

**The Effects of Potassium Currents on the Synchronization of  
Electrically Coupled Neural Oscillators**

By

Colin Baker Middleton  
B.A. (Duke University, Durham, North Carolina) 2005

THESIS

Submitted in Partial Satisfaction of the  
Requirements for the Degree of

MASTER OF SCIENCE

in

Applied Mathematics

in the

OFFICE OF GRADUATE STUDIES

of the

UNIVERSITY OF CALIFORNIA  
DAVIS

Approved:

---

Timothy Lewis, Chair

---

Robert Guy

---

Alexander Mogilner

Committee in Charge

2011

## **ACKNOWLEDGEMENTS**

I am forever indebted to my wonderful wife, Bina for her endless kindness and support in the completion of this thesis.

## TABLE OF CONTENTS

<b>Ch. 1 : Introduction .....</b>	<b>1</b>
1.1. Background .....	1
1.2. Mathematical Models of a Pair of Electrically Coupled Neurons .....	4
1.2.1. Neuronal Dynamics and the Hodgkin-Huxley model .....	4
1.2.2. The Leaky Integrate and Fire .....	12
1.2.3. Electrical Coupling .....	15
1.3. Theory of Weakly Coupled Oscillators & Reduction to Phase Models	17
1.4. Previous Modeling Results .....	21
1.4.1. Integrate and Fire Models .....	21
1.4.2. Effects of Potassium Currents .....	26
1.5. Outline of Thesis .....	28
 <b>Ch. 2 : Leaky Integrate and Fire (LIF) with an Explicit Potassium Current</b>	<b>31</b>
2.1. Model Description .....	31
2.1.1. LIF with an Explicit Summing Potassium Current .....	31
2.1.2. LIF with an Explicit Non-Summing Potassium Current .....	32
2.1.3. Non-dimensionalization .....	33
2.2. Effects of the Explicit Potassium Current on Firing Frequency .....	34
2.2.1. Numerical Simulations .....	34
2.2.2. Analytical Results .....	37
2.3. Electrically Coupled Cell-Pair Model with an Explicit Potassium Current .....	43
2.3.1. Numerical Simulations of Electrically Coupled Cells .....	44
2.4. Theory of Weakly Coupled Oscillators: Derivation of Phase Equation	46
2.4.1. The Effects of $\tau$ and $g_k$ on $G(\phi)$ .....	49
2.4.2. The Effects of $g_k$ and $\tau$ on $f^*$ .....	52
2.5. Insight from the Decomposition of $G(\phi)$ .....	57
2.5.1. $G_{SS}(\phi)$ .....	57
2.5.2. $G_K(\phi)$ .....	58
2.5.3. Interaction of $G_{SS}(\phi)$ and $G_K(\phi)$ .....	61
2.6. Conclusion and Discussion .....	65
2.6.1. Effects of the Summing versus the Non-Summing Potassium Current	67
2.6.2. Comparison to Previous Results of Pfeuty et al. and Mancilla et al.	69
2.6.3. Limitations of the Model .....	70
 <b>Ch. 3 : Leaky-Integrate-and-Fire with a Conductance Based Potassium Current .....</b>	<b>71</b>
3.1. Model Description .....	71
3.1.1. Non-dimensionalization .....	72

3.2. Effects of the Conductance-based Potassium Current on Frequency ..	73
3.2.1. Numerical Simulations .....	73
3.2.2. Analytical Results .....	75
3.3. Electrically Coupled Cell-Pair Model: Effects of a Conductance-based Potassium Current on Phase-Locking .....	79
3.3.1. Numerical Simulations of Electrically Coupled Cells .....	80
3.4. Theory of Weakly Coupled Oscillators: Derivation of Phase Equation	82
3.4.1. The Effects of $\tau$ on $G(\phi)$ .....	84
3.5. Conclusion and Discussion .....	89
3.5.1. Effects of Including Voltage Dependence in the Potassium Current	90
3.5.2. Comparison to Previous Results of Pfeuty et al. and Mancilla et al.	93
3.5.3. Limitations of the Model .....	95
<b>Ch. 4 : Full Conductance-Based Model .....</b>	<b>96</b>
4.1. Model Description .....	96
4.1.1. Potassium Channel Dynamics .....	98
4.2. Electrically Coupled Cell-Pair Model .....	100
4.3. Effect of the AHP Potassium Conductance on Phase-Locking: Theory of Weakly Coupled Oscillators .....	101
4.3.1. Effects of varying $I_{\text{applied}}$ , $g_{K_{AHP}}$ , and $\tau_{d_{AHP}}$ on the $G$ -functions .....	104
4.4. Discussion and Conclusions .....	113
4.4.1. Comparison to Previous Results of Pfeuty et al. and Mancilla et al.	113
4.4.2. Limitations of the Model .....	114
<b>App. A : .....</b>	<b>116</b>
A.1. The Infinitesimal Phase Resetting Curve $Z(t)$ .....	116
A.2. Reduction to Phase Model .....	117
<b>App. B : .....</b>	<b>119</b>
B.1. Choice of $\zeta(t)$ .....	119
B.2. Solutions for the LIF model with a Conductance-based Potassium Current for $g_K = 2$ .....	122
<b>App. C : .....</b>	<b>125</b>
C.1. Model Parameters .....	125
<b>Bibliography .....</b>	<b>127</b>

---

# Chapter 1

## Introduction

### 1.1 Background

The brain is characterized in part by its large-scale synchronous oscillatory electrical behavior [Buzsaki and Draguhn, 2004]. It is thought that synchronous oscillations are involved in cognition, sensory perception, and memory, but the exact mechanisms underlying synchrony and its exact function remain unknown [Buzsaki and Draguhn, 2004]. It is currently believed that oscillations in the  $\theta$  (3.5 - 7 Hz) and  $\gamma$  (30 - 70 Hz) frequency ranges affect memory processes and neural information encoding, while oscillations in the  $\alpha$  (8 - 13 Hz) and  $\gamma$  ranges correlate to cognitive attention [Ward, 2003; Sejnowski and Paulsen, 2006]. Synchronous oscillations appear to be ubiquitous throughout the brain. For example, oscillations in the  $\gamma$  frequency band have been found in numerous regions of the brain, including the neocortex, and oscillations in the  $\theta$  frequency band are commonly found in the hippocampus [Buzsaki and Draguhn, 2004; Buzsaki, 2002]. However, these examples represent only a small fraction of the frequencies where synchronous oscillatory activity has been observed, and we are only beginning to understand the biophysical and dynamical mechanisms underlying different oscillatory patterns [Ward, 2003].

An understanding of the oscillatory dynamics of subnetworks of neurons can provide insight into how and when synchronous oscillations arise in the brain. For example, many local populations of inhibitory interneurons in the cortex have been found to be extensively interconnected by electrical synapses [Galarreta and Hestrin, 2001], which are thought to promote synchrony. While there are many varieties of interneurons, electrical synapses are found predominately between interneurons of the same subpopulation. [Gibson et al., 1999; Beierlein et al., 2000]. This suggests that interneurons could be organized into functional subnetworks of cells. Certain subnetworks of interneurons have been found to play a fundamental role in the generation and maintenance of synchronous cortical oscillatory activity [Galarreta and Hestrin, 2001; Fries et al., 2007; Beierlein et al., 2000]. Although studies of electrically coupled cortical networks indicate that electrical coupling generally promotes the synchronization of electrical oscillations [Beierlein et al., 2000; Traub et al., 2001], theoretical studies have indicated that weak electrical coupling can support antisynchronous (i.e. antiphase) oscillatory activity in addition to synchronous behavior [Sherman and Rinzel, 1992; Chow and Kopell, 2000; Lewis and Rinzel, 2003]. However, this antisynchronous activity has not been observed experimentally, even though explicit attempts have been made to observe this phenomena [Mancilla et al., 2007]. Thus, it is thought that the contributions of certain intrinsic conductances in real neurons might “tune” networks for synchrony [Pfeuty et al., 2003; Mancilla et al., 2007].

The intrinsic electrical dynamics of neurons are controlled by the dynamics of numerous ionic channels. Potassium channels are among the most important, as they control the speed of depolarization, the strength and length of periods of hyperpolarization, and the duration of post-action potential refractory periods that prevent the formation of additional action potentials. More than 100 different potassium channels have been identified, and comprise a wide diversity of activation and deactivation properties. For instance, the Kv3.1 channel activates on a relatively fast time scale, between 10 - 20 *msec*, and also deactivates on a very fast time scale of 1.4 *msec* [see Coetzee et al., 1999]. Indeed, the Kv3.1 channel been found to deactivate at rates 7 - 10 times faster than those of nearly all other known voltage-gated potassium channels [Coetzee et al., 1999]. The Kv3.1 channel also activates at a relatively high threshold potential of  $-10mV$ . Conversely, the Kv1.3 channel activates on a slower time scale than the Kv3.1 channel, one greater than 20 *msec*, and deactivates on a slower time scale of 14 *msec* [Coetzee et al., 1999]. The Kv1.3 channel activates at a threshold potential of  $-50mV$ . Because of the importance of potassium channels in neuronal dynamics and the diversity of their properties, it behooves us to determine if and how the differences in potassium channel dynamics effect the synchronous behaviors of neuronal networks.

Two recent studies have suggested that potassium currents can have different effects on the synchronization of electrically coupled neurons. Research by Pfeuty et al. (2003) incorporated a model of a Kv1.3-like potassium current

in a Hodgkin-Huxley type model and found that such a current promoted synchronous oscillations. On the other hand, work by Mancilla et al. (2007) that incorporated models of both Kv1.3 and Kv3.1 potassium currents found that their inclusion promoted the formation of antisynchronous oscillations. Clearly, there is no uniform effect of potassium currents on the synchronization of electrically coupled oscillators. However, it seems likely that the exact activation and deactivation properties of individual potassium currents can influence whether antisynchronous oscillatory behavior arises. In this thesis, we hope to clarify how differences in the rates of activation and deactivation of potassium channels can influence the oscillatory behavior of electrically coupled neurons.

## **1.2 Mathematical Models of a Pair of Electrically Coupled Neurons**

### **1.2.1 Neuronal Dynamics and the Hodgkin-Huxley model**

The Hodgkin-Huxley model provides the formalism for the standard mathematical description of the electrical activity of a neuron [Hodgkin and Huxley, 1952]. It is based on the idea that the electrical properties of a neuron can be described by an equivalent electrical circuit. In this circuit, the current flowing across the membrane has two basic components: one is associated with charging the membrane capacitance and other is the “ionic currents” which are associated with the movement of ions across the membrane through specific ionic channels. The ionic current in the Hodgkin-Huxley model is subdivided into

distinct components corresponding to different types of channels: a sodium current  $I_{Na}$ , a potassium current  $I_K$ , and a leakage current  $I_L$  that accounts for all other ionic contributions.

The set of differential equations describing the Hodgkin-Huxley model is

$$C_m \frac{dV}{dt} = -I_{Na} - I_K - I_L + I_{applied}$$

where

$$I_{Na} = g_{Na}m^3h(V - E_{Na}) \quad (1.2.1)$$

$$I_K = g_Kn^4(V - E_K)$$

$$I_L = g_L(V - E_L)$$

and

$$\begin{aligned} \frac{dy}{dt} &= \alpha_y(V)(1 - y) - \beta_y(V)y \\ y_\infty(V) &= \frac{\alpha_y(V)}{\alpha_y(V) + \beta_y(V)} \\ \tau_y(V) &= \frac{1}{\alpha_y(V) + \beta_y(V)} \end{aligned} \quad (1.2.2)$$

where  $y = n, m, h$ .

Equation (1.2.1) is a conservation of current equation where  $C_m$  is the capacitance of the cell membrane,  $V$  is the cellular transmembrane potential, and  $I_{applied}$  is an external applied current. Each of the ionic currents can be modeled by an ohmic resistance in series with a “battery”, i.e. an electrochemical driving force that arises due to the differences in ionic concentrations across the cell membrane. The sodium and potassium conductances ( $g_{Na}m^3h$  and  $g_Kn^4$ ,

respectively) are modeled with variable resistances that are determined by time-dependent and voltage-dependent “gating” variables ( $m, h, n$ ); the leakage conductance is modeled with a constant resistance. The parameters  $g_{Na}$  and  $E_{Na}$  are the maximal conductance and the reversal potential for sodium, respectively;  $g_K$  and  $E_K$  are the maximal conductance and the reversal potential for potassium, respectively;  $g_L$  and  $E_L$  are the leakage conductance and the leakage potential, respectively. The reversal potentials are determined by the internal and external concentration of ions according to the Nernst equation and are typically  $E_{Na} \approx 50mV$ ,  $E_K \approx -75mV$ , and  $E_L \approx -55mV$  [Dayan and Abbott, 2001]. Note that, the sodium current acts to depolarize the neuron, i.e. make the membrane potential less negative, because of the relatively high value of its reversal potential, and that the potassium current acts to hyperpolarize the neuron, i.e. make the membrane potential more negative, because of its relatively low value of its reversal potential.

The ionic currents are controlled by the gating of their ion channels. In the Hodgkin-Huxley model,  $m$  and  $h$  are the gating variables for the sodium channels, and  $n$  is the gating variable for the potassium channels. Individually, each of the gating variables,  $(m, h, n)$ , can be thought of as a probability that a corresponding gate subunit is open, i.e., does not inhibit ionic flow through the channel pore. All gate subunits of an ion channel must be open for its channel to be open. Each sodium channel has three of the  $m$ -type activation gates and one  $h$ -type inactivation gate, while each potassium channel has four of the

$n$ -type activation gates. If we assume that all gates act independently, then  $m^3h$  and  $n^4$  give the probability that any given sodium or potassium channel is open, respectively. As the cell membrane contains numerous sodium and potassium channels,  $m^3h$  and  $n^4$  can alternatively be interpreted as the fraction of open sodium and potassium channels, respectively. Thus, the sodium and potassium conductances at a given state are  $g_{Na}m^3h$  and  $g_Kn^4$ , respectively.

Equation (1.2.2) describes the dynamics of each gating variable.  $\alpha_y(V)$  is the voltage dependent gate-subunit opening rate and  $\beta_y(V)$  is the voltage dependent gate-subunit closing rate. Both  $\alpha_y(V)$  and  $\beta_y(V)$  are determined by experimental fit via voltage clamp data. The dynamics of the gating variables can be more clearly understood by considering  $y_\infty(V)$  and  $\tau_y(V)$ .  $y_\infty(V)$  gives the gating variable's steady state value, the value to which  $y$  will evolve for a fixed membrane potential  $V$ .  $\tau_y(V)$  gives the gating variable's time constant, which quantifies how rapidly the gating variable approaches its instantaneous steady state value,  $y_\infty(V)$ .

Figure 1.2.1 plots the  $V$ -dependent the time-constant,  $\tau_y(V)$ , and steady state,  $y_\infty(V)$ , of the gating variables as a function of the membrane potential. The steady state values show the value that the gating variable will evolve to if the membrane potential is kept constant. Note that, when  $y_\infty = 0$ , all of the  $y$ -gating subunits evolve to the closed state, and when  $y_\infty = 1$ , all of the  $y$ -gating subunit evolve to the open state. At low voltages, the  $h$ -gating subunits tend to evolve to the closed state and the  $m$ - and  $n$ -gating subunits tend to

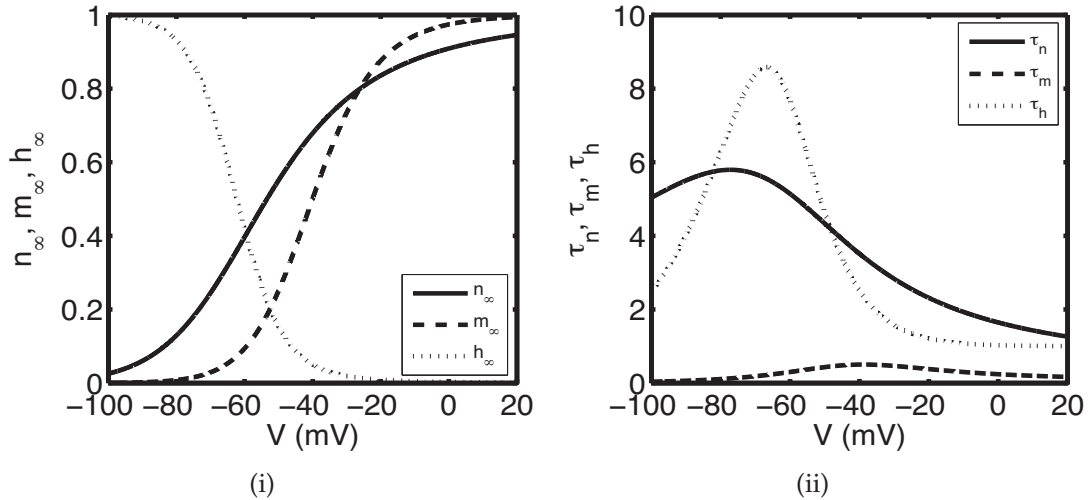


**Figure 1.2.1: The voltage dependence of the gating variables.** (i) Steady state value of the gating variables as a function of fixed  $V$ .  $n_\infty$ ,  $m_\infty$ , and  $h_\infty$  are solid, dashed, and dotted lines, respectively. (ii) Time constants of each gating variable.  $\tau_n$ ,  $\tau_m$ , and  $\tau_h$  are solid, dashed, and dotted, respectively. The smaller the time constant, the faster the gating variable reacts to changes in voltage. The  $m$  gating variable reacts quickly to voltage changes, while the  $h$  gating variable reacts much more slowly, especially at lower voltages.

evolve to the open state. At high voltages, the converse occurs (Figure 1.2.1(i)). Because of this behavior, the  $h$ -gating subunits are also known as inactivation gates, and the  $m$  and  $n$ -gating subunits are also called activation gates. Each gating variable's time constant indicates how rapidly the gating subunit reacts to changes in membrane potential at a given voltage. The smaller the value of  $\tau_y(V)$ , the faster the gating variable reacts to voltage changes. In general, the  $m$ -gating subunits are much faster to react to voltage changes than the  $n$ - or  $h$ -gating subunits (Figure 1.2.1(ii)).

In the absence of an external applied current, (i.e.  $I_{applied} = 0$ ), a Hodgkin-Huxley model neuron remains at an equilibrium potential of about  $-65mV$ .

The small sodium and potassium currents counterbalance the leakage current and force the membrane potential to this equilibrium value.

If a transient positive external current is applied to the cell, the neuron's membrane potential will increase. The size of this membrane potential increase depends on the magnitude and the duration of the applied current. In Figure 1.2.2(i), the dot-dashed line shows the effects of a small magnitude current.  $I_{applied}$  is increased from 0 to  $2nA$  at time  $t = 5msec$ . The membrane potential briefly increases before decreasing to a new, slightly higher equilibrium potential. In Figure 1.2.2(i), the solid line shows an action potential in the Hodgkin-Huxley model. At  $t = 0$ , the neuron is at equilibrium as  $I_{applied} = 0$ . At time  $t = 5msec$ ,  $I_{applied}$  is increased from 0 to  $10nA$ . The addition of the applied current  $I_{applied}$  causes the membrane potential to increase above a threshold potential. This elicits an action potential, which is characterized by a rapid increase in the membrane potential followed by a fast repolarization.

Examining the evolution of the gating variables provides insight into the formation of an action potential. Figure 1.2.2(ii) shows how the gating variables evolve during an action potential. As the voltage increases due to the application of  $I_{applied}$ , the  $m$ -gating variable rapidly increases and begins to activate the sodium conductance. The activation of the sodium conductance causes the membrane potential to depolarize further, which in turn causes the  $m$ -gating variable to rapidly increase further, and thus forming a positive feedback loop and the large, fast action potential upstroke. Note that concurrently,

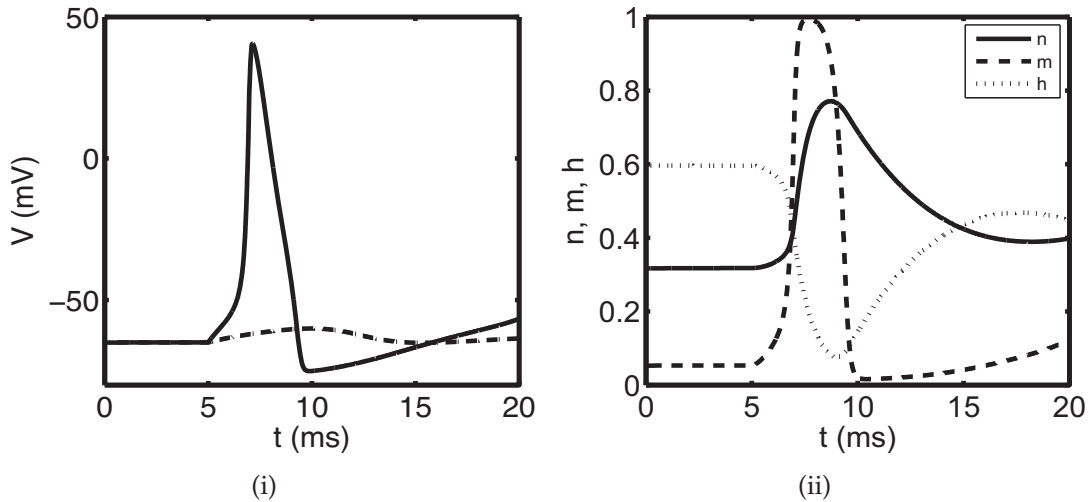


**Figure 1.2.2: An action potential in the Hodgkin-Huxley model neuron.** (i) In the time period  $[0, 5\text{msec}]$ ,  $I_{applied} = 0$  and the neuron is at  $V_m \simeq -65\text{mV}$ . At  $t = 5\text{msec}$ ,  $I_{applied}$  is set to  $10nA$  (solid) and  $2nA$  (dot-dashed). The addition of  $I_{applied} = 10nA$  leads to a rapid increase in membrane potential,  $V$ , then a fast repolarization. After repolarization, the cell slowly depolarizes back towards the equilibrium state. If  $I_{applied} = 2nA$ , the membrane potential increases but remains below the threshold potential. Therefore, no action potential occurs, and the neuron settles to a new, higher equilibrium potential (ii) The evolution of the gating variables  $n$  (solid),  $m$  (dashed), and  $h$  (dotted) in response to the changes in voltage as shown in (i) for the addition of  $I_{applied} = 10nA$  (solid line). [Parameters and gating variable function are as described in Dayan and Abbott, 2001, p. 173]

the  $h$ -gating variable decreases in response to increases in membrane potential.

However, because the  $h$ -gating variable responds much more slowly to voltage changes than the  $m$ -gating variable, the sodium conductance is able to activate and form the positive feedback loop before the  $h$ -gating variable significantly inactivates the sodium conductance. At the same time, the  $n$ -gating variable increases as the voltage increases. However, like the  $h$ -gating variable, the  $n$ -gating variable increases more slowly than the  $m$ -gating variable, and thus the activation of the potassium conductance lags that of the sodium conductance.

After a lag of a few milliseconds, the potassium conductance attains a significant level of activation and the sodium conductance becomes significantly inactivated. Therefore, the potassium conductance then causes a sharp repolarization of the neuron. If this repolarization drives the membrane potential below the resting potential, the neuron is said to have hyperpolarized. During the hyperpolarization phase, the  $m$ -gating variable quickly returns to a steady state value,  $m_\infty(V) \sim 0$ , and the sodium conductance is deactivated. The  $n$ -gating variable more slowly returns to a steady state value,  $n_\infty(V) \sim 0$ . Thus, the potassium conductance decays and the leakage current returns the neuron towards its resting equilibrium.

Immediately following an action potential, especially during a hyperpolarized period, it can be difficult or impossible to induce a new action potential via new stimulation. This property is known as refractoriness, and can be either absolute or relative. During an absolute refractory period, it is impossible to initiate the creation of another action potential, regardless of the strength of the stimulus. During a relative refractory period, it is possible to create an action potential but the threshold potential for its creation is increased. The refractory periods are due to the delay of the  $h$ - and  $n$ -gating variables to return to their values at equilibrium. As the neuron exits its refractory period, it becomes easier to evoke an action potential.

If the applied current,  $I_{\text{applied}}$ , is held constant at a supra-threshold value, i.e. above a certain threshold, a subsequent action potential can form. Indeed, this

process can continue indefinitely in a periodic fashion (Figure 1.2.3).

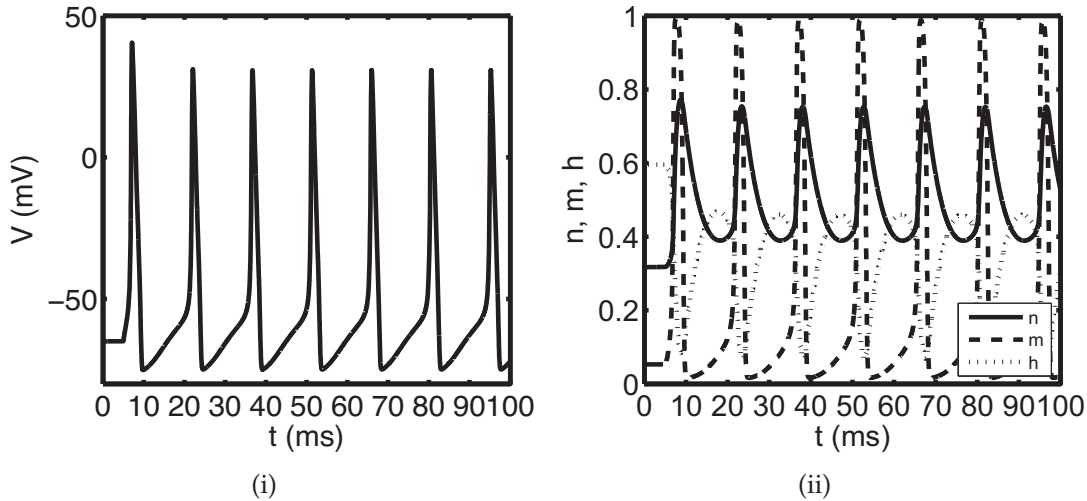


**Figure 1.2.3: Oscillations in the Hodgkin-Huxley model.** In the time period  $[0, 5\text{msec}]$ ,  $I_{\text{applied}} = 0$  and the model neuron is at  $V_m \approx -65\text{mV}$ . At  $t = 5\text{msec}$ ,  $I_{\text{applied}}$  is set to  $10\text{nA}$ . (i) Oscillations in the Hodgkin-Huxley model under a constant current. (ii) Evolution of the gating variables  $n$  (solid),  $m$  (dashed), and  $h$  (dotted) in response to the changes in voltage as shown in (i).

Since Hodgkin and Huxley first described their model for the squid giant axon in the 1950's, the Hodgkin-Huxley model formalism continues to be used because it reproduces electrophysiological measurements of neurons to a high degree of accuracy [Bower and Beeman, 1995; Koch and Segez, 1989]. It also provides a framework for the integration of additional types of ionic currents, such as the additional potassium current we add in Chapter 4.

### 1.2.2 The Leaky Integrate and Fire

The complexity of the Hodgkin-Huxley model makes it difficult to gain analytic insight. This limitation of the Hodgkin-Huxley model can be overcome by using an idealized model of neuronal dynamics which only captures the

basic properties of neurons, such as the Leaky Integrate and Fire (LIF) model. Instead of allowing the gating variables to determine the properties of the action potential, the standard LIF model includes only the leakage current and ignores the details of the action potential entirely. Whenever the membrane potential reaches a prescribed threshold potential,  $V_{th}$ , the neuron is said to “fire” an action potential and the membrane potential is immediately set to a reset potential,  $V_{reset}$ . Thus, the effects of the sodium and potassium currents are described by the threshold and reset conditions.

The intrinsic dynamics of the standard LIF model with a constant applied current are described by

$$C_m \frac{dV}{dt} = -g_L(V - E_L) + I_{app} \quad (1.2.3)$$

where if  $V(t_*^-) = V_{th}$ , then  $V(t_*^+) = V_{reset}$ .

As in the Hodgkin-Huxley model,  $t$  is time,  $C_m$  is the membrane capacitance,  $V$  is the transmembrane potential of the cell,  $g_L(V - E_L)$  is the leakage current, and  $I_{app}$  is a current applied to the cells.

For a constant applied current  $I_{app}$  and the initial condition  $V(0) = V_{reset}$ , the sub-threshold solution to the LIF model (1.2.3) is given by the following:

$$V(t) = V_{reset} + \frac{I_{app} + g_L(E_L - V_{reset})}{g_L} \left(1 - e^{-\frac{g_L}{C_m}t}\right).$$

Note that if  $I_{app} \leq g_L(V_{th} - E_L)$  that the cell approaches a steady state  $V^* = E_L + I_{app}/g_L \leq V_{th}$  and does not fire. Conversely, if  $I_{app} \geq g_L(V_{th} - E_L)$ , then  $V$

increases from  $V_{reset}$  until  $V = V_{th} \leq E_L + I_{app}/g_L$ , at which point the cell fires,  $V$  is reset to  $V_{reset}$ , and the process repeats, producing periodic firing of period

$$T = \frac{C_m}{g_L} \ln \left( \frac{I_{app} + g_L(E_L - V_{reset})}{I_{app} + g_L(E_L - V_{th})} \right).$$

Figure 1.2.4 illustrates examples of sub-threshold steady state behavior and periodic activity. Note that the LIF model captures the basic behavior of the Hodgkin-Huxley model as illustrated in Figure 1.2.3(i).

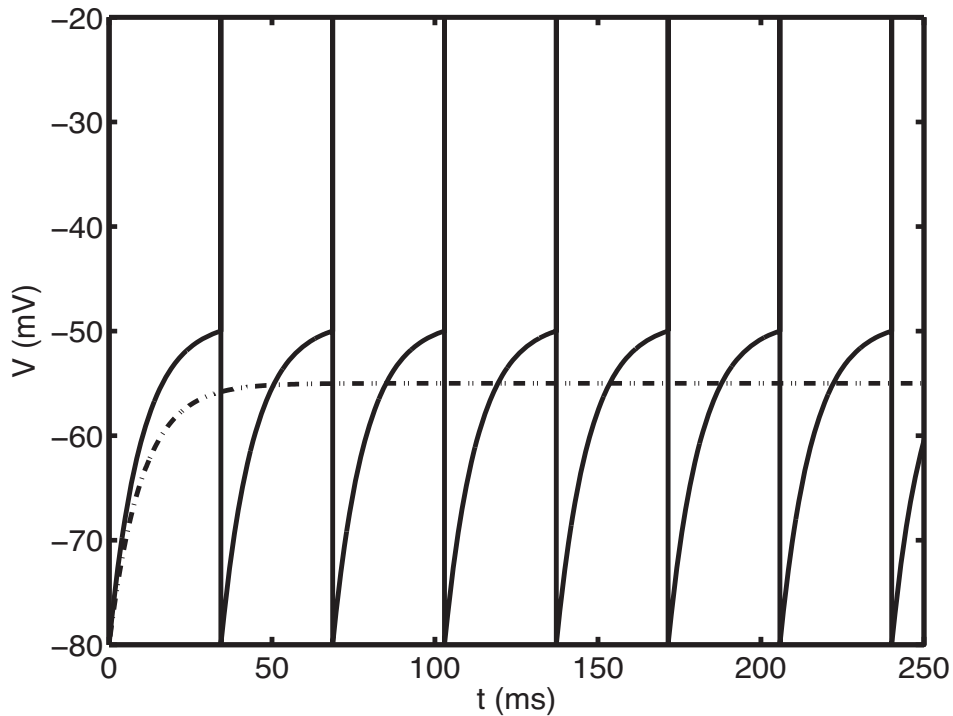


Figure 1.2.4: **LIF dynamics subject to a constant applied current.** The dot-dash line corresponds to  $I_{app} \leq g_L(E_L - V_{reset})$  with  $I_{app} = 1\text{nA}$ . This solution approaches a steady state that is less than the threshold voltage, and thus no action potential is fired. The solid line solution corresponds to  $I_{app} \geq g_L(E_L - V_{reset})$  with  $I_{app} = 1.6\text{nA}$ . This solution evolves to the threshold voltage and allows for the creation of action potentials. For both cases,  $V_{th} = -50\text{mV}$ ,  $V_r = -65\text{mV}$ ,  $V_{reset} = -80\text{mV}$ ,  $g_L = .1\mu\text{S}$ , and  $C_m = 1\text{nF}$ .

The standard LIF model can be extended to include a proscribed action potential which is “fired” when the neuron reaches its threshold potential. While the inclusion of a proscribed action potential does not influence the dynamics of an individual LIF neuron, its inclusion does affect the dynamics of electrically coupled LIF neurons. Here, we shall use a  $\delta$ -function “spike” to model the action potential, given by  $\beta\delta(t)$ , where  $\delta(t)$  is the  $\delta$ -function, and  $\beta$  is a measure of the size of the spike [Lewis and Rinzel, 2003]. Thus, when  $V$  reaches a threshold potential,  $V_{th}$ , from below, the cell “fires a spike” of size  $\beta$ .  $V$  is then set to the reset potential,  $V_{reset}$ .

### 1.2.3 Electrical Coupling

Electrical coupling between neurons is well-described by a simple ohmic resistance [Bennett and Zukin, 2004]. That is, the current flow from cell 1 into cell 2 can be described by  $I_{coup} = g_c(V_1 - V_2)$ , where  $g_c$  is the constant conductance of the electrical coupling and  $V_1$  and  $V_2$  are the voltages for cell 1 and cell 2, respectively. Therefore, to model electrical coupling,  $I_{coup}$  must be added to the current balance equation in the neuron models. Thus, a model describing a pair of identical, electrically coupled LIF neurons is

$$\begin{cases} C_m \frac{dV_1}{dt} = -g_L(V_1 - E_L) + I_{app} + g_c(V_2 - V_1) \\ C_m \frac{dV_2}{dt} = -g_L(V_2 - E_L) + I_{app} + g_c(V_1 - V_2) \end{cases} \quad (1.2.4)$$

where if  $V_i(t_*^-) = V_{th}$ , then the cell spikes and is reset,

$$V_i(t_*) = \beta\delta(t_*) \text{ and } V_i(t_*^+) = V_{reset} \text{ for } i = 1, 2.$$

Note that, it is important to include an explicit spike in the electrically coupled LIF neuron model, as the large depolarization during an action potential can greatly affect the membrane potential of the coupled cell, and thus affect the dynamics of phase-locking. Without the spike, the coupling term only accounts for sub-threshold activity, i.e. the rapid re-polarization during an action potential that is captured by the reset of a neuron from  $V_{th}$  to  $V_{reset}$  (i.e., standard LIF).

In non-dimensionalization terms, the system is

$$\begin{cases} \frac{dv_1}{d\bar{t}} = -v_1 + I + \bar{g}_c(v_2 - v_1) \\ \frac{dv_2}{d\bar{t}} = -v_2 + I + \bar{g}_c(v_1 - v_2) \end{cases} \quad (1.2.5)$$

where if  $v_i(t_*^-) = v_{th} = 1$ , then the cell spikes and is reset,

$$v_i(t_*) = \beta\delta(t_*) \text{ and } v_i(t_*^+) = v_{reset} = 0 \text{ for } i = 1, 2,$$

where  $v_i = (V_i - V_{reset})/(V_{th} - V_{reset})$ ,  $\bar{t} = t/(c_m/g_L)$ ,  $\bar{g}_c = g_c/g_L$ ,  $\bar{\beta} = \beta/(V_{th} - V_{reset})$ , and  $I = (I_{app} + g_L(E_L - V_{reset}))/(g_L(V_{th} - V_{reset}))$ . Note that this reduces the number of parameters from seven to three and sets  $v_{reset} = 0$  and  $v_{th} = 1$ . For convenience, we will omit the bars over the parameters for the duration of the chapter.

### 1.3 Theory of Weakly Coupled Oscillators & Reduction to Phase Models

The theory of weakly coupled oscillators allows for the reduction of the dynamics of any pair of weakly coupled oscillating neurons to a single equation that governs the phase difference between the two oscillatory cells [Kuramoto, 1984]. This simplified model, known as a phase model, allows for extensive analysis and insight into the existence and stability of the phase-locking states of the coupled systems. This approach is often used in the analysis of networks of neurons, e.g. Ermentrout and Kopell (1991), Grannan et al. (1993), Hansel et al. (1995), Golomb et al. (2001), Ermentrout and Kleinfeld (2001), and Lewis and Rinzel (2003). Below, we present a derivation of the phase-model for electrically coupled neurons.

Consider a pair of identical, weakly electrically coupled neurons (e.g. system (1.2.5) with “small”  $g_c$ ), where each isolated neuron oscillates with a period,  $T$ , and that this oscillation is the result of a strongly attracting limit cycle. We define the voltage component of the limit cycles as  $v_{LC}(t)$  (where  $t \in [0, T]$ ). Because of the weak coupling, the dynamics of each individual cell is dominated by its intrinsic dynamics rather than the dynamics of the coupled cell. Thus, each coupled cell strongly adheres to its intrinsic limit cycle  $v_{LC}(t)$  and has a period very close to  $T$ . The state of each cell is therefore well described solely by its position or “phase” on the limit cycle, where the phase of cell  $j$  is defined as  $\phi_j(t) = [(t/T) \bmod 1]$ , where  $t \in [0, T]$ ,  $\phi_j \in [0, 1]$  (phase 0 is an arbitrary point

on the limit cycle). Although each cell is dominated by its intrinsic dynamics, the weak electrical coupling between the cells can cause small changes in the relative phases of the cells. While these changes are negligible over a single cycle, these small effects can accumulate over many cycles and lead to specific phase-locking patterns between the cells (i.e. synchrony, antisynchrony, or other asynchronous patterns). This relationship can be quantified by the phase difference between two cells, given by  $\phi = \phi_j - \phi_k$ .

To understand these small phase shifts due to coupling, we first need to know how each cell will react to a “small, brief” current pulse at a given phase and how much current will be delivered by its coupled cell at a given time. The infinitesimal phase resetting curve (iPRC),  $Z(t)$  quantifies how each cell will react to a small, brief current pulse at any given phase in the cell’s cycle. To determine  $Z(t)$ , suppose that a small current of amplitude  $A$  and duration  $\Delta\tilde{t}$  is delivered to cell  $j$  at a phase in the oscillation corresponding to  $\phi_j = \tilde{t}/T$ , and it causes a phase shift of  $\Delta\phi$ . The iPRC is the phase shift as a function of the phase of the stimulus,  $\tilde{t}$ , normalized by the total charge of the stimulus current,  $A\Delta\tilde{t}$ .

$$Z(\tilde{t}) = \frac{\Delta\phi}{A\Delta\tilde{t}}. \quad (1.3.1)$$

As long as  $A\Delta\tilde{t}$  is sufficiently small,  $Z(t)$  is approximately independent of the size of the stimulus.

The amount of current that cell  $j$  receives at time  $\tilde{t}$  due to its electrical coupling to cell  $k$  is given by

$$I_{coupling_{jk}}(\tilde{t}) = g_c[V_k(t) - V_j(t)] \simeq g_c[v_{LC}(\tilde{t} + \phi_k T) - v_{LC}(\tilde{t} + \phi_j T)]. \quad (1.3.2)$$

Using  $Z(t)$ , (Equation (1.3.1)), and setting its current amplitude  $A$  to be the coupling current  $I_{coupling}$ , the coupling current flowing during the time  $t$  to  $t + \Delta\tilde{t}$ , (Equation (1.3.2)), we can find the approximate shift in relative phase of cell  $j$  due to the coupling current from cell  $k$  over the small time  $\Delta\tilde{t}$ ,

$$\Delta\phi_j = Z(\tilde{t} + \phi_j T)g_c[v_{LC}(\tilde{t} + \phi_k T) - v_{LC}(\tilde{t} + \phi_j T)]\Delta\tilde{t}. \quad (1.3.3)$$

Dividing both sides of Equation (1.3.3) by  $\Delta\tilde{t}$  and taking the appropriate limit as  $\Delta\tilde{t} \rightarrow 0$  gives a differential equation governing the evolution of the relative phase  $\phi_j$  due to coupling,

$$\frac{d\phi_j}{d\tilde{t}} = Z(\tilde{t} + \phi_j T)g_c[v_{LC}(\tilde{t} + \phi_k T) - v_{LC}(\tilde{t} + \phi_j T)]. \quad (1.3.4)$$

Because we assume that the neurons are weakly coupled,  $g_c$  is small, implying that the time scale for the evolution of the relative phase  $\phi_j$  is much larger than that of the period,  $T$ . Therefore, we can average the right hand side of Equation (1.3.4) over the full period of an oscillation while holding  $\phi_j$  and  $\phi_k$  fixed to

obtain an equation that describes the rate of change in  $\phi_j$  on a slow time scale

$$\begin{aligned}\frac{d\phi_j}{d\tilde{t}} &= \frac{1}{T} \int_0^T Z(\tilde{t} + \phi_j T) g_c [v_{LC}(\tilde{t} + \phi_k T) - v_{LC}(\tilde{t} + \phi_j T)] d\tilde{t} \\ &= \frac{1}{T} \int_0^T Z(\tilde{t}) g_c [v_{LC}(\tilde{t}) - v_{LC}(\tilde{t} - (\phi_j - \phi_k)T)] d\tilde{t} \\ &= H(-(\phi_j - \phi_k)).\end{aligned}\quad (1.3.5)$$

Note that the explicit time dependence of equation (1.3.4) has been eliminated.

By subtracting the differential equation (1.3.5) for cell 2 from that for cell 1, a single differential equation which describes the evolution of the phase difference between the two coupled cells,  $\phi = \phi_1 - \phi_2$ , is obtained.

$$\frac{d\phi}{dt} = H(-\phi) - H(\phi) = G(\phi) \quad (1.3.6)$$

The so-called “ $G$ -function” allows for the use of familiar nonlinear dynamics analysis to determine how changes to the parameters can lead the coupled oscillators to evolve to stable phase-locked states [Strogatz, 1994]. As a reminder,  $G(\phi^*) = 0$  indicates that  $\phi^*$  is a phase-locked state. The stability of phase-locked states can be determined by the sign of  $G'(\phi^*)$ . If  $G'(\phi^*) > 0$ , the phase-locked state is unstable, and if  $G'(\phi^*) < 0$ , the phase-locked state is stable. When two identical neurons are electrically coupled, as a result of symmetry,  $\phi = 0$  and  $\phi = T/2$  are always fixed points. In the following chapters, we use the  $G$ -function to probe how changes in parameters, particularly those associated with an explicit potassium current, affect the stability of the antisynchronous

phase-locked state,  $\phi = T/2$ .

## 1.4 Previous Modeling Results

### 1.4.1 Integrate and Fire Models

Recent theoretical work has shown that two electrically coupled neural oscillators can exhibit both stable synchrony and asynchrony [Chow and Kopell, 2000; Lewis and Rinzel, 2003; Lewis, 2003]. Chow and Kopell (2000) used an integrate and fire model to show that the shape and size of the action potentials and the strength of the gap junction plays an important role in the existence and stability of phase locked states in electrically coupled neurons. Using the electrically coupled LIF model given in Equation (1.2.5), Lewis and Rinzel found that cell pairs connected by electrical coupling can support both synchronous and asynchronous firing below a critical frequency. Additionally, they found that increasing the size of the instantaneous threshold spikes decreased the frequency range where antisynchronous firing patterns were stable.

As the research presented in this thesis is an extension of the work published in Lewis and Rinzel (2003), their methods and specific results are reproduced here.

Numerical simulations of the pair of electrically coupled LIF model neurons (Equation (1.2.5)) show that changes in action potential frequency can affect whether the neurons evolve to a stable synchronous or antisynchronous firing pattern (Figure 1.4.1).

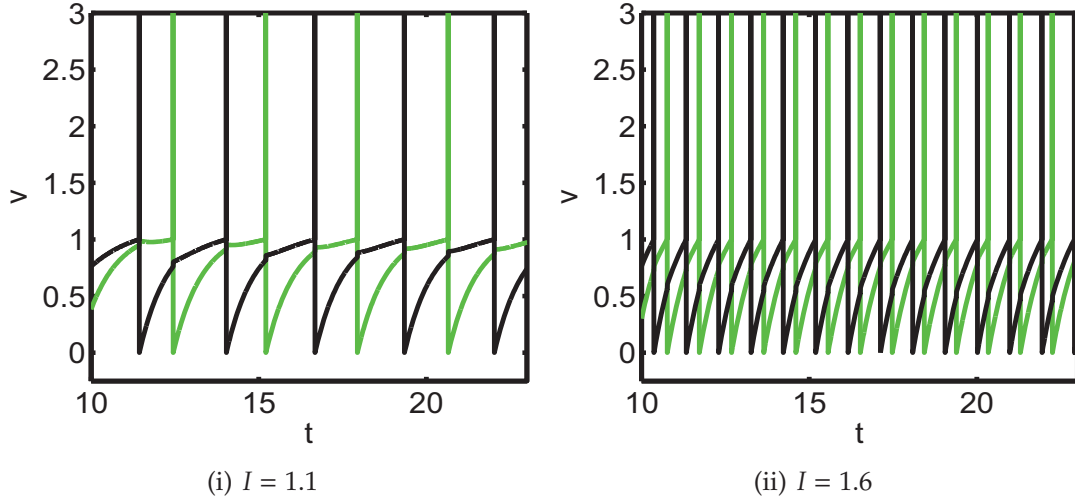


Figure 1.4.1: Response patterns of electrically coupled LIF cell pairs. For both graphs,  $\beta = 0.2$  and  $g_c = 0.2$  with initial conditions of  $v_j = 0.59$  and  $v_k = 0.0$ . The black lines and green lines correspond to cell  $j$  and cell  $k$  respectively. In (i) where  $I = 1.1$ , the cells fire at a relatively low intrinsic frequency and cells can exhibit stable antisynchronous activity. In (ii) where  $I = 1.6$  there is a relatively high intrinsic frequency and the cells synchronize.

To gain analytical insight, the system was reduced to a phase model. The membrane potential of an isolated non-dimensionalized LIF neuron during  $T$ -periodic oscillations is described by

$$v_{LC}(t) = I(1 - e^{-t}) + \beta\delta(t - T) \quad \text{for } 0 < t < T, \quad (1.4.1)$$

where  $T = \ln\left(\frac{I}{I-1}\right)$ .

The iPRC is

$$Z(t) = \begin{cases} \frac{e^t}{IT} & \text{for } 0 < t < T. \\ 0 & \text{for } t = 0, T. \end{cases} \quad (1.4.2)$$

(See Appendix A.1 for a derivation of  $Z(t)$ .)

Therefore, the  $G$ -function for the electrically coupled LIF cell pair can be calculated through the steps outlined in Section 1.3 (and Appendix A.2). This gives

$$G_c(\phi) = \frac{1}{T} \int_0^T Z(t) g_c [(v_{LC}(t - \phi T) - v_{LC}(t + \phi T))] dt$$

$$= \begin{cases} \frac{g_c}{T} [G_{SUB}(\phi) + G_{SPIKE}(\phi)], & \text{for } 0 < \phi < 1, \\ 0, & \text{for } \phi = 0, 1. \end{cases} \quad (1.4.3)$$

where

$$G_{SUB}(\phi) = 2(\phi \sinh((1 - \phi)T) - (1 - \phi) \sinh(\phi T)), \quad \text{for } 0 \leq \phi \leq 1,$$

$$G_{SPIKE}(\phi) = \begin{cases} \beta [e^{\phi T} - e^{T(1-\phi)}] & \text{for } 0 < \phi < 1, \\ 0 & \text{for } \phi = 0, 1. \end{cases}$$

Note that the strength of coupling,  $g_c$ , does not affect the existence or stability of phase-locked states. It simply scales the  $G$ -function and therefore, only affects the speed with which the system approaches or retreats from a phase-locked state.

Figure 1.4.2(i) shows the full  $G$ -function for  $f = 0.49$ ,  $I = 1.15$  and  $\beta = 0.1$ . Both the synchronous states (black diamonds) and the antisynchronous state (black circle) are stable. The unstable asynchronous states (open circles) define the boundaries between the region of attraction between the stable synchronous and antisynchronous phase-locked states.

The  $G$ -function is composed of two terms:  $G_{SPIKE}(\phi)$ , which accounts for the

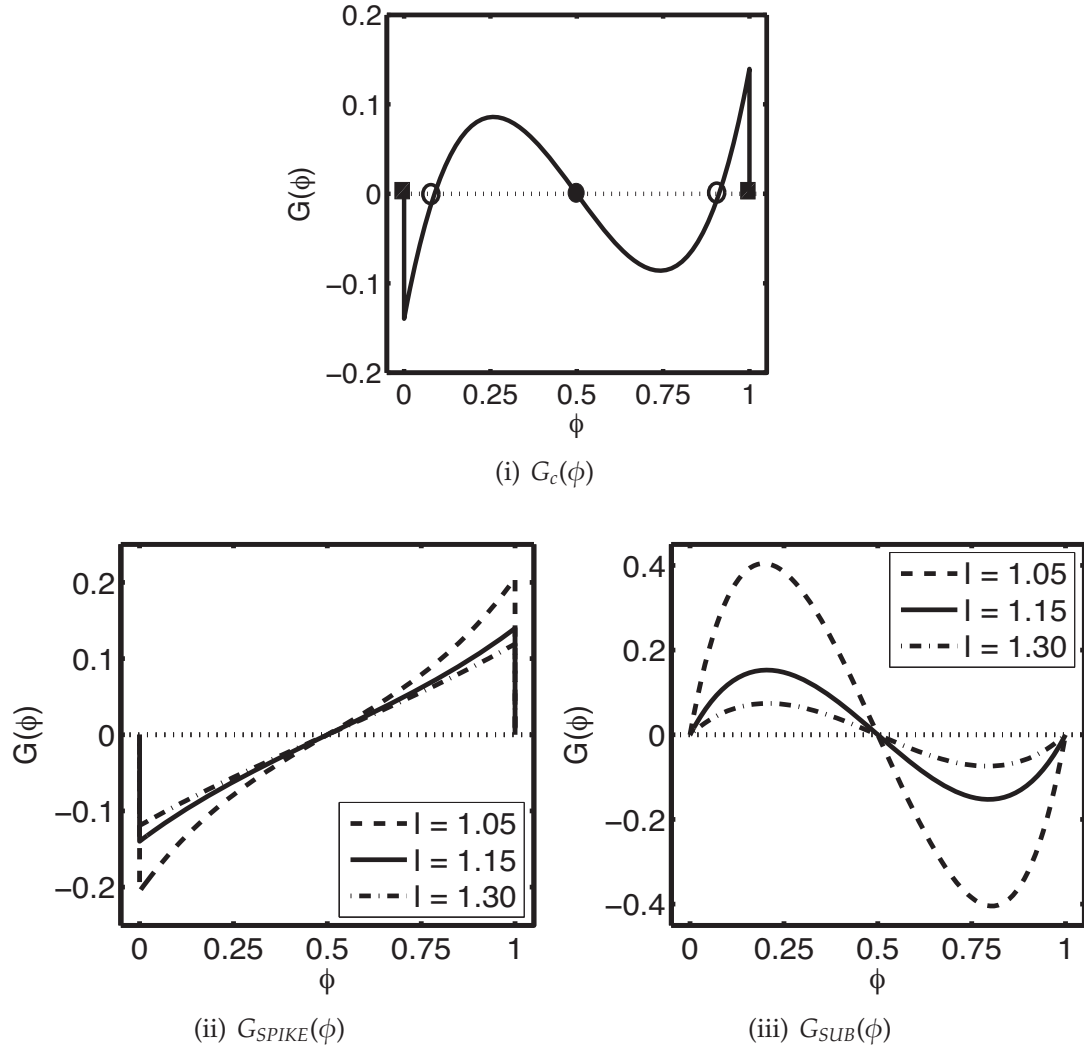


Figure 1.4.2: ***G*-functions for weakly electrically coupled LIF cell pairs.** (i) The full *G*-function for  $I = 1.15$ . Filled squares, filled circles, and open circles indicate the stable synchronous state, the stable antisynchronous state, and the unstable asynchronous states respectively. In (ii) and (iii), dashed, solid, and dot-dashed lines correspond to  $I = 1.05$ ,  $I = 1.15$ , and  $I = 1.3$  respectively. (ii) The portion of the *G*-function that accounts for the effects of the supra-threshold portion of the spike. This portion of the *G*-function always tends to synchronize activity. (iii) The portion of the *G*-function that accounts for effects of the sub-threshold activity. This portion of the *G*-function always tends to desynchronize activity. In all panels  $g_c = 1$ ,  $\beta = .1$ .

supra-threshold portion of the spike, and  $G_{SUB}(\phi)$ , which accounts for the sub-threshold activity of the cell. Note that, when  $\beta = 0$ ,  $G_c(\phi)$  is equal to  $G_{SUB}(\phi)$ .  $G_{SUB}(\phi)$  shows that for the given parameters, that the synchronous state is unstable and the antisynchronous state is stable (Figure 1.4.2(iii)). Conversely,  $G_{SPIKE}(\phi)$  always tends to synchronize the coupled cells (Figure 1.4.2(ii)). That is, this term has a stabilizing effect on the synchronous phase-locked state and a destabilizing effect on the antisynchronous phase-locked state. Note that this term is scaled by the size of the spike,  $\beta$ , and that increases in  $\beta$  lead to increased stability of the synchronous state and decreased stability of the antisynchronous state. Because  $G_c(\phi)$  is the scaled linear combination of  $G_{SPIKE}(\phi)$  and  $G_{SUB}(\phi)$ , the relative contributions of both portions of  $G_{SPIKE}(\phi)$  and  $G_{SUB}(\phi)$  determine the stability of the antisynchronous state.

The bifurcation diagram is an efficient way to show how the phase-locking behavior of the electrically coupled LIF neurons depends on the parameters for the neurons over a range of values (Figure 1.4.3). For small  $I$ , both antisynchrony and synchrony are stable, while for large  $I$ , only synchrony is stable.  $I_c^*$  denotes the critical value of  $I$  at which the antisynchronous state,  $\phi = 0.5$ , switches stability.  $I_c^*$  depends on the strength of the spike,  $\beta$ . The relationship between  $I_c^*$  and the spike strength,  $\beta$ , can be found by investigating where  $G'(0.5) = 0$ . This gives

$$\beta = \left( I_c^* - \frac{1}{2} \right) \ln \left( \frac{I_c^*}{I_c^* - 1} \right) - 1, \quad (1.4.4)$$

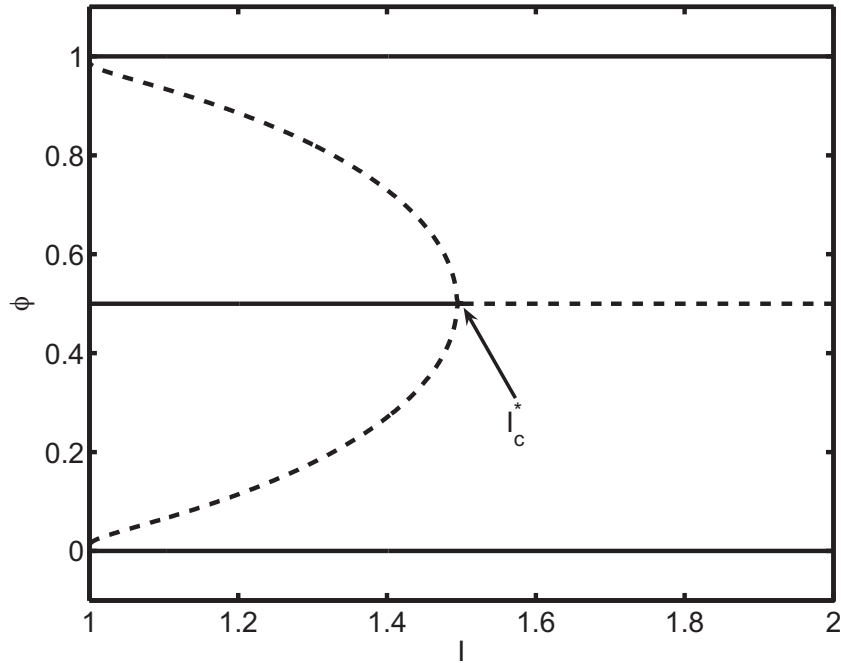


Figure 1.4.3: **Bifurcation diagram for the LIF cell-pair with weak electrical coupling with  $\beta = 0.1$ .** Solid and dashed lines indicate stable and unstable phase-locked states respectively.  $I_c^*$  indicates the critical value of  $I$  at which the antisynchronous state  $\phi^* = 0.5$  changes stability. Where  $I > I_c^*$  only synchrony is stable; where  $I < I_c^*$  both synchrony and antisynchrony are stable.

which implies that  $I_c^*$  increases as  $\beta$  decreases. That is, the spike suppresses the stability of the antisynchronous phase-locked state.

Note that one gains considerable insight into the mechanisms generating the phase locking dynamics by understanding how the model parameters affect  $Z(t)$ ,  $v_{LC}(t)$ , and  $G(\phi)$ .

#### 1.4.2 Effects of Potassium Currents

Ermentrout et al. (2001) studied the effects of a slow, voltage-dependent potassium current on the synchronization of a pair of conductance-based model

neurons connected by excitatory chemical synapses. They found that the magnitude of the potassium current can affect the stability of the synchronous phase-locked state. At a fixed frequency of 40 Hz, the synchronous phase-locked state is stable when the magnitude of the potassium current is small. As the magnitude of the potassium current is increased, the synchronous phase-locked state becomes less robustly stable. For a sufficiently large magnitude of the potassium current, the synchronous phase-locked state becomes unstable. Interestingly, the antisynchronous phase-locked state remains stable regardless of the magnitude of the potassium current.

Studies by Pfeuty et al. (2003) and Mancilla et al. (2007) investigated the effects of potassium currents on the synchronization of electrically coupled neurons. Pfeuty et al. modified the magnitude of two potassium currents, a delayed rectifier current and a slow, modified Kv1.3 type current, in numerical simulations to see how these currents effected synchronization. They found that both types of potassium currents independently promote the synchronization of the coupled cells. As an analog to their full conductance based model, Pfeuty et al. considered a quadratic integrate and fire (QIF) model, which similarly to the LIF model, qualitatively captures the dynamics of a neuron. Pfeuty et al. used the QIF model to link the synchronizing effects of potassium conductances to a “rightward” shift in the peak of the phase response curve Mancilla et al. (2007) considered both Kv1.3 and Kv3.1 type potassium channels as described by Erisir et al. (1999) in a conductance based model. They found

that both conductances promoted stabilization of the antisynchronous state. Mancilla et al. found that Kv1.3 shifted the PRC leftwards, while Kv3.1 shifted the PRC rightwards. Additionally, Mancilla et al. compared their theoretical model to biological data from neocortical inhibitory interneurons. They found that unlike the model cells, the real neurons were never able to support antisynchronous oscillatory activity. Furthermore, they found no significant difference between the location of peaks in model PRCs and experimentally determined PRCs, suggesting that it is unlikely that changes to the PRC alone are responsible for determining phase-locking behavior. Mancilla et al. provided evidence that differences in the shapes of the action potential and after-hyperpolarization currents are responsible for the differences between phase-locking in the modeled neurons and real neurons.

In this thesis, we hope to extend on both of these studies, and clarify how intrinsic differences in potassium channels can influence the phase-locking behavior of electrically coupled neurons.

## 1.5 Outline of Thesis

In this thesis, we study the effects of potassium currents on the synchronization of electrically coupled neural oscillators. We take advantage of the finding of Jolivet et al. (2004) that the reduction from a full conductance based Hodgkin-Huxley type model to an Integrate and Fire (IF) type model can quantitatively capture the dynamics of the more detailed full conductance

based model. Therefore, in Chapters 2 and 3, we will extend the LIF model as used by Lewis and Rinzel (2003) to gain analytic insight into the effect of potassium currents on synchronization, and then check in Chapter 4 whether these results hold in a full Hodgkin-Huxley type conductance based model.

In Chapter 2, we introduce two explicit potassium currents that activate during the hyperpolarization (reset) of a neuron following an action potential. We first show how these currents affect a single uncoupled LIF neuron. Next, we electrically couple two LIF neurons with explicit potassium currents and show that the explicit potassium currents can affect the stability of phase-locked states via numerical simulations. To gain insight into how changes in parameters can affect the stability of phase-locked states, we reduce our system of electrically coupled LIF neurons with explicit potassium current to a phase model. We investigate the  $G$ -function to understand how the explicit potassium current affects the existence and stability of phase-locked states. We then dissect the  $G$ -function and examine its decomposition to gain insight into the mechanisms underlying synchronization.

In Chapter 3, we again add a potassium current to the standard LIF model; however, we use a voltage-dependent potassium current. Similar to Chapter 2, we examine the effects of the voltage-dependent, conductance based potassium current on a single LIF neuron, before examining how the addition of the conductance based potassium current affects the synchronization of electrically coupled LIF neurons. As before, we use numerical simulations and a reduction

to phase models to examine how this conductance based potassium current affects the existence and stability of phase-locked states. Additionally, we compare the results from this chapter with those of Chapters 2 to see whether the results from the simpler model hold in an increasingly realistic one.

In Chapter 4, we use a modified Hodgkin-Huxley type model to investigate how differences in potassium channel dynamics effect the synchronization of electrically coupled neurons. Through numerical simulations and phase models, we compare results from this model with those of our earlier models in order to see whether the results hold in a more biologically realistic model.

## Chapter 2

### Leaky Integrate and Fire (LIF) with an Explicit Potassium Current

In this chapter, we modify the standard LIF model by adding explicit spike-activated potassium currents. We consider both a “summing” potassium current and a “non-summing” potassium current. For both kinds of explicit potassium currents, an action potential instantaneously triggers the activation of the potassium current, and the current exponentially decays after the action potential. The summing potassium current models a current that linearly sums all potassium currents activated by successive action potentials, which is a good approximation when an ionic conductance is far from saturation. The non-summing potassium current models a current that rapidly activates so that it attains its (near) maximal value during each spike, i.e., the current saturates with each spike. We determine how the addition of the explicit potassium current affects the dynamics of a single LIF neuron and investigate how the addition of the explicit potassium current affects the phase-locking behavior of a pair of electrically coupled neurons.

#### 2.1 Model Description

##### 2.1.1 LIF with an Explicit Summing Potassium Current

The LIF model with the addition of the summing potassium current is

$$C_m \frac{dV}{dt} = -g_L(V - E_L) + I_{app} + \eta_{K_s}(t),$$

where if  $V(t_*^-) = V_{th}$ , then

(i) the cell spikes and is reset,

$$V(t_*) = \beta \delta(t_*) \text{ and } V(t_*^+) = V_{reset}$$

(ii) the spike times are updated  $t_0 = t_*, t_{n-1} = t_n$

(iii) the spike-triggered decaying potassium current is activated such that

$$\eta_{K_s}(t) = \sum_{n=-\infty}^0 -q_s \frac{1}{\tau} e^{-(t-t_n)/\tau}. \quad (2.1.1)$$

The potassium current is the linear sum of the individual potassium currents triggered by each spike (which occurred at time  $t_n$ ). The parameter  $\tau$  is the time constant of the deactivation of the potassium current, and  $-q_s$  is the total charge carried by the potassium current triggered by each spike, i.e.,  $\eta_{K_s}(t)$  is normalized by  $1/\tau$ .  $\beta$  scales the effect of the supra-threshold portion of the spike.

### 2.1.2 LIF with an Explicit Non-Summing Potassium Current

The LIF model with the addition of the non-summing potassium current is

$$C_m \frac{dV}{dt} = -g_L(V - E_L) + I_{app} + \eta_{K_{ns}}(t),$$

where if  $V(t_*^-) = V_{th}$ , then

(i) the cell spikes and is reset,

$$V(t_*) = \beta\delta(t_*) \text{ and } V(t_*^+) = V_{reset}$$

(ii) the time of the most recent spike is updated  $t_0 = t_*$

(iii) the spike-triggered decaying potassium current is activated such that

$$\eta_{K_{ns}}(t) = -q_s \frac{1}{\tau} e^{-(t-t_0)/\tau} \text{ for } t \geq t_0. \quad (2.1.2)$$

The potassium current is triggered by the most recent spike at time  $t_0$ . As for the summing potassium current, the parameter  $\tau$  is the time constant of the deactivation of the potassium current and the parameter  $-q_s$  is a measure of the strength of the potassium current and  $\beta$  scales the effect of the supra-threshold portion of the spike

### 2.1.3 Non-dimensionalization

We apply a similar non-dimensionalization as presented in Chapter 1. We let  $v = (V - V_{reset})/(V_{th} - V_{reset})$ , so that  $v_{reset} = 0$  and  $v_{th} = 1$ . Likewise, we let  $\bar{t} = t/(C_m/g_L)$ . After applying this non-dimensionalization, we group our parameters as such:  $\bar{\tau} = \tau/(C_m/g_L)$ ,  $\bar{\beta} = \beta/(V_{th} - V_{reset})$ ,  $\bar{I} = (I_{app} + g_L(E_L - V_{reset}))/(g_L(V_{th} - V_{reset}))$ ,  $\bar{g}_K = q_s/(C_m(V_{th} - V_{reset}))$ , and  $\bar{\eta}_K(\bar{t}) = \eta_K(t/\tau)$ . In the non-dimensionalized form,  $\bar{I}$  is the dimensionless applied current,  $\bar{\tau}$  is the dimensionless time constant of the potassium current, and  $\bar{g}_K$  is the dimensionless strength of the explicit potassium current. For convenience, the bars

over the parameters will be omitted for the remainder of this chapter. Thus, the non-dimensionalized LIF model with an explicit potassium current is

$$\frac{dv}{dt} = -v + I - g_K \eta_K(t)$$

where if  $v(t_*^-) = v_{th}$ , then

(i) the cell spikes and is reset,

$$v(t_*) = \beta \delta(t_*) \text{ and } v(t_*^+) = v_{reset}$$

(ii) the spike times are updated  $t_0 = t_*, t_{n-1} = t_n$

(iii) the spike-triggered decaying potassium current is activated such that

$$\eta_K(t) = \begin{cases} \eta_{K_s}(t) = \sum_{n=-\infty}^0 \frac{1}{\tau} e^{-(t-t_n)/\tau} & \text{for } t \geq t_0, \\ \eta_{K_{ns}}(t) = \frac{1}{\tau} e^{-(t-t_0)/\tau} & \text{for } t \geq t_0. \end{cases} \quad (2.1.3)$$

## 2.2 Effects of the Explicit Potassium Current on Firing Frequency

Before considering the effects of coupling, we examine the effects of an explicit potassium current on the dynamics of a single LIF neuron. We limit our analysis to the case in which the neuron is stimulated by a constant applied current  $I$ , and we determine the effects of the potassium currents on the firing frequency, the voltage-profile, and the model neuron's phase resetting curve.

### 2.2.1 Numerical Simulations

Figure 2.2.1 presents numerical simulations of the periodic firing of a single LIF cell with the summing potassium current (left) and the non-summing

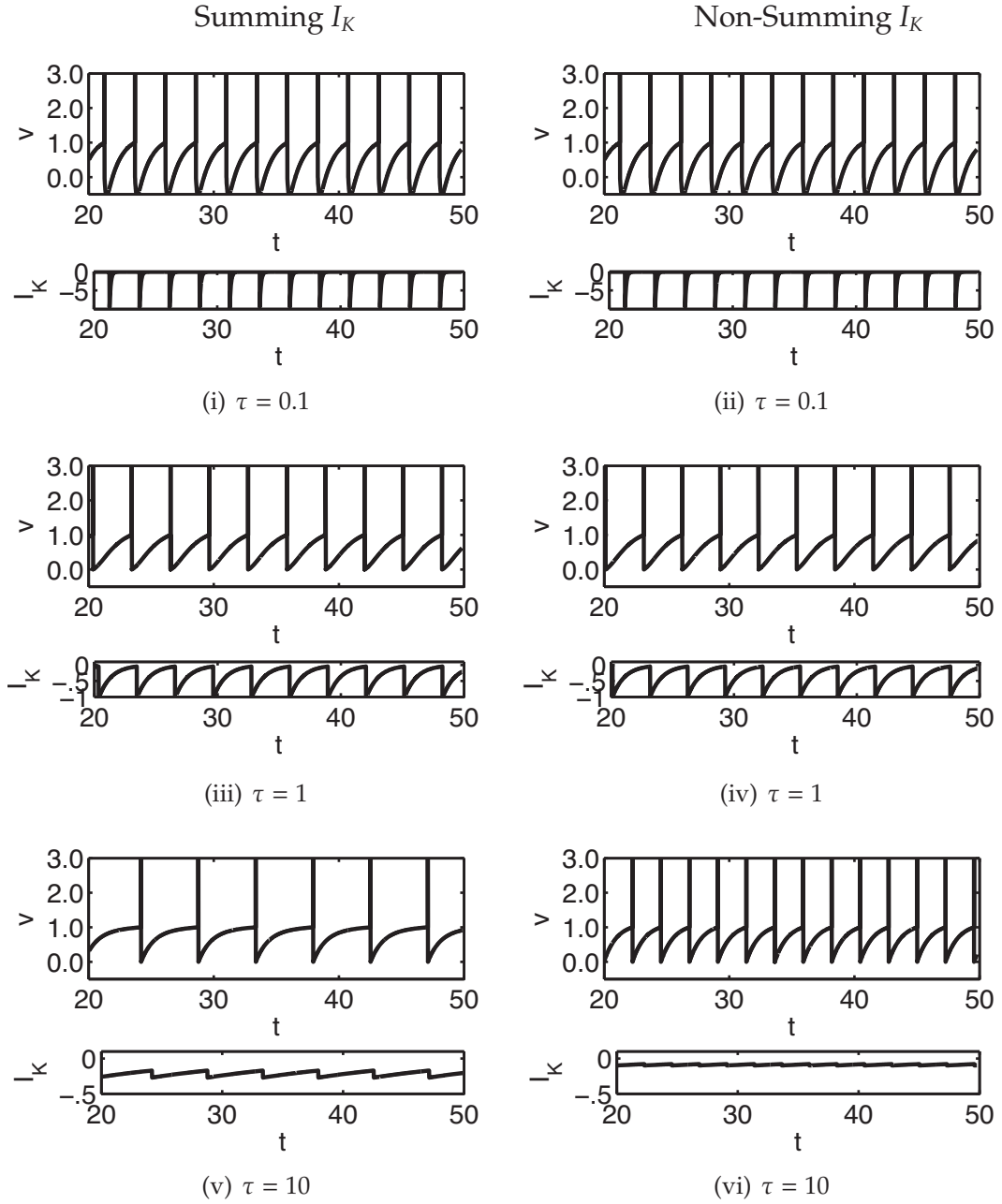


**Figure 2.2.1: Periodic firing of LIF model with the summing (left) and the non-summing (right) potassium current.** For all graphs,  $I = 1.2$  and  $g_K = 1$ . In each panel, plots of the voltage are in the upper graphs and plots of the explicit potassium current are in the lower graphs. (i), (ii) For  $\tau = 0.1$ , the explicit potassium current drives  $v$  below  $v_{reset} = 0$ . (iii), (iv) For  $\tau = 1$ ,  $v$  is always greater than  $v_{reset}$  (upper). (v), (vi) For  $\tau = 10$ , the exponential decay in the explicit potassium current becomes less apparent. The substantial accumulated amount of potassium current causes (v) the case with the summing potassium current to have a considerably lower firing frequency compared to (vi) the case with the non-summing potassium current.

potassium current (right) for deactivation time constants of  $\tau = 0.1$  (top),  $\tau = 1$  (middle), and  $\tau = 10$  (bottom). Note that, in the model with the summing potassium current, as the deactivation time constant of the potassium current  $\tau$  increases, the firing frequency decreases. Whereas in the model with the non-summing potassium current, increasing  $\tau$  causes non-monotonic changes to the frequency. Increasing  $\tau$  from  $\tau = 0.1$  to  $\tau = 1$  causes the firing frequency to decrease while increasing  $\tau$  from  $\tau = 1$  to  $\tau = 10$  causes the firing frequency to increase. For  $\tau = 0.1$  and  $\tau = 1$ , there is little difference between the firing frequencies of the LIF model with either the summing potassium current or the non-summing potassium current. However, the more slowly deactivating potassium constant  $\tau = 10$ , the LIF model with the summing potassium current fires with a substantially lower frequency than for the model with the non-summing potassium current.

Examining the explicit potassium currents (given in the lower half of each subfigure), we see that the maximum of the potassium current decreases as  $\tau$  increases. For small  $\tau$  (e.g.,  $\tau = 0.1$ ), the current consists of a sharp spike, i.e., a large current is quickly activated and rapidly decays. For large  $\tau$  (e.g.,  $\tau = 10$ ), the potassium current is always present throughout the entire period. For  $\tau = 0.1$  and  $\tau = 1$ , there is little difference between the shape and magnitude of the summing and non-summing potassium currents. However for  $\tau = 10$ , the average magnitude of the current is over two times greater for the summing potassium current than for the non-summing potassium current, and this leads

to the lower firing frequency in the LIF model with the summing potassium current.

### 2.2.2 Analytical Results

To obtain a more complete picture of the effects of the explicit potassium current on the dynamics of the LIF model seen via the numerical simulations, we investigate the analytic solutions to the modified LIF model (Equation (2.1.3)).

Note that when  $I < 1$ , the LIF neuron never spikes, and thus the explicit potassium current is never activated. The neuron simply exponentially approaches the steady state,  $v = I$ .

However when  $I > 1$ ,  $v$  increases to threshold,  $v_{th} = 1$ , which triggers a spike, resets  $v$  to  $v_{reset} = 0$ , and activates the explicit potassium current. Because the explicit potassium current exponentially decays towards zero,  $v$  will always reach  $v_{th}$  and cause another spike to be fired. The system will always evolve to  $T$ -periodic activity.

During  $T$ -periodic firing, the non-dimensionalized summing potassium current can be written in closed form.

$$\begin{aligned}\eta_{K_s}(t) &= \sum_{n=-\infty}^0 \frac{1}{\tau} e^{-(t-t_n)/\tau} \\ &= \left( \frac{1}{1 - e^{-T/\tau}} \right) \frac{1}{\tau} e^{-t/\tau}, \quad t \in [0, T]\end{aligned}\tag{2.2.1}$$

and the non-dimensionalized non-summing potassium current is

$$\eta_{K_{ns}}(t) = \frac{1}{\tau} e^{-t/\tau}, \quad t \in [0, T]. \quad (2.2.2)$$

Note that, during periodic firing,  $\eta_{K_s}(t)$  and  $\eta_{K_{ns}}(t)$  only differ by the scaling factor  $1/(1 - e^{-T/\tau})$  (compare Equation (2.2.1) to Equation (2.2.2)). Because  $(1 - e^{-T/\tau})$  is always less than 1, the summing current will contribute more hyperpolarizing current than the non-summing current, for a given fixed period  $T$ , but the form of the current will be the same.

Because of the similarity between the form of the summing potassium current,  $\eta_{K_s}$ , and the non-summing potassium current,  $\eta_{K_{ns}}$ , solutions will be given for the generic potassium current,  $\eta_K$ , but any differences between the summing and non-summing potassium currents will be noted explicitly.

The general solution for the non-dimensionalized LIF neurons with an explicit potassium current, (2.1.3), during  $T$ -periodic activity is <sup>1</sup>

$$v_{LC}(t) = I(1 - e^{-(t-t_n)}) - g_K A_K(\tau) (e^{-t/\tau} - e^{-t_n/\tau - (t-t_n)}) + \beta \delta(t - (t_n + T)), \quad t \in [t_n, t_{n+1} = t_n + T]. \quad (2.2.3)$$

where  $t_n$  is the time of the  $n^{th}$  spike. For the summing potassium current

$$A_K(\tau) = \frac{1}{\tau - 1},$$

---

<sup>1</sup>We note that this solution is valid for  $\tau \neq 1$ . This solution can easily be extended to  $\tau = 1$  because  $\tau = 1$  is removable singularity. However for simplicity, we omit the specific solution for  $\tau = 1$ .

and for the non-summing potassium current

$$A_K(\tau) = \left( \frac{1}{1 - e^{-T/\tau}} \right) \frac{1}{\tau - 1}. \quad (2.2.4)$$

Note that, for any given period  $T$ , the term  $g_K A_K(\tau)(e^{-t/\tau} - e^{-t})$  captures the effects of the potassium current on the periodic oscillations of the membrane potential  $v_{LC}(t)$ .

The period  $T$  can be found by solving  $v_{LC}(T^-) = v_{th} = 1$ , for  $T$ ,

$$1 = I(1 - e^{-T}) - g_K A_K(\tau)(e^{-T/\tau} - e^{-T}). \quad (2.2.5)$$

Although this equation cannot be solved for  $T$  explicitly, the period,  $T$ , can be found numerically.

Equation (2.2.5) can be rearranged to give  $I$  as a function of the firing frequency,  $f$  ( $= 1/T$ ), as well as the magnitude of the potassium current,  $g_K$ , and the deactivation rate of the potassium current,  $\tau$ , (i.e., the inverse  $f$ - $I$  curve).

$$I = \frac{1 + g_K A_K(\tau)(e^{-T/\tau} - e^{-T})}{(1 - e^{-T})}. \quad (2.2.6)$$

Note that when  $g_K = 0$ ,  $I$  is identical to that of the standard LIF model.

Figure 2.2.2 illustrates the relationship between the firing frequency,  $f$ , and the applied current,  $I$ . Note that,  $I = 1$  is the threshold current for the repetitive firing of action potentials in the standard LIF model as well as both modified models. In both the model with the summing potassium current and the

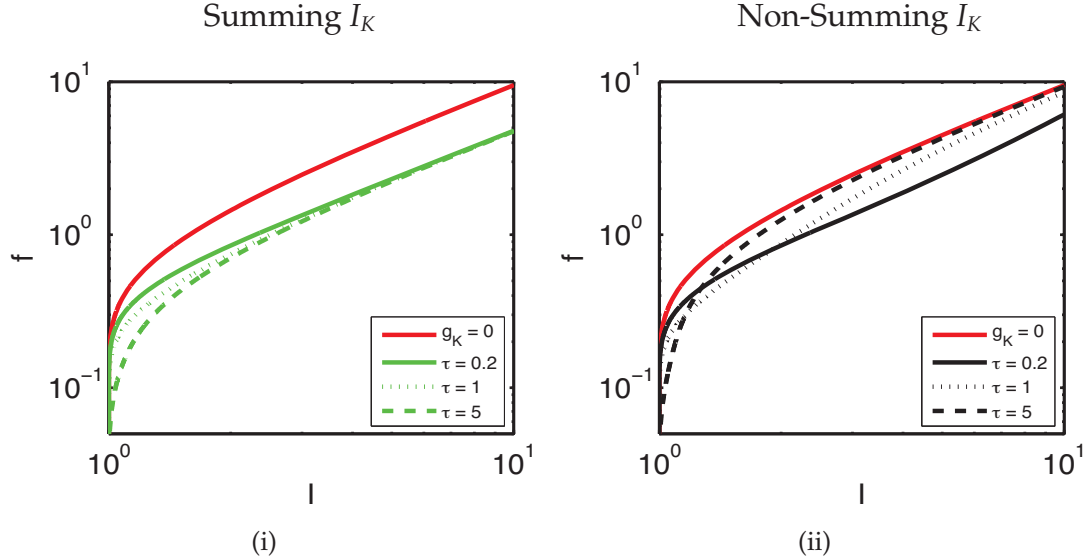
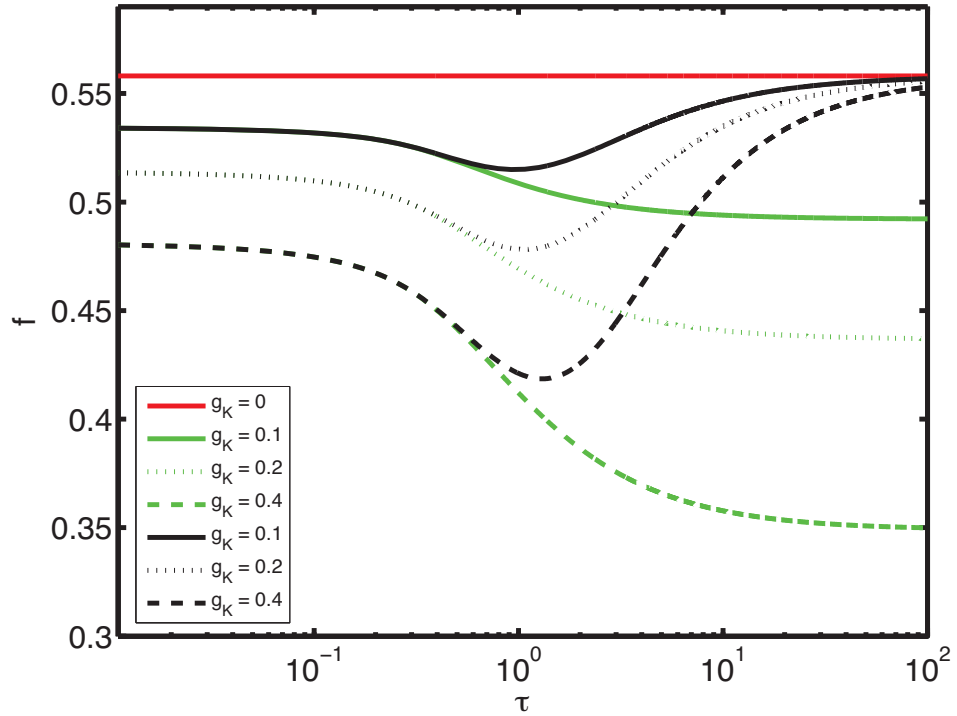


Figure 2.2.2: **The applied current,  $I$ , vs. the firing frequency,  $f$ .** The solid red line shows the frequency for the standard LIF neuron (no explicit potassium current, i.e.,  $g_K = 0$ ). Solid, dotted, and dashed green and black lines correspond to  $\tau = 0.2$ ,  $\tau = 1$ , and  $\tau = 5$ , respectively. For all plots,  $g_K = 1$ . As  $I$  increases,  $f$  increases. The addition of the explicit potassium current decreases the firing frequency compared to a standard LIF neuron.

model with the non-summing potassium current,  $f$  increases as  $I$  increases for all values of  $\tau$ . As  $I$  increases from  $I = 1$ , the  $f$ - $I$  curves for the various values of  $\tau$  rapidly diverge. As  $I$  continues to increase, the contribution of  $I$  begins to dominate over the contribution of the explicit potassium current, and the  $f$ - $I$  curves for all values of  $\tau$  for the models with the explicit potassium currents converge toward the  $f$ - $I$  curve for the standard LIF model. However, the small contribution of the explicit potassium current prevents the  $f$ - $I$  curves from becoming identical for the models with the explicit potassium currents and the standard LIF model.

Equation (2.2.5) also provides the complete relationship between the deac-



**Figure 2.2.3: Effects of the deactivation rate of the explicit potassium current on the firing frequency of an LIF cell.** The green lines correspond to the model with the summing potassium current, while the black lines correspond to the model with the non-summing potassium current. The solid red line indicates the frequency for the standard LIF cell (no explicit potassium current, i.e.,  $g_K = 0$ ). For both current types, solid, dotted, and dashed lines correspond to  $g_K = 0.1$ ,  $g_K = 0.2$ , and  $g_K = 0.4$ , respectively. For small  $\tau$ , the plots for the two types of explicit potassium currents are virtually identical. However, for large  $\tau$ , the summing potassium current caused the model to fire at a lower frequency compared to the non-summing potassium current. All plots were produced with  $I = 1.2$ . Similar patterns hold for all  $I > 1$  and  $g_K > 0$ .

tivation rate of the potassium current,  $\tau$ , and the firing frequency,  $f$ . Figure 2.2.3 plots the  $f$  versus  $\tau$  relationship for  $I = 1.2$  and  $g_k = 0.1, 0.2$ , and  $0.4$ , but similar relationships holds for all  $I > 1$  and  $g_k > 0$ . For the case with the summing potassium current, the firing frequency monotonically decreases with increasing  $\tau$ . On the other hand, the LIF model with the non-summing potassium current exhibits a non-monotonic relationship between frequency

and  $\tau$ . When  $\tau$  is sufficiently small, the behavior of the summing potassium current is indistinguishable from that of the non-summing potassium current. This is because both explicit potassium currents effectively fully decay before the neuron fires the subsequent action potential. Therefore, there is very little “leftover” current to significantly accumulate from the previous firing in the case with the summing current. However, for large  $\tau$ , a considerable amount of potassium current can accumulate in the summing potassium current model, which significantly decreases the firing frequency in comparison to the model with the non-summing potassium current.

For very large deactivation time constants,  $\tau \rightarrow \infty$ , the summing potassium current accumulates over many periods to become an approximately constant negative current of magnitude  $g_K/T$ . This accumulated current effectively decreases the applied current  $I$  to  $I - g_K/T$ , and thus decreases the firing frequency of the model with the summing potassium current versus the standard LIF model. Conversely, the magnitude of the non-summing potassium current decreases to 0 for very large deactivation constants due to the scaling term  $(1/\tau)$ . Thus, the non-summing explicit potassium current is not significantly present, and this model behaves similarly to the standard LIF model. Hence, for large  $\tau$ , the model with the summing potassium current has a lower firing frequency than that of the model with the non-summing potassium current.

Additionally, Figure 2.2.3 shows that as  $g_K$  increases, the firing frequency decreases for both the model with the summing and the non-summing potas-

sium currents. This is expected because  $g_K$  is a scaling factor of the potassium currents, and as  $g_K$  increases, the magnitude of the hyper-polarizing potassium current increases, which causes a decrease in the firing frequency in the LIF model.

### 2.3 Electrically Coupled Cell-Pair Model with an Explicit Potassium Current

To examine the effects of an explicit potassium current on the phase-locking behavior in a pair of electrically coupled LIF neurons, we add the non-dimensionalized spike-triggered potassium currents to the LIF cell-pair model given in the introduction, (1.2.4).

$$\begin{cases} \frac{dv_1}{dt} = -v_1 + I - g_K \eta_{K_1}(t) + g_c(v_2 - v_1) \\ \frac{dv_2}{dt} = -v_2 + I - g_K \eta_{K_2}(t) + g_c(v_1 - v_2) \end{cases}$$

where if  $v_i(t_*^-) = v_{th}$ , then

(i) the cell spikes and is reset,

$$v_i(t_*) = \beta \delta(t_*) \text{ and } v_i(t_*^+) = v_{reset}$$

(ii) the spike times are updated  $t_{0,i} = t_*, t_{n-1,i} = t_{n,i}$

(iii) the spike-triggered decaying potassium current is activated such that

$$\eta_{K_i}(t) = \begin{cases} \eta_{K_{s,i}}(t) = \sum_{n=-\infty}^0 \frac{1}{\tau} e^{-(t-t_{n,i})/\tau}, & \text{for } i = 1, 2. \\ \eta_{K_{ns,i}}(t) = \frac{1}{\tau} e^{-(t-t_{0,i})/\tau}, \end{cases} \quad (2.3.1)$$

As before,  $\beta$  scales the effect of the supra-threshold portion of the spike, and  $g_c$  is the dimensionless strength of the electrical coupling between the cells. The explicit potassium currents,  $g_K \eta_{K_i}(t)$  are defined as in Equation (2.2.1) for the summing potassium current and Equation (2.2.2) for the non-summing potassium current. The subindex  $i$  on  $\eta_{K_i}(t)$  simply denotes that it refers to the explicit potassium current of cell  $i$ .

### 2.3.1 Numerical Simulations of Electrically Coupled Cells

Studies have shown that electrically coupled cells can evolve to either stable synchrony or antisynchrony depending on the strength of the electrical coupling,  $g_c$ , the “size” of the spike,  $\beta$ , and the magnitude of the applied current,  $I$  [Chow and Kopell, 2000; Lewis and Rinzel, 2003]. Here, we investigate whether the addition of an explicit potassium current can also affect whether electrically coupled cells evolve to stable synchrony or antisynchrony.

Figure 2.3.1 shows that an explicit potassium current can influence whether the system evolves to synchrony or antisynchrony. This influence depends on the values of the parameters describing the potassium current,  $g_k$  and  $\tau$ . Consider the two LIF cell system with  $I = 1.6$ ,  $g_c = 0.2$ , and  $\beta = 0.2$ . Without a potassium current ( $g_K = 0$ ), the system evolves to stable synchrony (not shown). For the LIF model with the summing potassium current (Figure

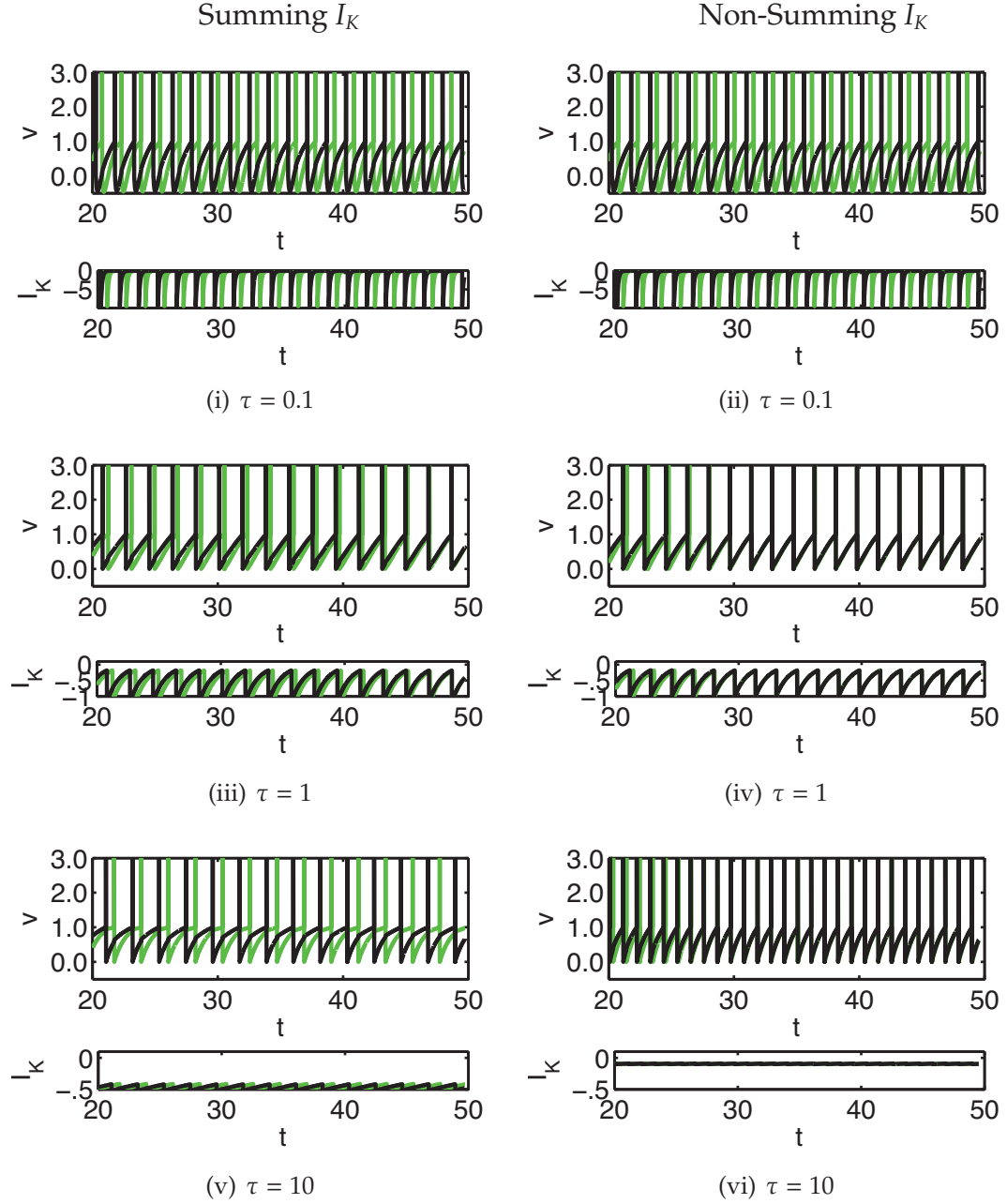


**Figure 2.3.1: Electrically coupled LIF neurons with the summing (left column) and the non-summing (right column) potassium currents.** The cells oscillate independently from initial conditions  $v_1 = 0.59$  (black) and  $v_2 = 0.0$  (green) until the coupling term was activated at  $t = 10$ . For the summing potassium current: the system evolves to antisynchrony for (i)  $\tau = 0.1$  and (v)  $\tau = 10$ , and evolves to synchrony (iii) for  $\tau = 1$ . For the non-summing potassium current: the system evolves to antisynchrony for (ii)  $\tau = 0.1$ , and to synchrony for (iv)  $\tau = 1$  and (vi)  $\tau = 10$ . For all subfigures,  $I = 1.6$ ,  $g_K = 1$ ,  $g_c = 0.2$ , and  $\beta = 0.2$ . Note: for  $g_K = 0$ , the system evolves to synchrony.

2.3.1, left column), the system displays stable antisynchronous activity when the potassium current's deactivation time constant is relatively short,  $\tau = 0.1$  (Figure 2.3.1(i)). When the deactivation time constant is increased to  $\tau = 1$ , the system evolves to stable synchronous activity (Figure 2.3.1(iii)). However, when the deactivation time constant is increased to  $\tau = 10$ , the system evolves to stable antisynchrony (Figure 2.3.1(v)). For the non-summing current (right column), the system evolves to stable antisynchrony when  $\tau = 0.1$  (Figure 2.3.1(ii)) and evolves to stable synchrony when  $\tau = 1$  or  $\tau = 10$  (Figures 2.3.1(iv) and 2.3.1(vi)).

## 2.4 Theory of Weakly Coupled Oscillators: Derivation of Phase Equation

To gain insight into how changes in the magnitude of the potassium current,  $g_K$ , and its deactivation time constant,  $\tau$ , affect the phase-locking dynamics of coupled LIF neurons, we use the theory of weakly coupled oscillators [Kuramoto, 1984]. We apply the steps outlined in Section 1.3 as detailed in Appendix A.1 to produce the infinitesimal phase resetting function (iPRC) and the corresponding cell-pair interaction function,  $G(\phi)$ .

The infinitesimal phase resetting curve for the LIF model with an explicit potassium current is

$$Z_K(t) = \begin{cases} \frac{e^t}{TB_K(\tau, I)} & \text{for } 0 < t < T \\ 0 & \text{for } t = 0, T \end{cases} \quad (2.4.1)$$

where  $B_K(\tau, I) = \left( I + g_K A_K(\tau) \left[ \frac{1}{\tau} e^{T(\tau-1)/\tau} - 1 \right] \right)$ , where  $A_K(\tau)$  is given in Equation (2.2.4) [See Appendix A.1 for derivation]. When  $g_K = 0$ ,  $Z_K(t)$  reduces to the iPRC for a standard LIF neuron. The term  $g_K A_K(\tau) \left( \frac{1}{\tau} e^{T(\tau-1)/\tau} - 1 \right)$  captures the effects of the potassium current on  $Z_K(t)$ . Because  $B_K(\tau, I) > I$ , the addition of the explicit potassium current always decreases the iPRC for any given period  $T$ , and thus decreases the sensitivity of the LIF neurons to perturbations, as shown in Figure 2.4.1.

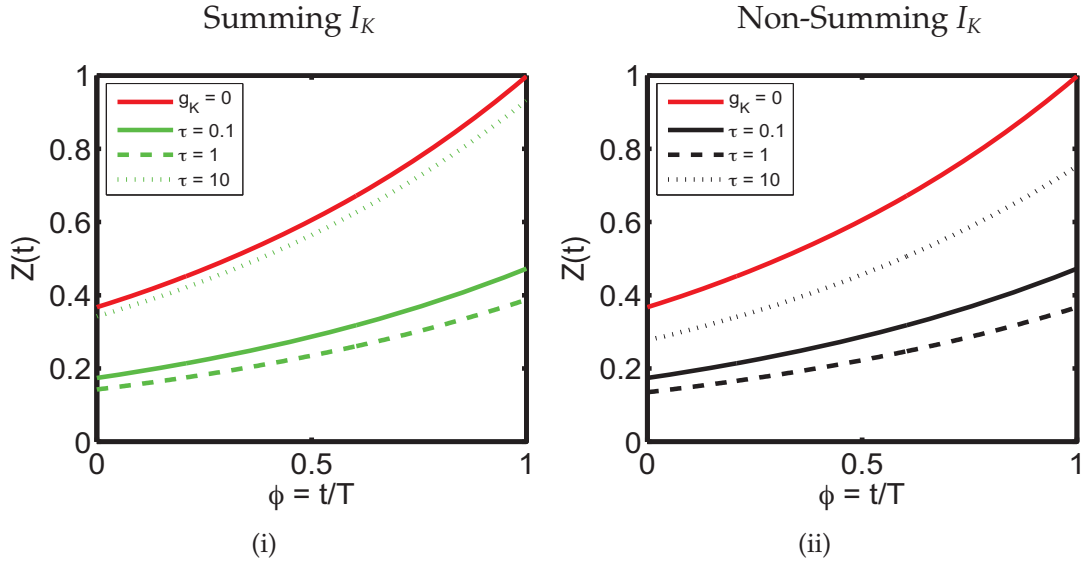


Figure 2.4.1: **The dependence of the iPRCs,  $Z_K(t)$ , on the explicit potassium currents.** All iPRCs have been normalized by fixed period  $T = 2.5$ . The green lines correspond to the model with the summing potassium current, and the black lines correspond to the model with the non-summing potassium current. For both,  $g_K = 1$ . The solid red line indicates the iPRC for the standard LIF cell (no explicit potassium current, i.e.,  $g_K = 0$ ). For both current types, solid, dashed, and dotted lines correspond to  $\tau = 0.1$ ,  $\tau = 1$ , and  $\tau = 10$ , respectively. For both the summing and non-summing potassium currents,  $Z_K(t)$  decreases as  $\tau$  is increased from  $\tau = 0.1$  to  $\tau = 1$  and increases when  $\tau$  is increased from  $\tau = 1$  to  $\tau = 10$  for all phases. All iPRCs were produced with  $T = 2.5$ .

Figure 2.4.1 also shows that for  $T = 2.5$  that  $Z_K(t)$  decreases as  $\tau$  is increased from  $\tau = 0.1$  to  $\tau = 1$ , but it increases as  $\tau$  is increased from  $\tau = 1$  to  $\tau = 10$  at all phases for both types of potassium currents.

By combining the expressions for the iPRC,  $Z_K(t)$ , and the electrical coupling current between two oscillating neurons,  $g_c(v_{LC}(t - \phi T) - v_{LC}(t + \phi T))$ , we obtain an equation for the evolution of the phase difference,  $\phi$ , between the electrically coupled LIF neurons with an explicit potassium current.

$$\frac{d\phi}{dt} = G(\phi)$$

where

$$G(\phi) = \frac{1}{T} \int_0^T Z_K(t) g_c [(v_{LC}(t - \phi T) - v_{LC}(t + \phi T))] dt$$

$$= \begin{cases} \frac{g_c}{TB_K(\tau, I)} [G_{SUB}(\phi) + G_K(\phi) + G_{SPIKE}(\phi)], & \text{for } 0 < \phi < 1, \\ 0, & \text{for } \phi = 0, 1. \end{cases} \quad (2.4.2)$$

and

$$G_{SUB}(\phi) = 2T \left( \frac{1}{1 - e^{-T}} \right) (\phi \sinh((1 - \phi)T) - (1 - \phi) \sinh(\phi T)) \quad \text{for } 0 \leq \phi \leq 1,$$

$$G_K(\phi) = g_K A_K(\tau) \left[ \left( \frac{\tau}{\tau - 1} \right) \left[ (1 - e^{-T/\tau}) (e^{\phi T} - e^{T(1-\phi)}) - (1 - e^T) (e^{-\phi T/\tau} - e^{-T(1-\phi)/\tau}) \right] \right. \\ \left. - 2T \left( \frac{1 - e^{-T/\tau}}{1 - e^{-T}} \right) [\phi \sinh((1 - \phi)T) - (1 - \phi) \sinh(\phi T)] \right] \quad \text{for } 0 \leq \phi \leq 1,$$

$$G_{SPIKE}(\phi) = \begin{cases} \beta [e^{\phi T} - e^{T(1-\phi)}] & \text{for } 0 < \phi < 1, \\ 0 & \text{for } \phi = 0, 1. \end{cases}$$

Note that, to focus on the effects of the frequency, we have used the  $f$ - $I$  rela-

tionship (Equation (2.2.6)) to write  $I$  in terms of  $T$ . This allows us to consider  $f$  as a parameter, instead of as a function of  $g_k$ ,  $\tau$ , and  $I$ .

As a reminder,  $G(\phi^*) = 0$  indicates that  $\phi^*$  is a phase-locked state. When  $G'(\phi^*) > 0$ , the phase-locked state is unstable, and when  $G'(\phi^*) < 0$ , the phase-locked state is stable. As with any symmetrically coupled pair of identical oscillating cells, the synchronous phase-locked state  $\phi^* = 0, 1$  and the antisynchronous phase-locked state  $\phi^* = 0.5$  always exist (i.e.,  $G(0) = G(1) = 0, G(0.5) = 0$ ). Because of the  $\delta$ -function spike and the monotonically increasing  $Z(t)$ , the synchronous state is always stable [Lewis and Skinner, 2011]. On the other hand, the antisynchronous state can be either stable or unstable depending on the parameters (i.e.,  $G'(0.5)$  can be either negative or positive). Note that, the strength of coupling,  $g_c$ , does not affect the existence or stability of the phase-locked states: it simply scales the  $G$ -function, and therefore, it only affects the speed with which the system approaches or departs from the phase-locked states.

#### 2.4.1 The Effects of $\tau$ and $g_k$ on $G(\phi)$

To better understand the influence of the potassium currents on the existence and stability of phase-locked states, we examine how changes in  $\tau$  and  $g_k$  affect the function  $G(\phi)$ .

Figure 2.4.2 shows the full  $G$ -functions for the summing (left column) and the non-summing (right column) potassium currents as  $\tau$  varies (top row) and

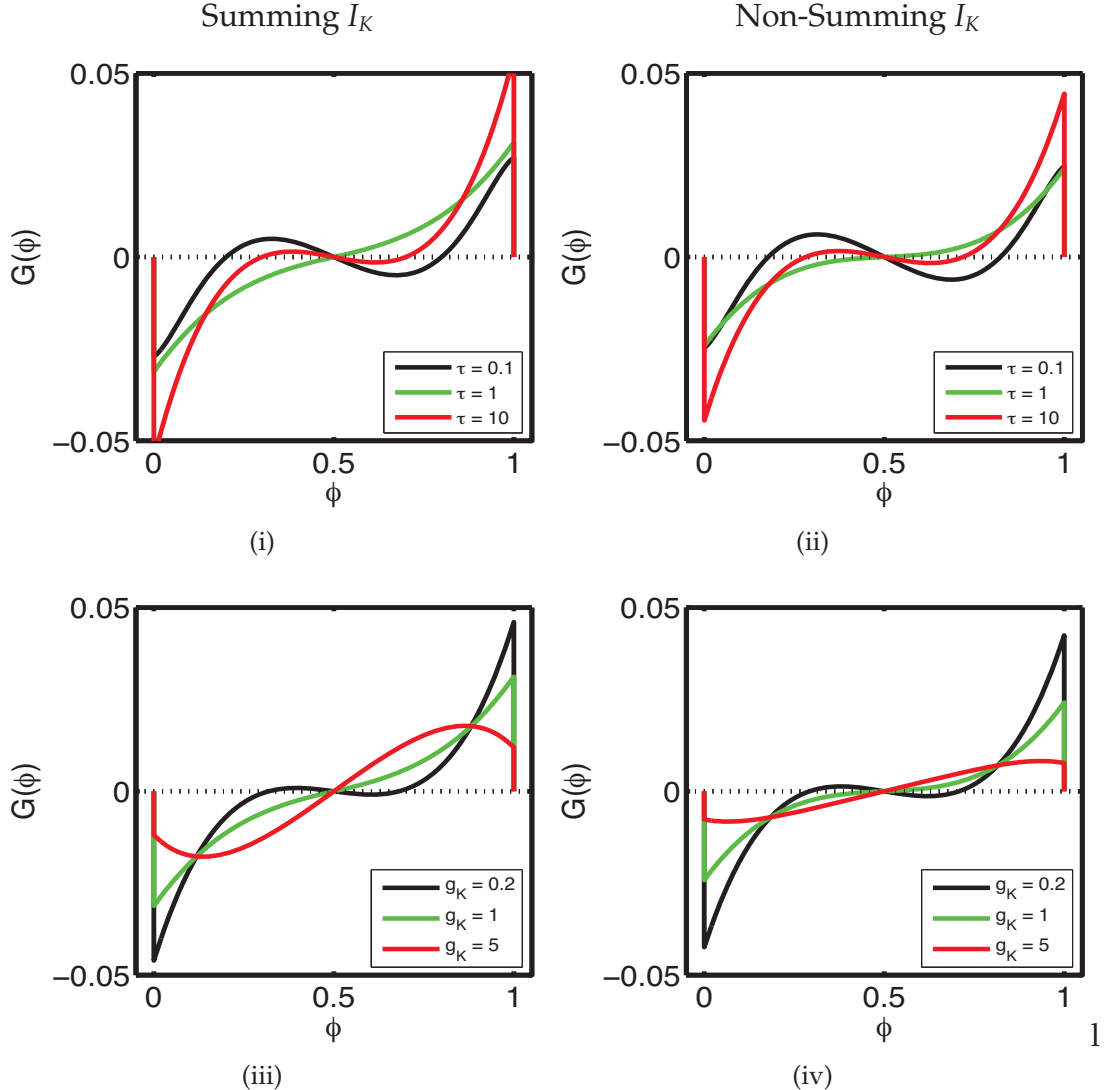


**Figure 2.4.2:  $G$ -functions for the summing (left) and the non-summing (right) potassium currents.** For all graphs,  $f = 0.55$  and  $\beta = 0.2$ . In (i – ii),  $g_K = 1$ , and the black, green, and red lines correspond to  $\tau = 0.1$ ,  $\tau = 1$  and  $\tau = 10$  respectively. In (iii – iv),  $\tau = 1$  and the black, green, and red lines correspond to  $g_K = 0.2$ ,  $g_K = 1$  and  $g_K = 5$  respectively. (i – ii)  $G$ -functions for the model with the summing potassium current and for the model with the non-summing potassium current indicate that the system is bistable for  $\tau = 0.1$ . When  $\tau = 1$ , the antisynchronous state destabilizes, leaving the synchronous state as the sole stable solution. For  $\tau = 10$ , both the synchronous and antisynchronous states are stable. (iii – iv)  $G$ -functions for the model with the summing potassium current and for the model with the non-summing potassium current indicate that the system is bistable for  $g_K = 0.2$ . When  $g_K = 1$  and  $g_K = 5$ , the antisynchronous state is unstable. These graphs show that changes in both  $\tau$  and  $g_K$  can affect the stability of phase-locked states.

as  $g_K$  varies (bottom row) for  $f = 0.55$  and  $\beta = 0.2$ . Plots of the  $G$ -function for the model with the summing potassium current and for the model non-summing potassium currents are qualitatively similar for changes of  $\tau$  and  $g_K$ . Figures 2.4.2(i) and 2.4.2(ii) show that the  $G$ -function indicates that both the synchronous and antisynchronous phase-locked states are stable for  $\tau = 0.1$  (black curve). When  $\tau$  is increased to  $\tau = 1$  (green curve), the antisynchronous state becomes unstable, while the synchronous state remains stable. A further increase in  $\tau$  to  $\tau = 10$  (red curve) restores the bistability of the synchronous and antisynchronous states. Figures 2.4.2(iii) and 2.4.2(iv) shows that the anti-synchronous and the synchronous phase-locked states are bistable for  $g_K = 0.2$  (black curve). For  $g_K = 1$  (green curve) and  $g_K = 5$  (red curve), the antisynchronous phase-locked state is unstable, while the synchronous phase-locked state is stable.

To more generally demonstrate the effects of the explicit potassium currents on the stability of phase-locked states over a wide range of frequencies, we plot the bifurcation diagrams for the phase difference  $\phi$  versus the firing frequency  $f$  for select values of  $\tau$  and  $g_K$  for the summing potassium current and the non-summing potassium current (Figure 2.4.3). Note that stable phase-locked states are indicated by solid lines, and unstable phase-locked states are indicated by dashed lines. The unstable curve defines the boundaries between the domain of attraction for the synchronous state and the antisynchronous state. For small  $f$ , the cell-pair system is bistable; however, the domain of attraction is

larger for the antisynchronous state,  $\phi = 0.5$ , than for the synchronous state,  $\phi = 0, 1$ , and thus the antisynchronous state dominates. As  $f$  increases, the domain of attraction for the antisynchronous steady state shrinks. With further increases in  $f$ , the synchronous state becomes dominant, and eventually a critical frequency  $f^*$  is reached, after which only the synchronous phase-locked state is stable. This critical frequency  $f^*$  occurs where the unstable steady state coalesces with the the antisynchronous state to form a subcritical pitchfork bifurcation.

We will use changes in the value of this critical frequency  $f^*$  as a convenient way to assess how the stability of the antisynchronous steady state depends on  $g_K$  and  $\tau$ . Figure 2.4.3 presents the bifurcation diagrams for several values of  $\tau$  and  $g_K$  for  $\beta = 0.2$ . In both the model with the summing potassium current (Figure 2.4.3(i)) and the model with the non-summing potassium current (Figure 2.4.3(ii)),  $f^*$  decreases as  $\tau$  is increased from  $\tau = 0.1$  (black curve) to  $\tau = 1$  (green curve). However,  $f^*$  increases as  $\tau$  is increased from  $\tau = 1$  to  $\tau = 10$  (red curve). In both models,  $f^*$  decreases as  $g_K$  is increased from  $g_K = 0.1$  to  $g_K = 1$  to  $g_K = 10$  (Figures 2.4.3(iii) and 2.4.3(iv)).

#### 2.4.2 The Effects of $g_k$ and $\tau$ on $f^*$

The relationship between the critical frequency,  $f^*$ , where the antisynchronous phase-locked state changes stability and the parameters  $g_k$  and  $\tau$  can be found by investigating  $G'(\phi)$  at  $\phi = 0.5$ . The critical frequency where the

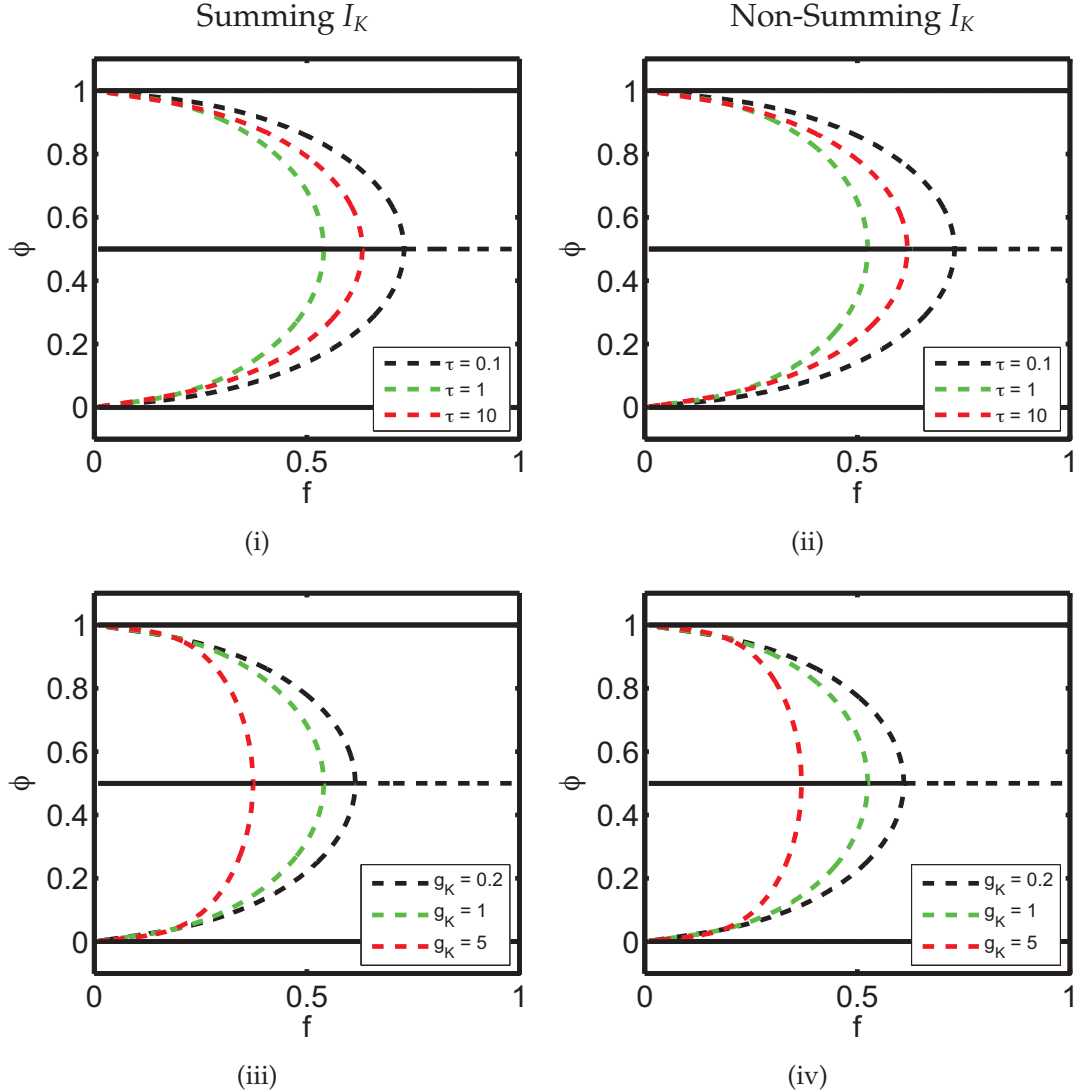


**Figure 2.4.3: Bifurcation diagrams for the models with the summing (left column) and the non-summing (right column) potassium currents.** In (i) and (ii),  $g_K = 1$  and black, green and red dashed lines correspond to  $\tau = 0.1$ ,  $\tau = 1$ , and  $\tau = 10$ , respectively. In (iii) and (iv),  $\tau = 1$  and black, green and red dashed lines correspond to  $g_K = 0.2$ ,  $g_K = 1$ , and  $g_K = 5$ , respectively. For all graphs,  $\beta = 0.2$ . Solid lines indicate stable state, while dashed lines indicate unstable states. We define  $f^*$  as the critical value of  $f$  where the subcritical pitchfork bifurcation originates. For  $f < f^*$ , both the antisynchronous and synchronous states are stable, while for  $f > f^*$  only the synchronous state is stable. (i), (ii) As  $\tau$  is increased from  $\tau = 0.1$  to  $\tau = 1$ ,  $f^*$  decreases. However, when  $\tau$  is increased from  $\tau = 1$  to  $\tau = 10$ ,  $f^*$  increases. (iii), (iv) As  $g_K$  increase,  $f^*$  decreases.

antisynchronous phase,  $\phi = 0.5$ , changes stability occurs were  $G'(\phi = 0.5) = 0$ .

For notational simplicity, we let  $T^* = 1/f^*$ , (i.e.,  $T^*$  is the critical period).

$$G'(\phi = 0.5) = \frac{2g_c}{B_K(\tau, I)} [G'_{SUB}(\phi = 0.5) + G'_K(\phi = 0.5) + G'_{SPIKE}(\phi = 0.5)] = 0. \quad (2.4.3)$$

where

$$G'_{SUB}(\phi = 0.5) = \left( \frac{1}{1 - e^{-T^*}} \right) (2 \sinh(0.5T^*) - T^* \cosh(0.5T^*)),$$

$$G'_K(\phi = 0.5) = g_K A_K(\tau) \left[ \left( \frac{\tau}{\tau - 1} \right) \left[ e^{0.5T^*} \left( 1 - e^{-T^*/\tau} \right) + \frac{1}{\tau} e^{-0.5T^*/\tau} (1 - e^{T^*}) \right] - \left( \frac{1 - e^{-T^*/\tau}}{1 - e^{-T^*}} \right) [2 \sinh(0.5T^*) - T^* \cosh(0.5T^*)] \right],$$

$$G'_{SPIKE}(\phi = 0.5) = \beta e^{0.5T^*}.$$

Equation (2.4.3) can be solved numerically for  $f^*$  as a function of  $\tau$ ,  $g_K$ , and  $\beta$ .

Figure 2.4.4 shows how the critical frequency  $f^*$  changes as  $\tau$  increases for several values of  $g_K$ . The dependence of  $f^*$  on  $\tau$  is similar for both the model with the summing potassium current and the model with the non-summing potassium current. The region above each curve corresponds to parameter sets for which only the synchronous state is stable, while the region below each curve corresponds to parameters sets for which both the synchronous and antisynchronous states are stable. For both models, as  $\tau$  increases, the

critical frequency  $f^*$  decreases to a minimum value  $f_{min}^*$  at  $\tau = \tau_{min}$  and then it increases, asymptotically approaching the critical frequency of a pair of electrically coupled LIF neurons without an explicit potassium current,  $f = f_{LIF}^*$  (red curve).

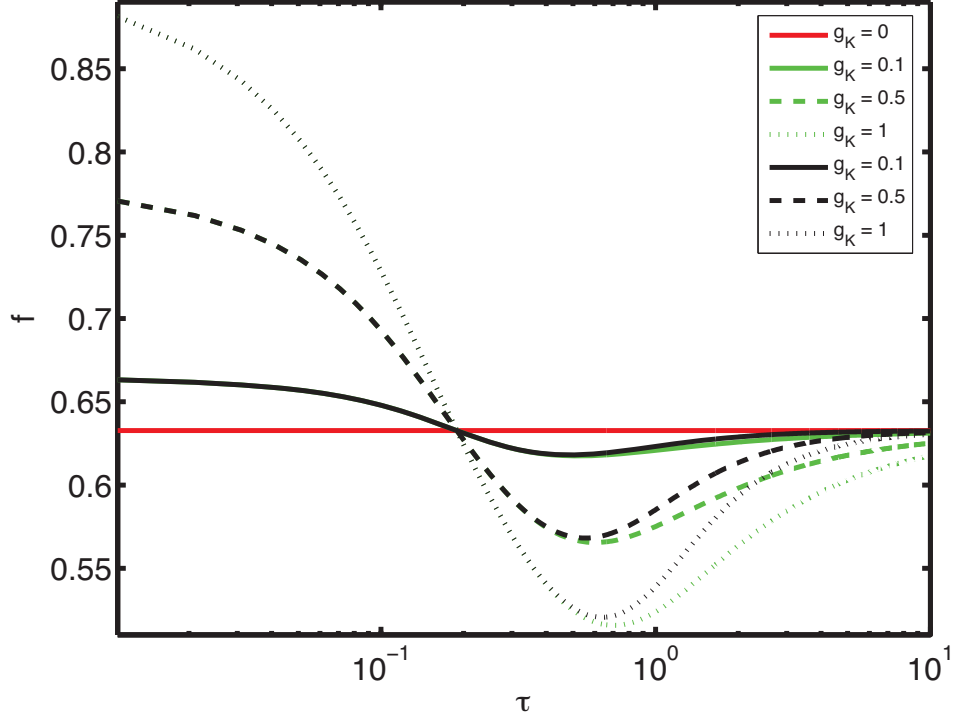


Figure 2.4.4:  $f^*$  as a function of  $\tau$  for several values of  $g_K$ . Green lines are for the model with the summing potassium current and black lines are for the model with the non-summing potassium current. Solid, dashed, and dotted lines correspond to  $g_K = 0.1$ ,  $g_K = 0.5$ , and  $g_K = 1$ , respectively. For all curves,  $\beta = 0.2$ . The solid red line is the critical frequency  $f_{LIF}^*$  for a standard LIF neuron (i.e.,  $g_K = 0$ ). All curves intersect at a specific potassium current deactivation time constant  $\tau = \tau_{int}$  regardless of  $g_K$ . Note that, for  $\tau < \tau_{int}$ , increasing  $g_K$  promotes the stability of antisynchrony. For  $\tau > \tau_{int}$ , increasing  $g_K$  hinders the stability of antisynchrony.

In Figure 2.4.4, all curves intersect at a specific potassium current deactivation time constant  $\tau = \tau_{int}$  regardless of the value of  $g_K$ . At  $\tau_{int}$ , the critical frequency,  $f^*$  is the same for all models, regardless of whether an explicit

potassium current is added to the standard LIF model, and regardless of which explicit potassium current is added to the standard LIF model. Note that, for  $\tau < \tau_{int}$ , increasing  $g_K$  increases the region in the  $f$  parameter space where antisynchrony is stable. Conversely, for  $\tau > \tau_{int}$ , increasing  $g_K$  decreases the region in the  $f$  parameter space where antisynchrony is stable.

Figure 2.4.4 shows how increasing  $\tau$  affects the stability of the electrically coupled LIF system at a given frequency. If  $f < f_{min}^*$ , antisynchrony and synchrony are bistable regardless of the value of  $\tau$ . If  $f_{min}^* < f < f_{LIF}^*$ , the antisynchrony and synchrony are bistable for small  $\tau$ . As  $\tau$  is increased, the system transitions to synchrony being the sole stable state. Further increases to  $\tau$  restore the bistability of the electrically coupled system. If  $f > f_{LIF}^*$  but less than the critical frequency when  $\tau \rightarrow 0$ ,  $f_{\tau \rightarrow 0}^*$ , antisynchrony and synchrony are bistable. As  $\tau$  is increased, the electrically coupled transitions to having synchrony as its sole stable phase-locked state. If  $f > f_{\tau \rightarrow 0}^*$ , the antisynchronous state is unstable, and the system always evolves to synchrony. The pattern of  $f^*$  versus  $\tau$  observed in the  $G$ -functions, Figure 2.4.2, corresponds to the choice of  $f_{min}^* < f < f_{LIF}^*$ .

In the next subsection, we use the decomposition of the  $G$ -function (see Equation (2.4.2)) to further understand the effects of the explicit potassium currents on the stability of the antisynchronous state, specifically by investigating the interplay between  $\tau$  and  $g_K$ .

## 2.5 Insight from the Decomposition of $G(\phi)$

The  $G$ -function is a scaled linear combination of three terms,  $G_{SUB}(\phi)$ ,  $G_K(\phi)$ , and  $G_{SPIKE}(\phi)$  (see Equation (2.4.2)). This description of  $G(\phi)$  allows us to gain insight into the mechanisms that determine the stability of phase-locked states. For any given frequency,  $f$ ,  $G_{SUB}(\phi)$  captures the portion of the  $G$ -function that depends on the sub-threshold dynamics of the LIF neuron without the non-potassium current,  $G_{SPIKE}(\phi)$  only contains the effects of the supra-threshold portion of the spike, and  $G_K(\phi)$  captures all of the direct effects of the explicit potassium current on the existence and stability of phase-locked states. Therefore, we can systematically assess the relative contribution of each portion of the  $G$ -function to gain further insight into the stability of the antisynchrony phase-locked state.

### 2.5.1 $G_{SS}(\phi)$

$G_{SUB}(\phi)$  and  $G_{SPIKE}(\phi)$  are similar to those given in Lewis and Rinzel (2003) (see Section 1.4). Lewis and Rinzel showed that the sub-threshold dynamics of the standard LIF model, as described by  $G_{SUB}(\phi)$ , always acts to stabilize the antisynchronous state ( $\phi = 0.5$ ) and acts to destabilize the synchronous state ( $\phi = 0, 1$ ), whereas the supra-threshold portion of the spike, as described by  $G_{SPIKE}(\phi)$ , always acts to destabilize the antisynchronous state and stabilize the synchronous state. Furthermore, they determined how the stability of the antisynchronous phase-locked state for the LIF cell pair without the explicit

potassium current  $G_{SS}(\phi) = G_{SUB}(\phi) + G_{SPIKE}(\phi)$ , depends on the frequency,  $f$  (see Figure 1.4.3). At low frequencies,  $G_{SUB}(\phi)$  dominates  $G_{SS}(\phi)$  and the antisynchronous state is robustly stable. As the frequency is increased, the relative contribution of  $G_{SUB}(\phi)$  compared to  $G_{SPIKE}(\phi)$  in  $G_{SS}(\phi)$  diminishes and the antisynchronous state becomes less robust until it loses stability altogether. We define the critical frequency  $f_{SS}^*$  as the frequency where the antisynchronous phase-locked state transitions from stable to unstable, i.e., the frequency at which  $G'_{SS}(0.5) = 0$ . This critical frequency  $f_{SS}^*$  depends on  $\beta$  through  $G_{SPIKE}(\phi)$ . As  $\beta$  is increased, the relative strength of  $G_{SPIKE}(\phi)$  increases,  $f_{SS}^*$  decreases, and antisynchrony is suppressed.

As  $G_{SS}(\phi)$  is well understood, we rewrite  $G(\phi)$  in Equation (2.4.2) as

$$G(\phi) = (g_c/TB_K(\tau, I))(G_{SS}(\phi) + g_K G_K(\phi)).$$

This will facilitate a discussion of how the explicit potassium combines with the sub-threshold dynamics and the supra-threshold portion of the spike to affect the overall stability of the antisynchronous phase-locked state.

### 2.5.2 $G_K(\phi)$

To assess how changes to  $\tau$  or  $g_K$  affect the stability of the antisynchronous state, we examine the zeros of  $G_K(\phi)$ . Note that  $g_K$  scales  $G_K(\phi)$  and does not affect the location of the zeros of  $G_K(\phi)$ . Figure 2.5.1 plots the zeros of  $G_K(\phi)$  as a function of  $f$  for several values of  $\tau$ . The dashed lines indicate the unstable

zeros, while solid lines indicate the stable zeros of  $G(\phi)$ . We note that the branches of the zeros of  $G_K(\phi)$  have the same shape as the bifurcation diagram for  $G_{SS}(\phi)$  (see Figure 1.4.3). We define the critical frequency  $f_K^*$  of  $G_K(\phi)$  analogously to  $f_{SS}^*$ . That is,  $f_K^*$  is the critical frequency at which  $G'_K(0.5) = 0$ . This defines where the explicit potassium current transitions from promoting to hindering antisynchrony. For both the model with the summing potassium current and the model with the non-summing potassium current, the critical frequency  $f_K^*$  decreases as  $\tau$  increases.

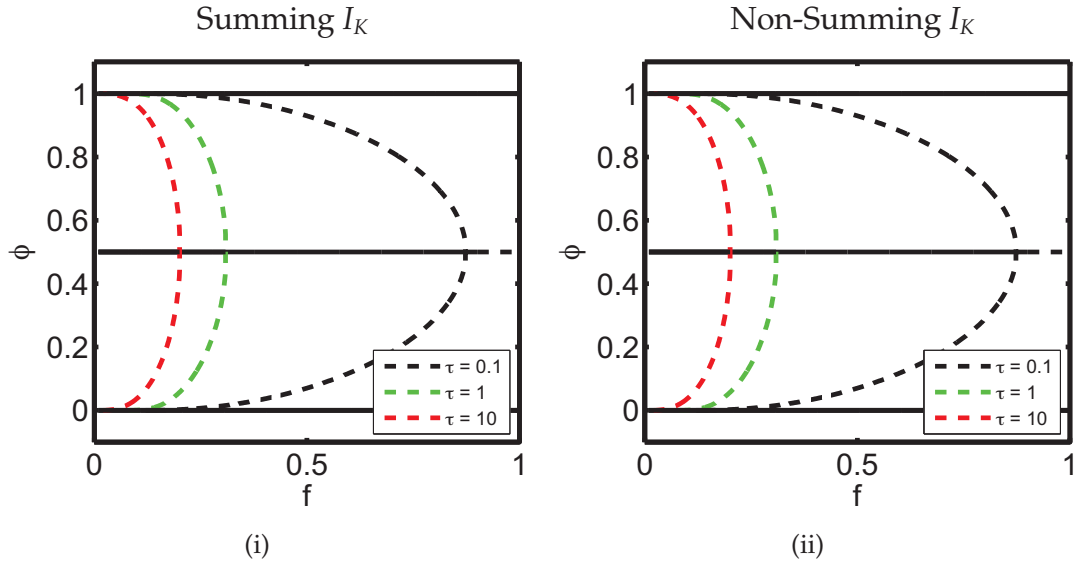


Figure 2.5.1: **Zeros of  $G_K(\phi)$  for the (i) summing and the (ii) non-summing potassium currents.** Black, green, and red dotted lines indicate the unstable zeros for  $\tau = .1$ ,  $\tau = 1$ , and  $\tau = 10$ , respectively. Solid black lines indicate stable zeros. In both graphs, the region where  $G_K(\phi)$  promotes the stability of the antisynchronous state decreases as  $\tau$  increases.

To more generally demonstrate the relationship between the critical frequency  $f_K^*$  and  $\tau$ , we examine  $G'_K(\phi) = 0$  at  $\phi = 0.5$  (see Equation (2.4.3)). Note that the zeros of  $G'_K(\phi = 0.5)$  do not depend on  $g_K$ , as  $g_K$  simply scales  $G'_K(\phi)$ .

Similarly, because  $A_K(\tau)$  scales  $G'_K(\phi)$ , the solutions of  $G'_K(\phi = 0.5) = 0$  do not depend on whether the summing or non-summing potassium current is added to the LIF model. That is, the solutions of  $G'_K(\phi = 0.5) = 0$  are identical for both the model with the summing potassium current and the non-summing potassium currents. Figure 2.5.2 plots the solutions of  $G'_K(\phi = 0.5) = 0$  and shows that  $f_K^*$  decreases as  $\tau$  increases. This implies that the region where  $G_K(\phi)$  promotes antisynchrony always decreases as  $\tau$  increases. That is, the explicit potassium currents promote antisynchrony for a larger range of frequencies at low potassium deactivation time constants than at large ones.

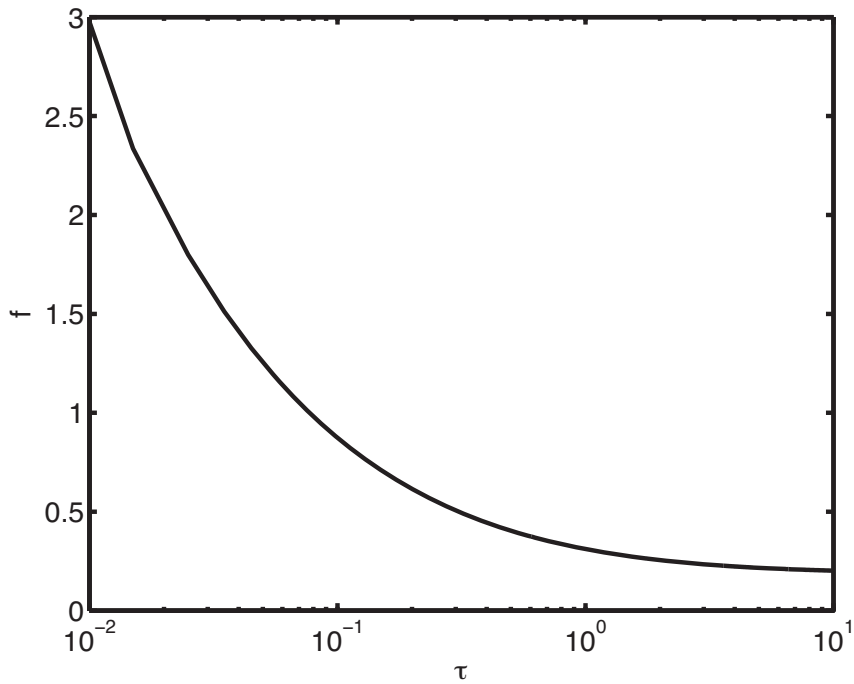


Figure 2.5.2: **Dependence of the critical frequency  $f_K^*$  on  $\tau$ , i.e.,  $G'_K(\phi = 0.5) = 0$ .** In the region below the curve,  $G_K(\phi)$  promotes antisynchrony, while in the region above the curve,  $G_K(\phi)$  suppresses antisynchrony. Note that this curve is identical for the LIF model with either the summing potassium current or the non-summing potassium current.

### 2.5.3 Interaction of $G_{SS}(\phi)$ and $G_K(\phi)$

The zeros of  $G(\phi)$  are determined by interaction between  $G_K(\phi)$  and  $G_{SS}(\phi)$ .  $G(\phi)$  is the scaled sum of  $G_K(\phi)$  and  $G_{SS}(\phi)$ . However, the scaling term  $g_c/(TB_K(\tau, I))$  does not affect the location of the zeros of  $G(\phi)$  or the value of  $f^*$ . Thus, the parameters for which the potassium current supports stable antisynchrony for any given frequency depends only on the relative weights of  $G_K(\phi)$  and  $G_{SS}(\phi)$ , or more specifically the locations of  $f_K^*$  and  $f_{SS}^*$ .

Figure 2.5.3 shows the zeros for  $G_K(\phi)$  and  $G_{SS}(\phi)$  for  $g_K = 1$  and  $\beta = 0.2$  and replots the bifurcation diagram for  $G(\phi)$  (see Figure 2.4.3). Figures 2.5.3(i) and 2.5.3(ii) show that  $f_{SS}^* < f^* < f_K^*$  for  $\tau = 0.1$ . This implies that the addition of the potassium current to the LIF model acts to stabilize the antisynchronous phase-locked state. Figures 2.5.3(iii) and 2.5.3(iv) for  $\tau = 1.5$  show that  $f_K^* < f^* < f_{SS}^*$ . This implies that the addition of the potassium current to the LIF model acts to destabilize the antisynchronous phase-locked state.

Examining  $G'(\phi) = 0$  at  $\phi = 0.5$  shows how the relative weights of  $G_K(\phi)$  and  $G_{SS}(\phi)$  affect the frequencies at which antisynchrony changes stability (Equation (2.4.3)). Note that  $f^*$  is found by considering

$$G'(\phi = 0.5) = \frac{2g_c}{B_K(\tau, I)} [G'_{SS}(\phi = 0.5) + G'_K(\phi = 0.5)] = 0, \quad (2.5.1)$$

which implies that

$$-G'_{SS}(\phi = 0.5) = G'_K(\phi = 0.5). \quad (2.5.2)$$

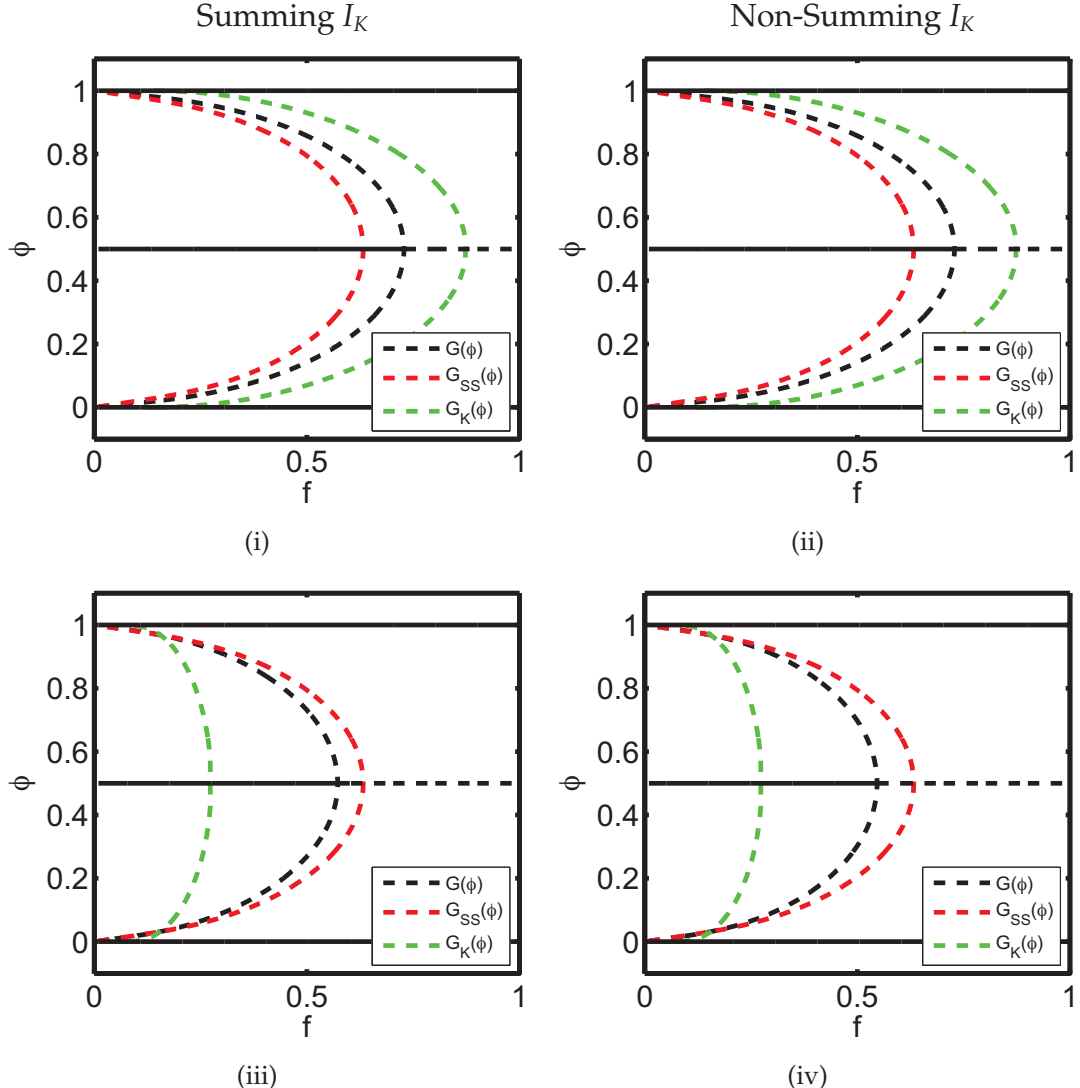


Figure 2.5.3: **Bifurcation diagram for  $G(\phi)$  (black) for the LIF model with the summing (left) and the non-summing (right) potassium currents.** Additionally, the zeros of  $G_K(\phi)$  (green) and  $G_{SS}(\phi)$  (red) are plotted. For all subfigures,  $g_K = 1$ ,  $\beta = .2$ . (i), (ii) When  $\tau = .1$ ,  $f_{SS}^* < f^* < f_K^*$  and implies that the addition of the potassium current to the LIF model promotes the stability of the antisynchronous phase-locked state. (iii), (iv) When  $\tau = 1.5$ ,  $f_K^* < f^* < f_{SS}^*$  and implies that the addition of the potassium current to the LIF model inhibits the stability of the antisynchronous phase-locked state.

Therefore, the critical frequency  $f^*$  is the  $f$ -value of the intersection of  $-G'_{SS}(\phi = 0.5)$  with  $G'_K(\phi = 0.5)$ .

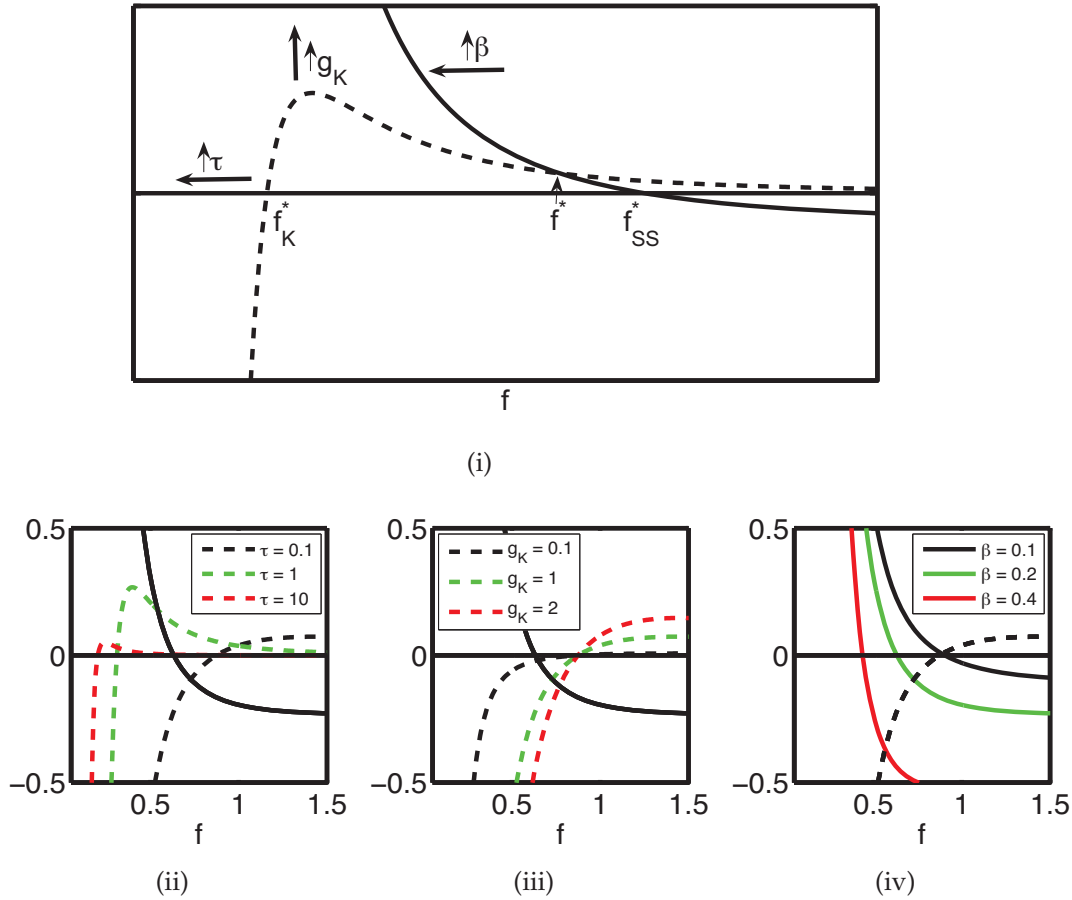


Figure 2.5.4: **Effects of the relative weighting of  $G_{SS}(\phi)$  and  $G_K(\phi)$  on  $f^*$ .** Solid and dotted lines indicate  $-G'_{SS}(\phi = 0.5)$  and  $G'_K(\phi = 0.5)$ , respectively. The zero of  $-G'_{SS}(\phi = 0.5)$  is  $f_{SS}^*$  and the zero of  $G'_K(\phi = 0.5)$  is  $f_K^*$ . The intersection of  $-G'_{SS}(\phi = 0.5)$  and  $G'_K(\phi = 0.5)$  is  $f^*$ . (i) Schematic view. As  $\tau$  increases,  $f_K^*$  decreases. As  $g_K$  increases,  $f_K^*$  remains stationary, but  $G'_K(\phi)$  becomes steeper, and “pulls”  $f^*$  toward  $f_K^*$ . As  $\beta$  is increased,  $f_{SS}^*$  decreases. (ii) Effects of  $\tau$  on  $f^*$  with  $g_K = 1$  and  $\beta = .2$ . Black, green, and red dashed lines correspond to  $\tau = 0.1$ ,  $\tau = 1$ , and  $\tau = 10$ , respectively.  $f_K^*$  decreases as  $\tau$  is increased. However,  $f^*$  displays non-monotonic changes in response to changes in  $\tau$ . (iii) Effects of  $g_K$  on  $f^*$  with  $\tau = .1$  and  $\beta = .2$ . Black, green, and red dashed lines correspond to  $g_K = 0.1$ ,  $g_K = 1$ , and  $g_K = 2$ , respectively.  $f^*$  increases as  $g_K$  increases. (iv) Effects of  $\beta$  on  $f^*$  with  $\tau = 0.1$  and  $g_K = 1$ . Black, green, and red solid lines correspond to  $\beta = .1$ ,  $\beta = .2$ , and  $\beta = .4$ , respectively. Plots are only shown for the model with the summing potassium current, but the non-summing potassium current produce qualitatively similar results.

Figure 2.5.4 plots  $-G'_{SS}(\phi = 0.5)$  and  $G'_K(\phi = 0.5)$  and examines the effects of  $\tau$ ,  $g_K$  and  $\beta$  on the critical frequency,  $f^*$ . Figure 2.5.4(i) is a schematic plot of  $-G'_{SS}(\phi = 0.5)$  and  $G'_K(\phi = 0.5)$ .  $f_{SS}^*$  and  $f_K^*$  correspond to the zeros of  $G'_{SS}(\phi = 0.5)$  and  $G'_K(\phi = 0.5)$ , respectively. The intersection of  $-G'_{SS}(\phi = 0.5)$  and  $G'_K(\phi = 0.5)$  correspond to the critical frequency  $f^*$  of where antisynchrony changes stability, i.e.,  $G(\phi = 0.5)$ . As the schematic indicates,  $f_K^*$  decreases as  $\tau$  increases. When  $g_K$  is increased,  $f_K^*$  remains stationary, and the graph of  $G'_K(\phi = 0.5)$  dilates larger. When  $\beta$  is increased,  $f_{SS}^*$  decreases and the value of  $f^*$  decreases.

Figures 2.5.4(ii), 2.5.4(iii), and 2.5.4(iv) illustrate how increases of  $\tau$ ,  $g_K$  and  $\beta$  affect the location of  $f^*$ . In Figure 2.5.4(ii), when  $\tau = .1$ ,  $f_{SS}^* < f^* < f_K^*$ , which implies that the addition of the potassium current is increasing the frequency range where antisynchrony is stable. As  $\tau$  is increased to  $\tau = 1$ ,  $f_K^*$  decreases,  $f_K^* < f^*$ , and thus  $f^*$  decreases. As  $\tau$  is increased to  $\tau = 10$ , while  $f_K^*$  decreases further,  $f^*$  increases because of the decrease in magnitude of  $G_K(\phi)$ . For both  $\tau = 1$  and  $\tau = 10$ , the addition of the potassium current decreases the frequency range where antisynchrony is stable.

Figure 2.5.4(iii) shows that as  $g_K$  is increased,  $f^*$  approaches  $f_K^*$ . Figure 2.5.4(iv) shows that, as  $\beta$  is increased,  $f_{SS}^*$  decreases and causes a decrease in  $f^*$ . Lastly, we note that when  $f_K^* = f_{SS}^* = f^*$  (i.e.,  $G'_K(\phi = 0.5) = G'_{SS}(\phi = 0.5) = G'(\phi = 0.5) = 0$ ) that the location of  $f^*$  is independent of  $g_K$ . This value of  $f^*$  corresponds to  $\tau_{int}$ , the intersection point of all plots in Figure 2.4.4.

## 2.6 Conclusion and Discussion

In this chapter, we analyzed how the addition of spike-triggered summing and non-summing potassium currents to two identical, electrically coupled LIF model neurons affects the existence and stability of phase-locked states. Numerical simulations indicated that the addition of a spike-triggered potassium current influences whether a system of electrically coupled LIF model neurons evolve to stable synchrony or antisynchrony. The theory of weakly coupled oscillators helped to generalize the results of the numerical simulations and provided further insight into how changes to the deactivation time constant,  $\tau$ , and the magnitude of the current,  $g_K$ , affect whether the addition of the spike-triggered potassium current promoted or suppressed the antisynchronous phase-locked state. The decomposition of the  $G$ -function into the sub-threshold and spike portion,  $G_{SS}(\phi)$ , and the potassium portion,  $G_K(\phi)$ , allowed for additional insight into how and under what conditions increasing  $\tau$  promoted the stability of the antisynchronous state. These results are summarized in Table 2.6.1.

We found that either increasing the intrinsic firing frequency by increasing the applied current,  $I$ , or increasing the magnitude of the spike effect,  $\beta$ , promoted synchrony. The effect on synchronization of increasing the magnitude of the potassium current,  $g_K$ , or increasing the size of the deactivation time constant,  $\tau$ , is less clear. The decomposition of the  $G$ -function into the sub-threshold and spike portion,  $G_{SS}(\phi)$ , and the potassium portion,  $G_K(\phi)$ ,

Parameter variation	Effect
Increasing Intrinsic Frequency ( $\uparrow I$ )	Promotes synchrony
Increasing Spike Effect ( $\uparrow \beta$ )	Promotes synchrony
Increasing the Magnitude of the Potassium Current ( $\uparrow g_K$ )	Promotes Antisynchrony if $f_K^* > f_{SS}^*$ Suppresses Antisynchrony if $f_K^* < f_{SS}^*$ .
Increasing the Deactivation Time Constant ( $\uparrow \tau$ )	Can Promote or Suppress Antisynchrony

Table 2.6.1: **Summary of Results**

allowed us to find conditions where antisynchrony is promoted or suppressed as  $g_K$  is increased. If the critical frequency of the sub-threshold and spike portion of the  $G$ -function,  $f_{SS}^*$ , is less than the critical frequency of the potassium portion of the  $G$ -function,  $f_K^*$ , i.e.  $f_{SS}^* < f_K^*$ , then increasing the magnitude of the potassium current promotes antisynchrony. Conversely, if  $f_{SS}^* > f_K^*$ , then increasing the magnitude of the potassium current suppresses antisynchrony. We refer the reader to Section 2.5.3 for a more thorough analysis of how varying  $g_K$  affects synchronization. Despite the insight gained by the decomposition of the  $G$ -function, we are unable to succinctly describe the region where antisynchrony is promoted or suppressed when  $\tau$  is increased. Figure 2.4.4 and its related text in Section 2.4.2 best explained how varying  $\tau$  can influence the region where stable antisynchrony exists.

Further decomposition of the  $G$ -function could provide insight into the individual influence and the relative importance of the phase resetting curve,

$Z(t)$ , and the voltage trace,  $v_{LC}(t)$ , on the existence and stability of the antisynchronous phase-locked state. We leave this analysis for future work.

### 2.6.1 Effects of the Summing versus the Non-Summing Potassium Current

In this chapter, we investigated how the phase-locking behavior of a pair of electrically coupled LIF neurons is affected by the addition of a “non-summing” potassium current and a “summing” potassium current to each model neuron. Recall that our model of the non-summing potassium current corresponds to a current that achieves its maximal conductance (i.e., saturates) whenever an action potential arises. Our model of the summing potassium current corresponds to a current that is far from saturation and allows for repeated activation that sums linearly.

We largely treated the summing and non-summing currents identically in our analysis as the LIF models with these two currents differ by a factor of  $1/(1 - e^{-T/\tau})$  in the potassium current specific term,  $A_K(\tau)$ . Because this factor  $1/(1 - e^{-T/\tau})$  is always greater than 1, the summing potassium current has a greater effect on frequency than the non-summing potassium current on the dynamics of the LIF model, an effect that becomes more pronounced at higher frequencies and for larger  $\tau$ ’s. For small values of  $\tau$ , the effects of the addition of the two currents to the LIF model on the firing frequency are virtually identical, while for larger values of  $\tau$ , the firing frequency of the LIF neuron with the non-summing potassium current is higher than that of the LIF neuron

with the summing potassium current (as seen in Figure 2.2.3).

By analyzing the phase-locking dynamics with respect to frequency, we separated the direct effects of the addition of a spike triggered potassium current from the indirect effects caused by changes in frequency. This allowed us to investigate the frequency-independent differences between the summing and non-summing potassium currents. The form of the  $G$ -function allowed us to identify the differences between the effects of the summing and non-summing potassium currents by considering two terms:  $g_c/(TB_K(\tau, I))$ , which scales the overall  $G$ -function, and  $g_K A_K(\tau)$ , which scales the portion of the  $G$ -function,  $G_K(\phi)$ . Because the scaling factor of the  $G$ -function,  $g_c/(TB_K(\tau, I))$ , is always positive, it does not affect the existence or stability of phase-locked states; only the speed with which the system approaches or departs from the phase-locked states. The scaling factor of  $G_K(\phi)$ ,  $g_K A_K(\tau)$ , affects the relative importance of the spike-triggered potassium current on the existence and stability of the phase-locked states of  $G(\phi)$ . Because the potassium specific term,  $A_K(\tau)$  for the summing potassium current is always greater than  $A_K(\tau)$  for the non-summing potassium current, the influence of the summing potassium current on the  $G$ -function is greater than that of the non-summing potassium current. For small values of  $\tau$ , the effects of the two potassium currents on the critical frequency,  $f^*$ , are virtually identical. However, for larger values of  $\tau$ ,  $f^*$  for the non-summing potassium current is greater than  $f^*$  for the summing potassium current, which indicates that the non-summing potassium current more

strongly promotes the stability of the antisynchronous phase-locked state than the summing potassium current.

### 2.6.2 Comparison to Previous Results of Pfeuty et al. and Mancilla et al.

To facilitate a comparison to the work of Pfeuty et al. (2003) and Mancilla et al. (2007), we can translate the non-dimensional parameters of our model into dimensional form. Using the values reported in Mancilla et al. (2007) of  $C_m \approx 40pF$  and  $g_L \approx 10nS$ , we find that the membrane time constant is  $\tau = 4ms$ , which implies that the actual frequency,  $f$ , corresponds to  $250\bar{f} \text{ Hz}$ , where  $\bar{f}$  is the non-dimensional frequency. The non-dimensional deactivation time constants  $\bar{\tau} = 0.1, 1.0$ , and  $10$ , correspond to the deactivation time constants of  $\tau = 0.4, 4.0$ , and  $40msecs$ , values which are representative of the reported deactivation rates for potassium channels in the Kv1 and Kv3 families [Coetzee et al., 1999]. The investigated non-dimensional  $\bar{f}$  frequency range of 0 to 1 corresponds to an actual frequency range of 0 to 250 Hz, a range that encompasses those investigated by Mancilla et al. (2007) and Pfeuty et al. (2003).

Our results unify those of Pfeuty et al. (2003) and Mancilla et al. (2007). We find that the addition of a potassium current can promote synchronous oscillatory activity, as Pfeuty et al. (2003) believe, and can promote antisynchronous oscillatory activity, as Mancilla et al. (2007) contend, depending on the magnitude of the potassium current,  $g_K$ , and the deactivation time constant,  $\tau$ . Pfeuty et al. found that as the magnitude of either of their potassium current

was increased that their model became more likely to evolve to synchrony. In our model, we also found that as the magnitude of the potassium current,  $g_K$ , is increased in our model, that antisynchrony is suppressed for sufficiently large values of  $\tau$  in certain parameter spaces (i.e., if  $f_K^* < f_{SS}^*$ ). That is, increasing  $g_K$  can promote synchrony for certain parameters. Mancilla et al. found that increasing the size of after-hyperpolarizations by increasing the magnitude of potassium conductances promoted antisynchronous activity. Similarly, we found that increasing the magnitude of the spike-triggered potassium current,  $g_K$ , can promote antisynchrony in certain parameter spaces (i.e., if  $f_K^* > f_{SS}^*$ ).

### 2.6.3 Limitations of the Model

We made numerous idealizations in order to create an analytically tractable model. Most prominently, we used an LIF model, instead of a full conductance based model, and chose an idealized current that allowed for easy manipulation and qualitatively fit the dynamics of potassium currents of the Kv1 and Kv3 families, instead of one that arose as a consequence of the dynamics of the gating of potassium channel. In Chapter 3, we introduce a more realistic potassium current, one that is voltage dependent, and investigate its effects on the phase-locking behavior of a pair of electrically coupled LIF neurons.

# Chapter 3

## Leaky-Integrate-and-Fire with a Conductance Based Potassium Current

In the previous chapter, we examined the effects of a time-dependent potassium current on the phase-locking behavior of a LIF cell-pair model. In this chapter, we modify a LIF cell-pair model by adding an explicit potassium current that more realistically captures the dynamics of potassium channels by considering both time and voltage dependences. That is, this explicit potassium current is modeled by a time-dependent conductance which depends on the magnitude of a driving force. We limit this study to non-summing synapses.

### 3.1 Model Description

The Leaky-Integrate-and-Fire model with a conductance-based potassium current is given by

$$C_m \frac{dV}{dt} = -g_L(V - E_L) + I_{app} - C_K \zeta(t - t_0)(V - E_K),$$

where if  $V(t_*)^- = V_{th}$ , then

(i) the cell spikes and is reset,

$$V(t_*) = \beta\delta(t_*) \text{ and } V(t_*^+) = V_{reset}$$

(ii) the time of the most recent spike is updated  $t_0 = t_*$

(iii) a spike-triggered decaying potassium conductance is activated such that

$$\zeta(t) = \frac{1}{t + \tau} \text{ for } t \geq 0. \quad (3.1.1)$$

$C_K$  scales the magnitude of the potassium channel,  $\tau$  is the time constant of the deactivation of the potassium conductance, and  $E_K$  is the reversal potential of the potassium current.  $\beta$  scales the effect of the supra-threshold portion of the spike. The form of  $\zeta(t)$  is chosen for analytical tractability (see Appendix B.1).

### 3.1.1 Non-dimensionalization

To non-dimensionalize this model, we let  $v = (V - V_{reset})/(V_{th} - V_{reset})$  so that  $v_{reset} = 0$  and  $v_{th} = 1$  and set  $\bar{t} = t/(C_m/g_L)$ . After applying this non-dimensionalization, we group our parameters as follows:  $\bar{g}_K = C_K/C_m$ ,  $\bar{\tau} = \tau/(C_m/g_L)$ ,  $\bar{I} = (I_{app} + g_L(V_r - V_{reset})/(g_L(V_{th} - V_{reset}))$ ,  $\bar{E}_K = (E_K - V_{reset})/(V_{th} - V_{reset})$ , and  $\bar{\zeta}(\bar{t}) = \zeta(t/\tau)$ . For convenience, we will omit the bars over the parameters. Thus, our non-dimensionalized LIF model with this conductance-based potassium current is given by

$$\frac{dv}{dt} = -v + I - g_K \zeta(t - t_0)(v - E_K)$$

where if  $v(t_*^-) = v_{th}$ , then

(i) the cell spikes and is reset,

$$v(t_*) = \beta\delta(t_*) \text{ and } v(t_*^+) = V_{reset}$$

(ii) the time of the most recent spike is updated  $t_0 = t_*$

(iii) a spike-triggered decaying potassium conductance is activated such that

$$\zeta(t) = \frac{1}{t + \tau} \text{ for } t \geq 0. \quad (3.1.2)$$

## 3.2 Effects of the Conductance-based Potassium Current on Frequency

Before considering the effects of coupling, we examine the effects of the conductance-based potassium current on the dynamics of a single LIF neuron. We limit our analysis to the case in which the neuron is stimulated by a constant applied current  $I$ , and we determine the effects of the conductance-based potassium current on the firing frequency, the voltage-profile, and the model neuron's phase resetting curve. Note that, analytical solutions for the model, (Equation (3.1.2)), are found most easily for integer values of  $g_K$ . In the text of this chapter, we only present equations for  $g_K = 1$ , though equations for  $g_K = 2$  can be found in Appendix B.2. However, we do present numerical solutions for both  $g_K = 1$  and  $g_K = 2$  where appropriate.

### 3.2.1 Numerical Simulations

Figure 3.2.1 presents numerical simulations of the periodic firing of a single

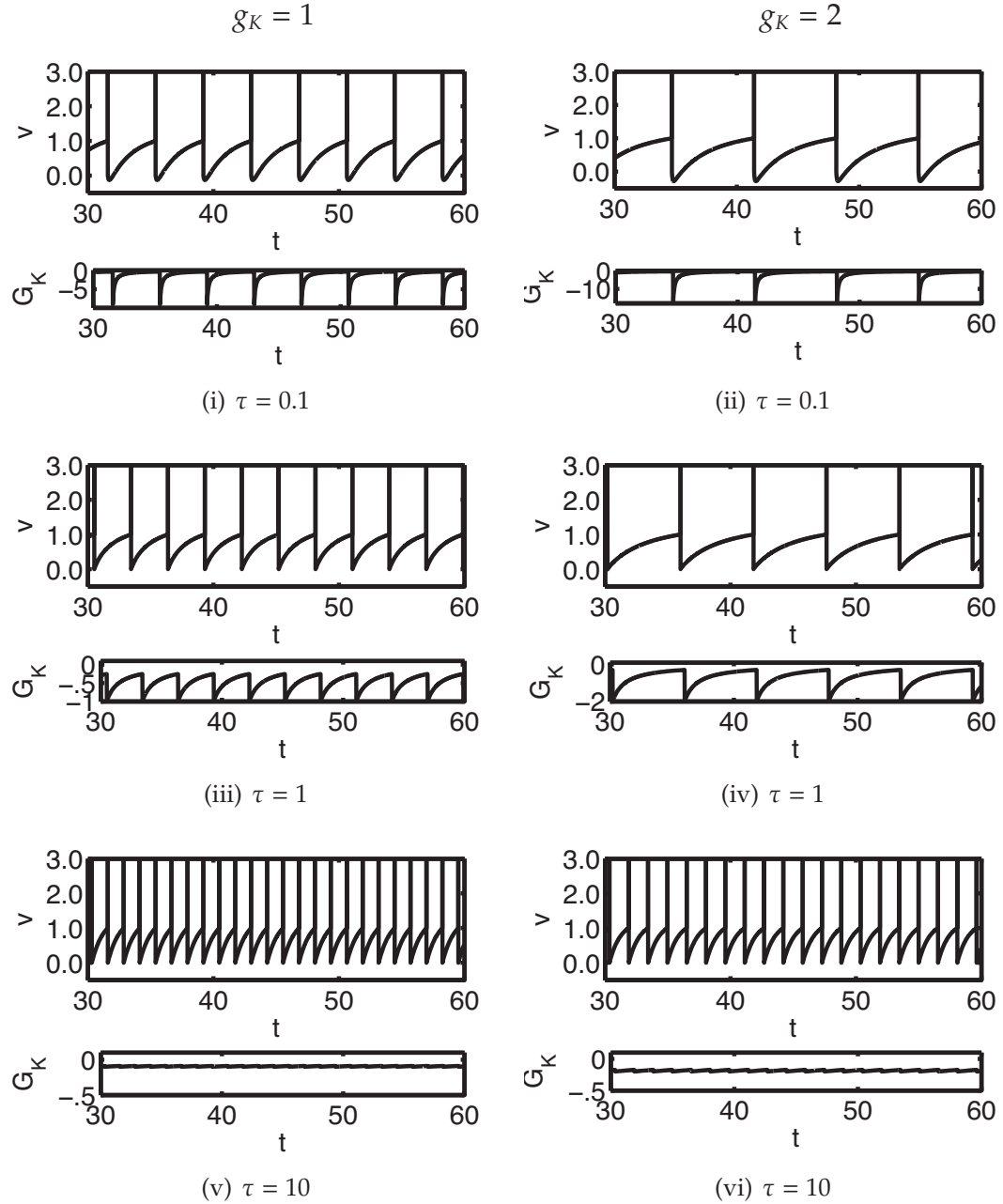


**Figure 3.2.1: Periodic firing of LIF model with explicit potassium conductance with  $g_K = 1$  (left column) and  $g_K = 2$  (right column).** For all graphs,  $I = 1.5$ ,  $E_K = -0.5$ , and  $\beta = 0.2$ . In each panel, plots of the voltage are in the upper graphs and plots of the explicit potassium conductance are in the lower graphs. For both  $g_K = 1$  and  $g_K = 2$ , the firing frequency of the model increases as  $\tau$  increases. For a given value of  $\tau$ , the firing frequency decreases as  $g_K$  is increased.

LIF neuron with a conductance-based potassium current for both  $g_K = 1$  (left column) and  $g_K = 2$  (right column) for time deactivation constants of  $\tau = .1$  (top row),  $\tau = 1$  (middle row) and  $\tau = 10$  (bottom row) when  $I = 1.5$ ,  $E_K = -0.5$ , and  $\beta = 0.2$ . We note that the firing frequency  $f$  of the neuron increases when  $\tau$  increases or  $g_K$  decreases.

### 3.2.2 Analytical Results

To obtain a more complete picture of the effects of the conductance-based potassium current on the dynamics of the LIF neuron model seen through the numerical simulations, we derive the analytical solutions to modified LIF model (Equation (3.1.2)).

Note that when  $I < 1$ , the LIF neuron never spikes, and thus the explicit potassium current is never activated. The neuron simply exponentially approaches the steady state,  $v = I$ .

However, when  $I > 1$ ,  $v$  increases to threshold,  $v_{th} = 1$ , and triggers a spike.  $v$  is then reset to  $v_{reset} = 0$ , and the explicit potassium conductance is activated. Because the explicit potassium conductance decays towards zero,  $v$  will always reach  $v_{th}$  and cause another spike to be fired.

It can readily be shown that the system will always evolve to  $T$ -periodic activity. The solution for the non-dimensionalized LIF neurons with an conductance-

based potassium current for  $g_K = 1$ , Eq (3.1.2), during  $T$ -periodic activity is

$$v_{LC}(t) = \frac{1}{t + \tau} \left( [I(\tau - 1) + E_k](1 - e^{-t-t_0}) + I(t - t_0 e^{-(t-t_0)}) \right) + \beta \delta(t - (t_0 + T)) \quad t \in [t_0, t_0 + T], \quad (3.2.1)$$

where  $t_0$  is the time of the most recent spike. The period  $T$  can be found by setting  $t_0 = 0$  and solving  $v_{LC}(T) = v_{th} = 1$ , for  $T$ .

$$1 = \frac{1}{T + \tau} \left( [I(\tau - 1) + E_k](1 - e^{-T}) + IT \right). \quad (3.2.2)$$

Equation (3.2.2) can be rearranged to give  $I$  as a function of the firing frequency,  $f$  ( $= 1/T$ ), as well as the deactivation rate of the potassium current,  $\tau$ , for any given magnitude of the potassium current,  $g_K$  (i.e., the inverse  $f$ - $I$  curve)

$$I = \frac{T + \tau - E_K(1 - e^{-T})}{(\tau - 1)(1 - e^{-T}) + T}. \quad (3.2.3)$$

Figure 3.2.2 illustrates the relationship between the firing frequency,  $f$ , and the applied current,  $I$ . For all cases,  $I = 1$  is the threshold current for the repetitive firing of action potentials, and  $f$  increases as  $I$  increases. The addition of the conductance-based potassium current to the LIF model decreases the firing frequency for all  $I$ . For a given value of  $I$ , the firing frequency,  $f$ , increases as  $g_K$  decreases for a given value of  $\tau$  (not shown) and the firing frequency increases as  $\tau$  increases. Because the conductance-based potassium current is truncated when the period ends and is normalized by  $\tau$ , changes in  $\tau$  and

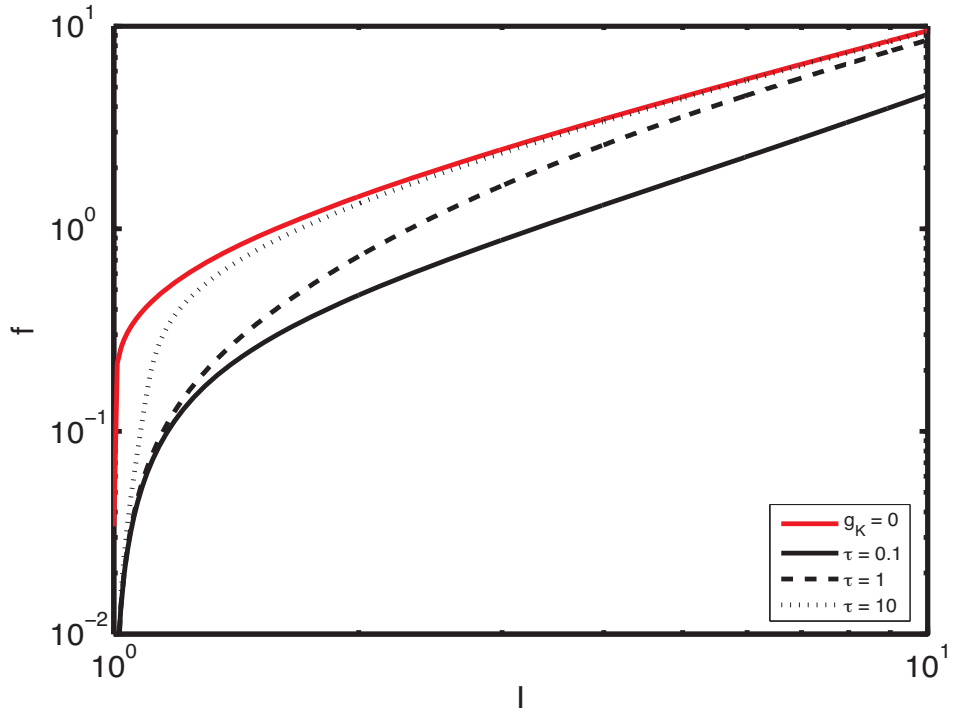


Figure 3.2.2: The firing frequency,  $f$ , versus the applied current,  $I$ , for  $g_K = 1$ . Solid, dashed and dotted black lines correspond to  $\tau = 0.1$ ,  $\tau = 1$ , and  $\tau = 10$ , respectively. The solid red line indicates the frequency for the standard LIF cell (no explicit potassium current or  $g_K = 0$ ). The addition of the explicit potassium current to the standard LIF model decreases the firing frequency for all  $I$ . For a given  $I$ , as  $\tau$  increases,  $f$  increases. Increasing  $g_K$  decreases  $f$  (not shown). For all plots,  $E_K = -0.5$ .

$g_K$  affect the total potassium current accumulated over a full period. These changes due to truncation and normalization likely primarily account for the effects of  $\tau$  and  $g_K$  on the  $f$ - $I$  curves.

Figure 3.2.3 plots the  $f - \tau$  relationship for  $I = 1.5$  and  $E_K = -0.5$  and more clearly illustrates the relationship between the time deactivation constant,  $\tau$ , of the potassium conductance and the firing frequency,  $f$ . For the LIF model with a conductance-based potassium current, the firing frequency  $f$  monotonically increases as  $\tau$  increases. As  $g_K$  is increased, the firing frequency decreases.

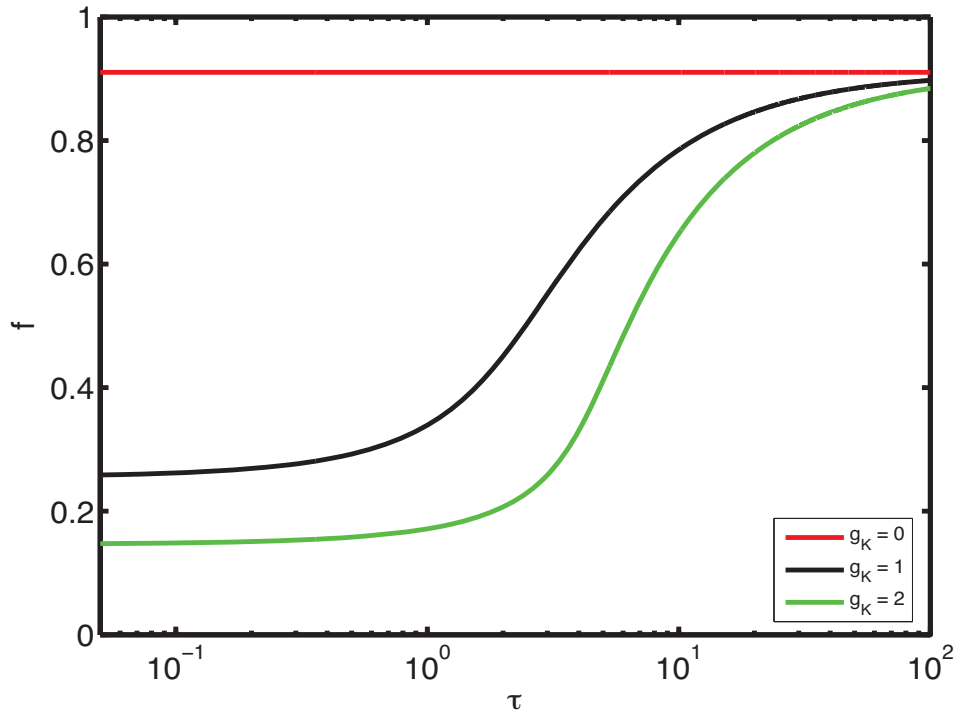


Figure 3.2.3: **Effects of the spike-triggered conductance-based potassium current on the firing frequency of an LIF cell.** The solid black line corresponds to the model with  $g_K = 1$ , while the green line corresponds to the model with  $g_K = 2$ . The solid red line indicates the frequency for the standard LIF cell (no explicit potassium current,  $g_K = 0$ ). For small  $\tau$  the firing frequency is much reduced compared to the LIF neuron. However, for large  $\tau$ , the firing frequency converges to the firing frequency for the LIF model. For all  $\tau$ , the firing frequency is decreased as  $g_K$  is increased. All plots were produced with  $I = 1.5$  and  $E_K = -0.5$ . While not shown, the same pattern holds for all  $I > 1$ .

For small values of  $\tau$ , which correspond to a quickly decaying potassium conductance, the firing frequency is much less than that for the standard LIF model. However for large values of  $\tau$ , which correspond to a more slowly decaying potassium conductance, the firing frequency is nearly identical to that of the standard LIF model. These results can be explained as follows. Note that, the total potassium conductance over a period is  $g_K \ln(1 + T/\tau)$ . If the period length is fixed, the total potassium conductance is greater for small

values of  $\tau$  than for large values of  $\tau$  due to the truncation of the potassium current and the effects of normalizing the potassium conductance by  $\tau$ , i.e.  $1/(t + \tau)$ . Therefore, we expect the conductance-based potassium current to more significantly reduce the firing frequency of the LIF model for smaller values of  $\tau$  than for large values of  $\tau$ . For very large values of  $\tau$ , the total potassium conductance over a period is  $g_K \ln(1 + T/\tau) \simeq 0$ , which is equivalent to omitting the conductance-based potassium current from the LIF model (i.e.  $g_K = 0$ ).

### 3.3 Electrically Coupled Cell-Pair Model: Effects of a Conductance-based Potassium Current on Phase-Locking

To examine the effects of a conductance-based potassium current on the phase-locking behavior in a pair of electrically coupled LIF neurons, we add the non-dimensionalized spike-triggered conductance-based potassium current to the LIF model cell-pair model given in the introduction, (1.2.4).

$$\begin{cases} \frac{dv_1}{dt} = -v_1 + I - g_K \zeta_1(t - t_{0,1})(v_1 - E_K) + g_c(v_2 - v_1) \\ \frac{dv_2}{dt} = -v_2 + I - g_K \zeta_2(t - t_{0,2})(v_2 - E_K) + g_c(v_1 - v_2) \end{cases}$$

where if  $v_i(t_*) = v_{th}$ , then

(i) the cell spikes and is reset,

$$v_i(t_*) = \beta \delta(t_*) \text{ and } v_i(t_*)^+ = v_{reset}$$

- (ii) the time of the most recent spike is updated  $t_{0,i} = t_*$
- (iii) a spike-triggered decaying potassium conductance is activated such that

$$\zeta_i(t) = \frac{1}{t + \tau} \text{ for } t \geq 0, i = 1, 2. \quad (3.3.1)$$

As before,  $\beta$  scales the effect of the supra-threshold portion of the spike and  $g_c$  is the dimensionless strength of the electrical coupling between the cells. The potassium conductance  $g_K \zeta_i(t)$  is the same as that defined in Equation (3.1.2). The subindex  $i$  on  $\zeta_i(t)$  simply denotes that it refers to the potassium conductance in cell  $i$ . Similarly, the subindex  $i$  on the time  $t_{i,0}$  denotes the most recent firing time of cell  $i$ .

### 3.3.1 Numerical Simulations of Electrically Coupled Cells

Studies have shown that electrically coupled LIF cells can evolve to either stable synchronous or antisynchronous phase-locked states depending on the strength of the electrical coupling,  $g_c$ , the “size” of the spike,  $\beta$ , and the magnitude of the applied current,  $I$  [Chow and Kopell, 2000; Lewis and Rinzel, 2003]. Chapter 2 reaffirmed these observations. Here, we investigate whether the addition of a conductance-based potassium current can also affect electrically coupled cells evolve to stable synchrony or antisynchrony.

Figure 3.3.1 shows that an conductance-based potassium current can influence whether the system evolves to synchrony or antisynchrony. This influence depends on the rate of decay of the potassium conductance  $\tau$ . For  $\tau = 0.1$  and

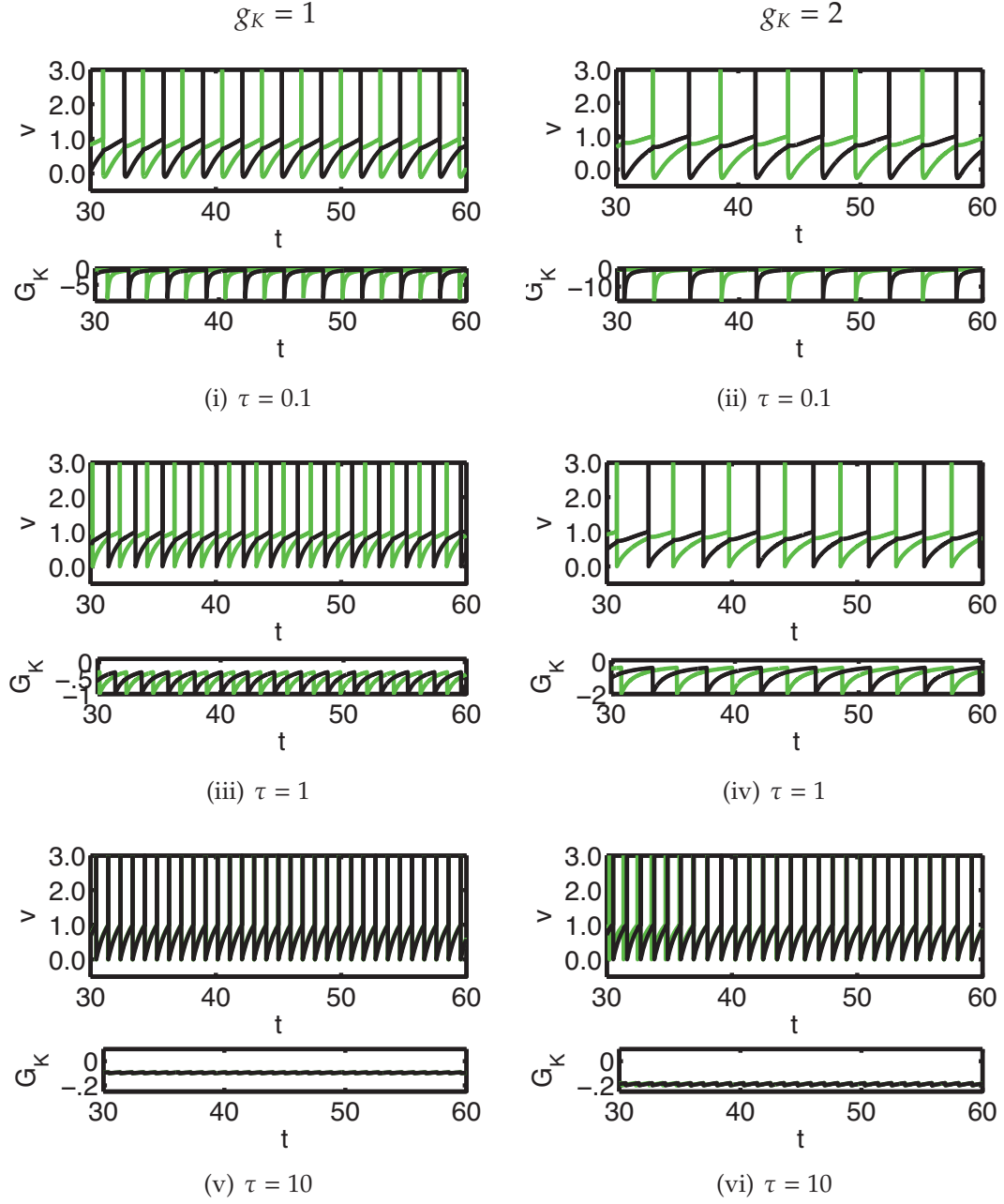


**Figure 3.3.1: Coupled LIF with the explicit potassium current for  $g_K = 1$  (left) and  $g_K = 2$  (right).** The cells evolved independently from initial conditions  $v_1 = 0.83$  (black) and  $v_2 = 0.0$  (green) in order to allow the cells to reach a uniform firing frequency until  $t = 20$ , at which time the electrical coupling term was activated. For  $\tau = 0.1$  and  $\tau = 1$ , the system evolves to antisynchrony for both  $g_K = 1$  and  $g_K = 2$ . For  $\tau = 10$ , the system evolves to synchrony for  $g_K = 1$  and  $g_K = 2$ . For all graphs,  $I = 1.7$ ,  $E_K = -0.5$ ,  $g_c = 0.2$ , and  $\beta = 0.2$ .

$\tau = 1$ , the system evolves to antisynchrony for both  $g_K = 1$  and  $g_K = 2$ . For  $\tau = 10$ , the system evolves to synchrony for both  $g_K = 1$  and  $g_K = 2$ .

### 3.4 Theory of Weakly Coupled Oscillators: Derivation of Phase Equation

As in Chapter 2, to gain insight into how changes in the magnitude of the potassium conductance,  $g_K$ , and its deactivation time constant,  $\tau$ , affect the phase-locking dynamics of electrically coupled LIF neurons, we use the theory of weakly coupled oscillators [Kuramoto, 1984]. We apply the steps outlined in Section 1.3 as detailed in Appendix A.1 to produce the infinitesimal phase resetting curve (iPRC) and the corresponding cell-pair interaction function,  $G(\phi)$ .

The infinitesimal phase resetting curve for the LIF model with a conductance-based potassium current for  $g_K = 1$  is

$$Z(t) = \frac{(t + \tau)e^t}{T(I(\tau - 1) + E_k + (I - 1)e^T)}. \quad (3.4.1)$$

Figure 3.4.1 shows  $Z(t)$  for the standard LIF model and  $Z(t)$  for the model with the conductance-based potassium current when  $T = 1.67$ . Both are qualitatively similar in that both monotonically increase as the phase increases. However, for fixed  $T$ ,  $Z(t)$  for the LIF model with the conductance-based potassium current increases more rapidly than that of  $Z(t)$  for the standard LIF model due to the factor  $(t + \tau)$  in Eq (3.4.1).

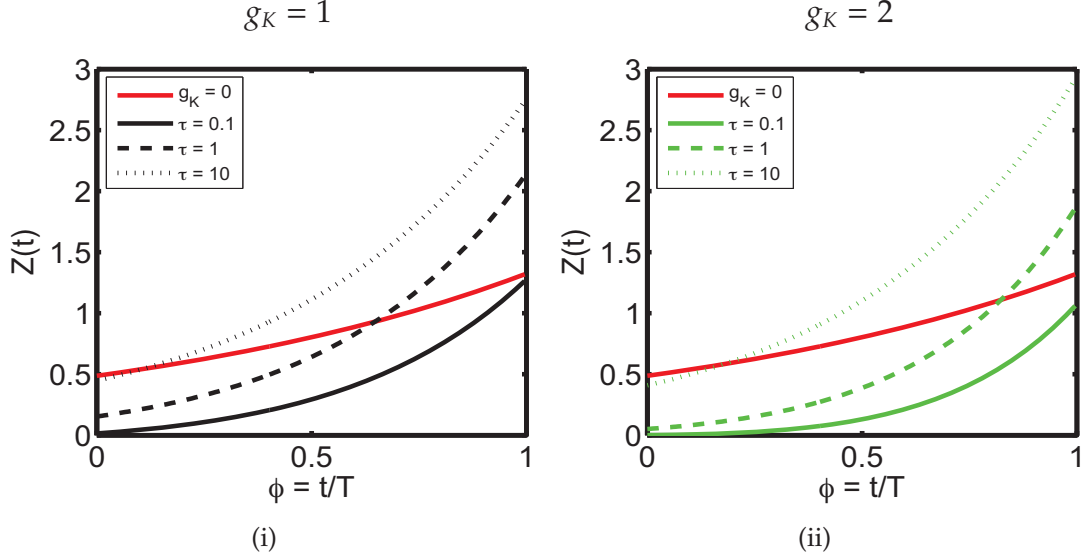


Figure 3.4.1: **The dependence of the iPRC,  $Z(t)$ , on the conductance-based potassium current.** The black lines correspond to the model with  $g_K = 1$ , while the green lines correspond to the model with  $g_K = 2$ . The solid red line indicates the frequency for the standard LIF cell (no explicit potassium current or  $g_K = 0$ ). Solid, dashed, and dotted lines correspond to  $\tau = 0.1$ ,  $\tau = 1$ , and  $\tau = 10$ , respectively. All plots were produced with  $T = 1.67$  and  $E_K = -0.5$ .

By combining the expressions for the iPRC,  $Z(t)$ , and the electrical coupling current between the two neurons,  $g_c(v_{LC}(t - \phi T) - v_{LC}(t + \phi T))$ , we obtain an equation for the evolution of the phase difference,  $\phi$ , between the electrically coupled LIF neurons with a conductance-based potassium current. For  $g_K = 1$ ,

$$\frac{d\phi}{dt} = G(\phi)$$

where

$$\begin{aligned}
 G(\phi) = \frac{g_c}{TD_1(\tau)} & \left[ \left( \int_0^{\phi T} (t + \tau) e^t v_{LC}(t + (1 - \phi)T) dt + \int_{\phi T}^T (t + \tau) e^t v_{LC}(t - \phi T) dt \right. \right. \\
 & - \int_0^{T(1-\phi)} (t + \tau) e^t v_{LC}(t + \phi T) dt - \int_{T(1-\phi)}^T (t + \tau) e^t v_{LC}(t - (1 - \phi)T) dt \Big) \\
 & \left. + \beta [(\phi T + \tau) e^{\phi T} - ((1 - \phi)T + \tau) e^{(1-\phi)T}] \right]
 \end{aligned} \tag{3.4.2}$$

and where  $D_1(\tau) = T(I(\tau - 1) + E_k + (I - 1)e^T)$ .

The  $G$ -function is evaluated through the use of numerical methods as the  $G$ -function for this model cannot be solved analytically. As a reminder,  $G(\phi^*) = 0$  indicates that  $\phi^*$  is a phase-locked state. The stability of phase-locked states can be determined by examining  $G'(\phi^*)$ . When  $G'(\phi^*) > 0$ , the phase-locked state is unstable, and when  $G'(\phi^*) < 0$ , the phase-locked state is stable. As with any symmetrically coupled pair of identical oscillating cells, the synchronous phase-locked state  $\phi^* = 0, 1$  and the antisynchronous phase-locked state  $\phi^* = 0.5$  always exist (i.e.,  $G(0) = G(1) = 0$ ,  $G(0.5) = 0$ ). Because of the  $\delta$ -function spike and the monotonically increasing  $Z(t)$ , the synchronous state is always stable [Lewis and Skinner, 2011]. On the other hand, the antisynchronous state can be either stable or unstable depending on the parameters (i.e.,  $G'(0.5)$  can be either negative or positive). Note that, the strength of coupling  $g_c$ , does not affect the existence or stability of the phase-locked states; it simply scales the  $G$ -function, and therefore it only affects the speed with which the system approaches or diverges from the phase-locked states.

### 3.4.1 The Effects of $\tau$ on $G(\phi)$

To better understand the influence of the conductance-based potassium current on the existence and stability of the phase-locked states, we examine how changes in  $\tau$  affect the function  $G(\phi)$ .

Figure 3.4.2 shows the full  $G$ -functions for  $g_K = 1$  and  $g_K = 2$  as  $\tau$  varies

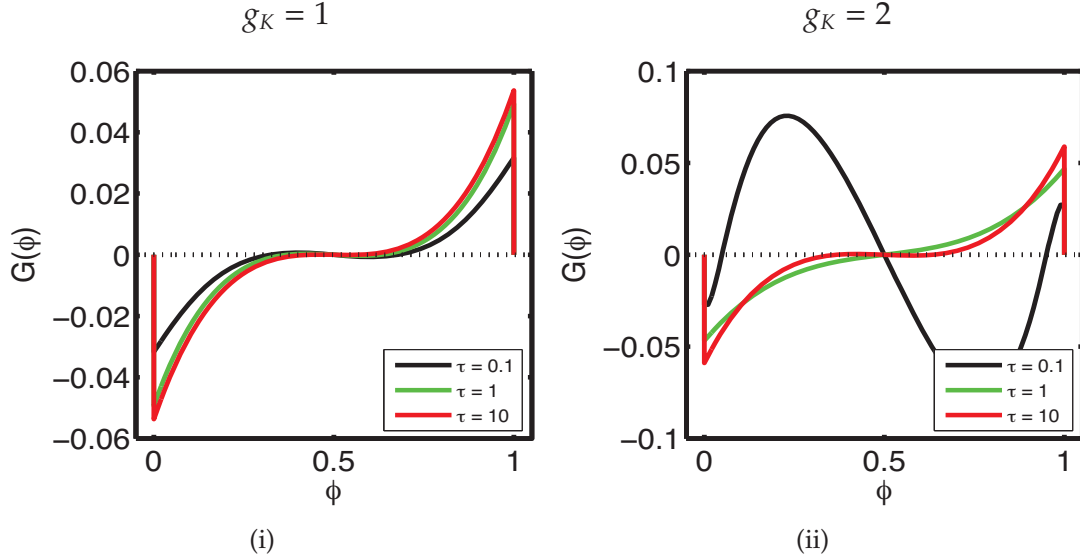
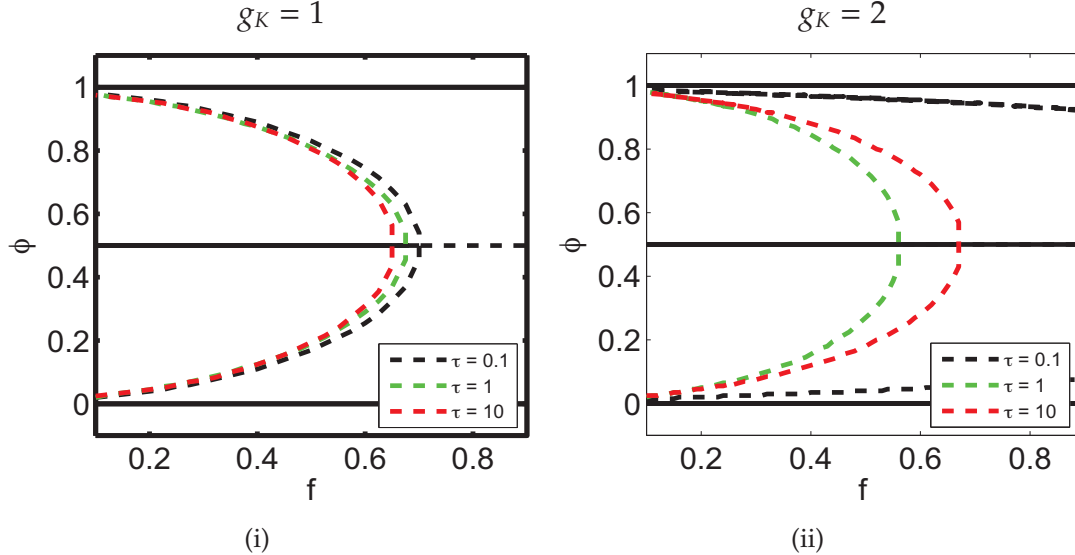


Figure 3.4.2: **G-functions with  $g_K = 1$  (left) and  $g_K = 2$  (right).** For all plots, with  $f = 0.65$ ,  $E_K = -0.5$ ,  $g_c = 0.2$ , and  $\beta = 0.2$ . In each graph, the black, green and red lines corresponds to  $\tau = 0.1$ ,  $\tau = 1$  and  $\tau = 10$ , respectively. (i) As  $\tau$  is increased from  $\tau = 0.1$  to  $\tau = 10$ , the antisynchronous state evolves from stable to unstable. (ii) For  $\tau = 0.1$ , the antisynchronous and synchronous states are both stable. As  $\tau$  is increased to  $\tau = 1$ , the antisynchronous state becomes unstable. When  $\tau$  is further increased to  $\tau = 10$ , the antisynchronous state returns to being stable.

for  $f = 0.65$ ,  $E_K = -0.5$ , and  $\beta = 0.2$ . Plots of the  $G$ -functions show that the synchronous state is stable for all values of  $\tau$ , while the stability of the antisynchronous state depends on the value of  $\tau$ . In Figure 3.4.2(i) for  $g_K = 1$ , as  $\tau$  is increased from  $\tau = 0.1$  (black curve) to  $\tau = 10$  (red curve), the antisynchronous phase-locked state becomes unstable, while the synchronous state remains stable. In Figure 3.4.2(ii) for  $g_K = 2$ , for  $\tau = 0.1$  (black curve), the antisynchronous state is stable. As  $\tau$  is increased from  $\tau = 0.1$  to  $\tau = 1$  (green curve), the antisynchronous state becomes unstable. As  $\tau$  is further increased from  $\tau = 1$  to  $\tau = 10$  (red curve), the antisynchronous state again becomes

stable.



**Figure 3.4.3: Bifurcation diagrams of the model with the explicit potassium current for the firing frequency  $f$ .** For all graphs,  $E_K = -0.5$  and  $\beta = 0.2$ . Solid lines indicate stable state and dotted lines indicate unstable states. Black, green, and red lines indicate  $\tau = 0.1$ ,  $\tau = 1$ , and  $\tau = 10$ , respectively. We define  $f^*$  to be the critical value of  $f$  where the pitchfork bifurcation originates. For  $f < f^*$ , both antisynchronous and synchronous states are stable, while for  $f > f^*$ , only the synchronous state is stable. (i) For  $g_K = 1$ , as  $\tau$  increases,  $f^*$  decreases. (ii) For  $g_K = 2$ , as  $\tau$  increases from  $\tau = 0.1$  to  $\tau = 1$ ,  $f^*$  decreases. However, when  $\tau$  is increased from  $\tau = 1$  to  $\tau = 10$ ,  $f^*$  increases. We note that the bifurcation diagrams for  $g_K = 2$  are much more greatly affected by changes in  $\tau$  than those for  $g_K = 1$ .

To demonstrate the effects of the conductance-based potassium current on the stability of phase-locked states over a wide range of frequencies, we plot the bifurcation diagrams for the phase difference  $\phi$  versus the firing frequency  $f$  for select values of  $\tau$  (Figure 3.4.3). Note that stable phase-locked states are indicated by solid lines, and unstable phase-locked states are indicated by dashed lines. The unstable curve defines the boundaries between the domain of attraction for the synchronous state and the antisynchronous state. For

small  $f$ , the cell-pair is bistable; however, the domain of attraction is larger for the antisynchronous state,  $\phi = 0.5$ , than for the synchronous state,  $\phi = 0, 1$ , and thus the antisynchronous state dominates. As  $f$  increases, the domain of attraction for the antisynchronous state shrinks. With further increases of  $f$ , the synchronous state becomes dominant, and eventually a critical frequency  $f^*$  is reached, after which only the synchronous phase-locked state is stable. This critical frequency  $f^*$  occurs where the unstable steady state coalesces with the stable antisynchronous state in a subcritical pitchfork bifurcation.

We will use changes in the value of this critical frequency  $f^*$  as a convenient way to assess how the stability of the antisynchronous steady state depends on  $\tau$ . Figure 3.4.3 presents the bifurcation diagrams for several values of  $\tau$  when  $E_K = -0.5$  and  $\beta = 0.2$ . When  $g_K = 1$ , Figure 3.4.3(i) shows that  $f^*$  decreases as  $\tau$  increases. Figure 3.4.3(ii), for  $g_K = 2$  shows that  $f^*$  decreases as  $\tau$  is increased from  $\tau = 0.1$  to  $\tau = 1$ . However,  $f^*$  increases when  $\tau$  is increased from  $\tau = 1$  to  $\tau = 10$ .

Figure 3.4.4 shows how the critical frequency  $f^*$  responds to increases in  $\tau$  when  $E_K = -0.5$  and  $\beta = 0.2$ . The area above each curve indicates the region in parameter space where only the synchronous state is stable, while the area below each curve indicates the region in parameter space where both the synchronous and antisynchronous states are stable. The solid red curve shows the critical frequency for the standard LIF model for the given parameters (i.e.,  $g_K = 0$ ). For  $g_K = 1$ , the LIF model with a conductance-based potassium cur-

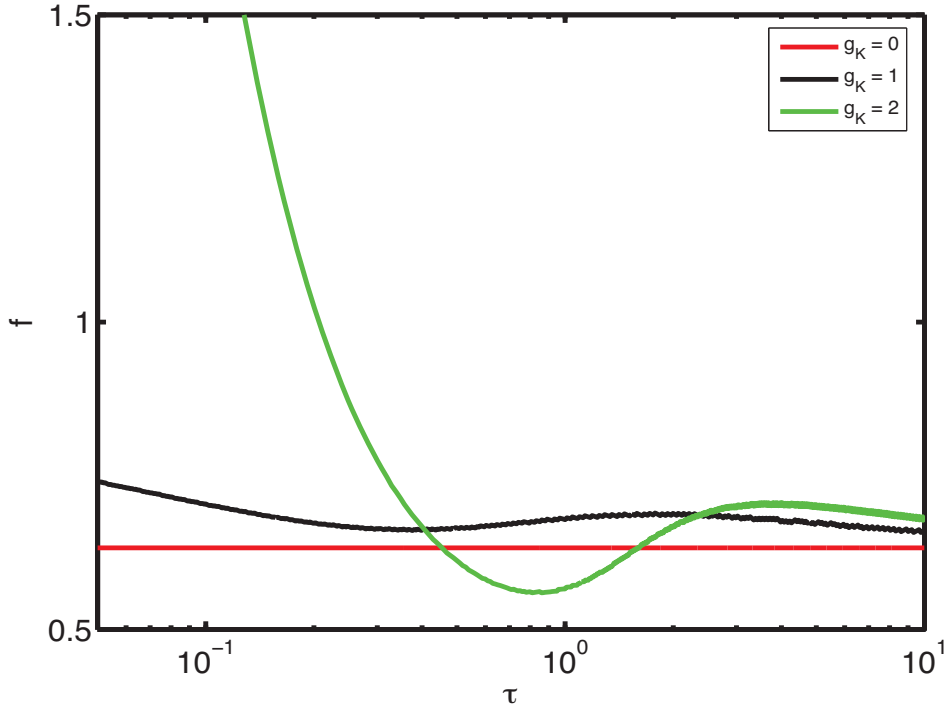


Figure 3.4.4: **Critical frequency,  $f^*$ , versus the potassium conductance deactivation time constant,  $\tau$ .** Black and green lines correspond to the model with  $g_K = 1$  and  $g_K = 2$ , respectively. The red line is for the standard LIF model without an explicit potassium current (or  $g_K = 0$ ). The model with  $g_K = 1$  always increases the  $f$  parameter space where antisynchrony is stable compared to the standard LIF model. However, the model with  $g_K = 2$  shows that for moderate values of  $\tau$ , that the model with an explicit potassium current can more strongly favor synchrony than than the standard LIF model.  $E_K = -0.5$  and  $\beta = 0.2$  for all graphs.

rent (black curve) always increases the region where antisynchrony is stable in comparison to the standard LIF model for all values of  $\tau$ , and thus promotes the asynchronous state. However for  $g_K = 2$ , the LIF model with a conductance-based potassium current (green curve) decreases the  $f$  parameter region where stable antisynchrony exists for moderate values of  $\tau$  and increases the  $f$  parameter region where stable antisynchrony exists for both small and large values of  $\tau$  in comparison to the standard LIF model.

Note that, it is expected that large values of  $\tau$  would cause the critical frequency of the LIF model with the conductance-based potassium current to converge to the critical frequency of the standard LIF model, because the potassium conductances goes to 0 as  $\tau \gg T$ , due to the potassium conductance being scaled by  $\tau$ , i.e.  $1/(t+\tau)$ . That is, the voltage-dependent explicit potassium current no longer impacts the dynamics of the LIF model for large values of  $\tau$  (see Section 3.2 and Figure 3.2.3).

Unfortunately, further analysis on the effects of the deactivation time constant,  $\tau$ , on the critical frequency,  $f^*$ , are limited, because of our reliance on numerical methods.

### 3.5 Conclusion and Discussion

In this chapter, we studied how the addition of a spike-triggered conductance-based potassium current to two identical, electrically coupled LIF model neurons affects the existence and stability of phase-locked states. Numerical simulations indicated that the addition of a spike-triggered conductance-based potassium current influences whether a system of electrically coupled LIF model neurons evolve to stable synchrony or antisynchrony. The theory of weakly coupled oscillators helped to generalize the results of the numerical simulations and provided more insight into how changes to the deactivation time constant,  $\tau$ , and the magnitude of the current,  $g_K$ , affect whether the addition of the spike-triggered potassium current promotes or suppresses the

antisynchronous phase-locked state. These results are summarized in Table 3.5.2.

Parameter variation	Effect
Increasing Intrinsic Frequency ( $\uparrow I$ )	Promotes synchrony
Increasing Spike Effect ( $\uparrow \beta$ )	Promotes synchrony
Increasing the Magnitude of the Potassium Current ( $\uparrow g_K$ )	Can Promote or Suppress Antisynchrony.
Increasing the Deactivation Time Constant ( $\uparrow \tau$ )	Can Promote or Suppress Antisynchrony

Table 3.5.2: **Summary of Results**

We found that either increasing the intrinsic firing frequency by increasing the applied current,  $I$ , or increasing the magnitude of the spike effect,  $\beta$ , promoted synchrony. The effect on synchronization of increasing the magnitude of the potassium current,  $g_K$ , or increasing the size of the deactivation time constant,  $\tau$ , is less clear. This chapter presented evidence that increasing either  $g_K$  or  $\tau$  can promote or suppress antisynchrony (see Figure 3.4.4); however, an exact description of the region where antisynchrony is promoted by increasing  $g_K$  or  $\tau$  remains elusive. Perhaps a decomposition of the  $G$ -function similar to that performed in Chapter 2 could provide insight into the effect of  $g_K$  and  $\tau$  on synchronization.

### 3.5.1 Effects of Including Voltage Dependence in the Potassium Current

In Chapters 2 and 3, we added a spike-triggered potassium current to a pair of electrically coupled LIF model neurons. In Chapter 2, we investigated how a non-summing potassium current affects the phase-locking behavior of a pair of electrically coupled LIF neurons, and in Chapter 3, we investigated how a conductance-based potassium current affects the phase-locking behavior of a pair of electrically coupled LIF neurons. These potassium currents differed in two ways: the shape and decay rate of their kernels,  $\eta_{K_{ns}}(t)$  and  $\zeta(t)$ , and the inclusion of the voltage dependence term,  $(v - E_K)$ , in the conductance-based potassium current. In Appendix B.1, we briefly examine the effects on phase-locking behavior of interchanging the potassium kernels in the electrically coupled LIF models (i.e., using  $\eta_{K_{ns}}(t)$  in place of  $\zeta(t)$  in the conductance-based potassium current model and using  $\zeta(t)$  instead of  $\eta_{K_{ns}}(t)$  in the spike-triggered potassium current). Numerical simulations indicate that the two different kernels for the potassium currents cause similar effects on the phase-locking behavior of electrically coupled LIF neurons. However, replacing  $\eta_{K_{ns}}(t)$  with  $\zeta(t)$  causes a significant decrease in the firing frequency for small values of  $\tau$ , but only a minimal decrease in  $f$  for large values of  $\tau$ . By investigating our models via frequency, we have minimized the frequency-dependent differences between the usage of either potassium kernel. Because the majority of the differences between the two kernels appear to be due to each kernel's effects on frequency, we can evaluate how the inclusion of voltage-dependence in the potassium current effects the dynamics of the model largely independent of

the choice of the kernel.

We first note that the voltage-dependence term,  $(v - E_K)$ , of the conductance-based potassium current affects the magnitude of the current. By choice, the kernel of the conductance-based potassium current always decreases as the phase advances. Because the membrane potential of the LIF neuron intrinsically increases, the voltage-dependence term,  $(v - E_K)$ , increases as the phase increases. The addition of the voltage-dependence term causes the magnitude of the potassium current to decrease near reset,  $\phi = 0$ , and increases near threshold,  $\phi = 1$ .

The inclusion of voltage-dependence in the potassium current affects the shape of the iPRC. For the model with the non-summing spike-triggered potassium current, the addition of the potassium current always decreases the iPRC versus that of the standard LIF model (Figure 2.4.2(ii)). However for the model with the conductance-based potassium current, the iPRC rapidly increases and can become larger than the iPRC for the standard LIF model (Figure 3.4.1). This rapid increase is due to the factor  $(t + \tau)$  in the iPRC (Equation (3.4.1)). Thus, the iPRC grows increasingly rapidly with increases in phase. We note that this factor,  $(t + \tau)$ , is a result of the inclusion of the voltage-dependence term,  $(v - E_K)$ , in the conductance based potassium current.

Because the  $G$ -function is a convolution of the voltage trace and iPRC, both of which are affected by the inclusion of the voltage-dependence term, the voltage-dependence term should impact the existence and stability of the

phase-locked states. However, because of our reliance on numerical methods to evaluate the  $G$ -function, we cannot isolate the influence of the voltage-dependence on the existence and stability of phase-locked states analytically. Nevertheless, we can gain insight into how the voltage-dependence term affects the existence of stable antisynchrony by comparing the effects of  $\tau$  on the critical frequency,  $f^*$ , for the electrically coupled LIF model with the non-summing potassium current and the model with the conductance-based potassium current. The model with the non-summing potassium current promotes antisynchrony more strongly than the standard LIF model for sufficiently small values of  $\tau$  ( $\tau < \tau_{int}$ ) and suppresses antisynchrony more strongly than the standard LIF model for sufficiently large values of  $\tau$  ( $\tau > \tau_{int}$ ) (see Figure 2.4.4). When  $g_K = 1$ , the model with the conductance-based potassium current promotes antisynchrony more strongly than the standard LIF model for all values of  $\tau$  (see Figure 3.4.4). However, when  $g_K$  is increased to  $g_K = 2$ , the model with the conductance-based potassium current suppresses antisynchrony more strongly than the LIF model for a small range of  $\tau$ . On the other hand, as the increase of  $g_K$  to  $g_K = 2$  can be thought of as the doubling of the effects of the voltage-dependence term rather than as the increase of the magnitude of the potassium current, the specific effects of the addition of the voltage-dependence on the phase-locking behavior of electrically coupled LIF neurons remain undetermined.

### 3.5.2 Comparison to Previous Results of Pfeuty et al. and Mancilla et al.

Similar to Chapter 2, we can translate the non-dimensional parameters of the electrically coupled LIF model with a spike-triggered conductance-based potassium current into dimensional form to facilitate a comparison to the work of Pfeuty et al. (2003) and Mancilla et al. (2007). Using the values reported in Mancilla et al. (2007) of  $C_m \approx 40\text{pF}$  and  $g_L \approx 10\text{nS}$ , we again find that the membrane time constant is  $\tau = 4\text{ms}$ , which implies that the actual frequency,  $f$ , corresponds to  $250\bar{f}\text{ Hz}$ , where  $\bar{f}$  is the non-dimensional frequency. The non-dimensional deactivation time constants  $\bar{\tau} = 0.1, 1.0$ , and  $10$ , correspond to the deactivation time constants of  $\tau = 0.4, 4.0$ , and  $40\text{msecs}$ , values which are representative of the reported deactivation rates for potassium channels in the Kv1 and Kv3 families [Coetzee et al., 1999]. The investigated non-dimensional  $\bar{f}$  frequency range of 0 to 1 corresponds to an actual frequency range of 0 to 250 Hz, a range that encompasses those investigated by Mancilla et al. (2007) and Pfeuty et al. (2003).

As the results presented in this chapter support those of Chapter 2, the results of Chapter 3 also unify those of Pfeuty et al. (2003) and Mancilla et al. (2007). Like the model of Pfeuty et al., our model from Chapter 3 shows that increasing the magnitude of the potassium current,  $g_K$ , can promote synchrony, at least for certain parameters. Similar to the results of Mancilla et al., our model indicated that if the size of after-hyperpolarizations are increased by increasing the magnitude of the potassium current,  $g_K$ , that antisynchrony is promoted for certain parameters.

### 3.5.3 Limitations of the Model

In this chapter we used a more realistic model of a potassium current than in Chapter 2 and investigated how it impacts the phase-locking behavior of a pair of electrically coupled LIF neurons. Although the LIF model captures the qualitative dynamics of a full conductance based model, it behooves us to see if the results from this chapter hold in a the more biophysically realistic, Hodgkin-Huxley type, full-conductance based model. Likewise, we should see if similar results arise when if a more realistic potassium current, one that arises due to the gating dynamics of potassium channels, is used instead of a spike-triggered one. In Chapter 4, we investigate the effects on the phase-locking behavior of altering a biophysically realistic potassium current on a pair of electrically coupled, Hodgkin-Huxley type conductance-based model neurons.

# Chapter 4

## Full Conductance-Based Model

In the previous two chapters, we added explicit potassium currents to a Leaky-Integrate-and-Fire model to see how changes in the strength and the rate of deactivation of explicit potassium currents affected the existence and stability of the oscillatory behavior of electrically coupled neurons. In this chapter instead of using an LIF type-model, we modify the Hodgkin-Huxley model (as introduced in Chapter 1) to investigate how differences in potassium channel dynamics might effect the synchronization of electrically coupled neurons.

### 4.1 Model Description

The modified Hodgkin-Huxley model is given by

$$C_m \frac{dV}{dt} = -I_{Na} - I_K - I_L + I_{applied}$$

where

$$I_{Na} = g_{Na}m^3h(V - E_{Na}) \quad (4.1.1)$$

$$I_K = (g_{K_{reset}}n_{reset} + g_{K_{AHP}}n_{AHP})(V - E_K)$$

$$I_L = g_L(V - E_L)$$

and

$$\frac{dy}{dt} = \alpha_y(V)(1 - y) - \beta_y(V)y, \quad (4.1.2)$$

where  $y = n_{reset}, n_{AHP}, m, h$ .

$C_m$  is the membrane capacitance,  $V$  is the transmembrane potential, and  $I_{Na}, I_K, I_L$ , and  $I_{applied}$  are the sodium, potassium, and leakage currents, respectively.  $E_{Na}, E_K$ , and  $E_L$  are the sodium, potassium, and leakage reversal potentials, respectively. The maximal conductances for the various currents are given by  $g_{Na}, g_{K_{reset}}, g_{K_{AHP}}$ , and  $g_L$ .

The dynamics of the gating variables,  $m$  and  $h$  for the sodium current and  $n_{reset}$  and  $n_{AHP}$  for the two potassium currents, are described by Eq (4.1.2), where  $\alpha_y(V)$  and  $\beta_y(V)$  are the voltage-dependent gate-subunit opening rate and closing rate, respectively.

The difference between this model and the standard Hodgkin-Huxley model is our description of the total potassium current,  $I_K$ . We consider two separate potassium currents,  $I_{K_{reset}} = g_{K_{reset}}n_{reset}(V - E_K)$  and  $I_{K_{AHP}} = g_{K_{AHP}}n_{AHP}(V - E_K)$ . The first potassium current,  $I_{K_{reset}}$  is a fast activating and deactivating current that primarily controls the fast repolarization of the model neuron following an action potential, have similar effects as the instantaneous reset of the modified LIF models used in Chapters 2 and 3, but modeled in a more realistic way. The second potassium current,  $I_{K_{AHP}}$  is qualitatively similar to  $I_{K_{reset}}$ , but the magnitude and deactivation rate of  $I_{K_{AHP}}$  are varied so that we can investigate how

changes in potassium channel dynamics effect the phase-locking behavior of the electrically coupled neurons.  $I_{K_{AHP}}$  can be thought of as being analogous to the explicit potassium currents of the previous models.

A full list of parameter values for the model can be found in Appendix C.

#### 4.1.1 Potassium Channel Dynamics

As both the gating variable for the resetting potassium current,  $n_{reset}$  and the gating variable for the after-hyperpolarization potassium current,  $n_{AHP}$ , are identical in form, we present the functions controlling the gating dynamics for a general “ $n$ ” gating variable.

We let the voltage-dependent steady state be the sigmoid function

$$n_\infty(V) = \frac{e^{V-V_{1/2}}}{1 + e^{V-V_{1/2}}} \quad (4.1.3)$$

and the voltage-dependent time constant be

$$\tau_n(V) = \frac{\tau_a e^{V-V_{1/2}} + \tau_d}{1 + e^{V-V_{1/2}}}, \quad (4.1.4)$$

where

$$n = n_{AHP}, n_{reset}.$$

(See Figure 4.1.1.)

The corresponding rate constants are

$$\alpha_n(V) = \frac{e^{V-V_{1/2}}}{\tau_a e^{V-V_{1/2}} + \tau_d} \quad (4.1.5)$$

and

$$\beta_n(V) = \frac{1}{\tau_a e^{V-V_{1/2}} + \tau_d} \quad (4.1.6)$$

In the above equations,  $V_{1/2}$  is the membrane potential where the potassium channel is half activated. We set  $V_{1/2} = 0mV$  for both the reset and AHP potassium currents. This potential is sufficiently high to ensure that neither potassium current prevents the formation of an action potential. The activation rate and the decay rate of the potassium current are given by  $\tau_a$  and  $\tau_d$ , respectively. Because we want the potassium currents to activate very quickly, we set both  $\tau_{a_{reset}} = 0.1ms$  for the resetting potassium current,  $I_{K_{reset}}$ , and  $\tau_{a_{AHP}} = 0.1ms$  for the AHP potassium current,  $I_{K_{AHP}}$ . We choose  $\tau_{d_{reset}} = 1ms$  so that the resetting potassium current remained activate for a sufficient duration to fully repolarize the neuron but still deactivated relatively quickly. To investigate the role of the deactivation constant of the AHP potassium current on the oscillatory behavior of electrically coupled neurons, we vary  $\tau_{d_{AHP}}$ .

Figure 4.1.1 shows the function that governs the dynamics of the potassium conductances. Figure 4.1.1(i) shows that at low voltages,  $n_\infty \sim 0$ , and thus the potassium gates tend to be closed; at high voltages,  $n_\infty \sim 1$ , and thus the potas-

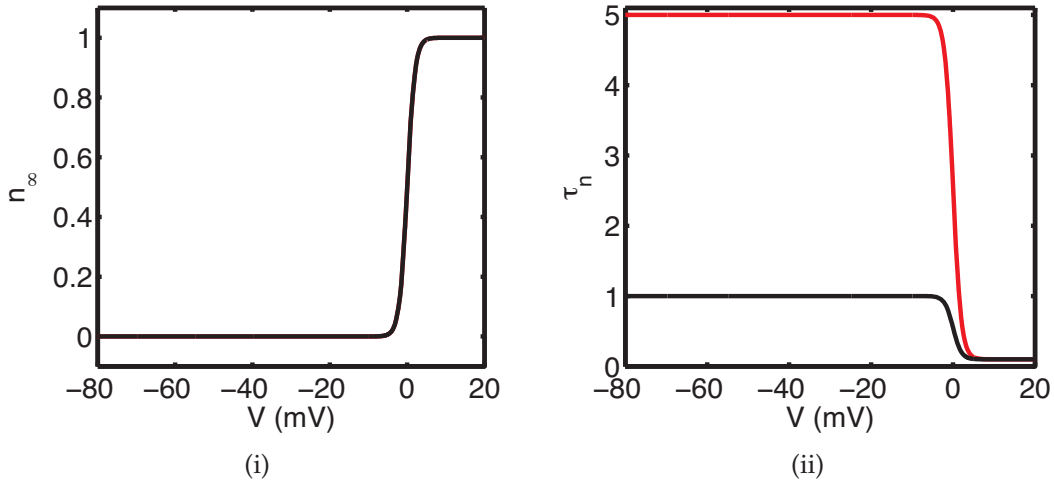


**Figure 4.1.1: Dynamics of the Potassium Currents** In all plots, black and red lines correspond to  $I_{K_{reset}}$  and  $I_{K_{AHP}}$ , respectively. For  $I_{K_{reset}}$ ,  $\tau_{a_{reset}} = 0.1ms$  and  $\tau_{d_{reset}} = 1ms$ . For  $I_{K_{AHP}}$ ,  $\tau_{a_{AHP}} = 0.1ms$  and  $\tau_{d_{AHP}} = 5ms$ . (i) Plot of  $n_\infty(V)$ . At low voltages, neither potassium current is significantly activated. As the membrane potential increases past the threshold voltage,  $V_{1/2} = 0mV$ , the potassium currents become fully activated. Note that,  $n_\infty$  is identical for both the reset potassium current and the AHP potassium current. (ii) Plot of  $\tau_n(V)$ . At low voltages, both potassium current are much slower to achieve their  $n_\infty$  values than at high voltages.

sium gates tend to be open. The gates transition from being predominately closed to being predominately open as the membrane potential is increased past  $V_{1/2} = 0mV$ . This indicates that at low voltages, the potassium conductance will be inactive, while at high voltages, the potassium current will be active. Figure 4.1.1(ii) shows how quickly the potassium gates can achieve their  $n_\infty$  value. The potassium currents are much faster to approach their  $n_\infty$  values at high voltages than at low voltages, i.e., the potassium conductances are much faster to activate than deactivate.

## 4.2 Electrically Coupled Cell-Pair Model

The full conductance-based model of a pair of electrically coupled cells is

$$\begin{cases} C_m \frac{dV_1}{dt} = -I_{Na_1} - I_{K_1} - I_{L_1} + I_{applied} + g_c(V_2 - V_1) \\ C_m \frac{dV_2}{dt} = -I_{Na_2} - I_{K_2} - I_{L_2} + I_{applied} + g_c(V_1 - V_2) \end{cases}$$

where

$$\begin{aligned} I_{Na_i} &= g_{Na} m_i^3 h_i (V_i - E_{Na}) \\ I_{K_i} &= (g_{K_{reset}} n_{reset_i} + g_{K_{AHP}} n_{AHP_i}) (V_i - E_K) \\ I_{L_i} &= g_L (V_i - E_L) \end{aligned} \tag{4.2.1}$$

and

$$\frac{dy_i}{dt} = \alpha_{y_i}(V_i)(1 - y_i) - \beta_{y_i}(V_i)y_i, \tag{4.2.2}$$

where  $y = n_{reset_i}, n_{AHP_i}, m_i, h_i$ . for  $i = 1, 2$

The variables and parameters are the same as defined earlier, Eq (4.1.1); the sub-index  $i$  simply denotes the differences between the two neurons, cell 1 and cell 2. The magnitude of the current that flows from cell  $j$  to cell  $k$  through simple ohmic resistance is given,  $g_c(V_j - V_k)$ , where  $g_c$  is the constant conductance of the electrical coupling.

### 4.3 Effect of the AHP Potassium Conductance on Phase-Locking: Theory of Weakly Coupled Oscillators

To determine how changes to the deactivation time constant and the mag-

nitude of the AHP potassium current affect the phase-locking behavior of the electrically coupled neurons, we use the theory of weakly coupled oscillators. Numerical methods allowed us to determine the voltage trace over a single period for a model neuron and its corresponding phase-response curve. Together, these can be combined to find the  $G$ -function, which allows for the easy determination of the existence and stability of the phase-locked states as described in Section 1.3. In general, we will vary the the decay rate,  $\tau_{d_{AHP}}$ , and magnitude,  $g_{K_{AHP}}$ , of the AHP current and examine the  $G$ -functions to investigate how changes in these parameters affect the stability of the phase-locked states.

Figure 4.3.1 shows the voltage trace, PRC, gating variables, and corresponding  $G$ -function for the model without the AHP current activated ( $g_{K_{AHP}} = 0$ ) (*i, iii, v*) and with the AHP current activated ( $g_{K_{AHP}} = 100nS, \tau_{d_{AHP}} = 5ms$ ) (*ii, iv, vi*) at a firing frequency of  $f \approx 30Hz$ . The voltage traces of the model with and without the AHP current are similar, though the model with the AHP current repolarizes slightly more strongly and is initially slower to depolarize. The PRCs are also similar, as both are all positive, Type I PRCs [Ermentrout and Rinzel, 1988] and are very similar to PRCs measured for real cortical inhibitory interneurons [Mancilla et al., 2007]. However, they differ as the PRC for the model with the AHP current is right-shifted and has a higher peak response to stimulus than the PRC for the model without the AHP current. The evolution of both the  $n_{reset}$  and  $m$ -gating variables appear identical for the model

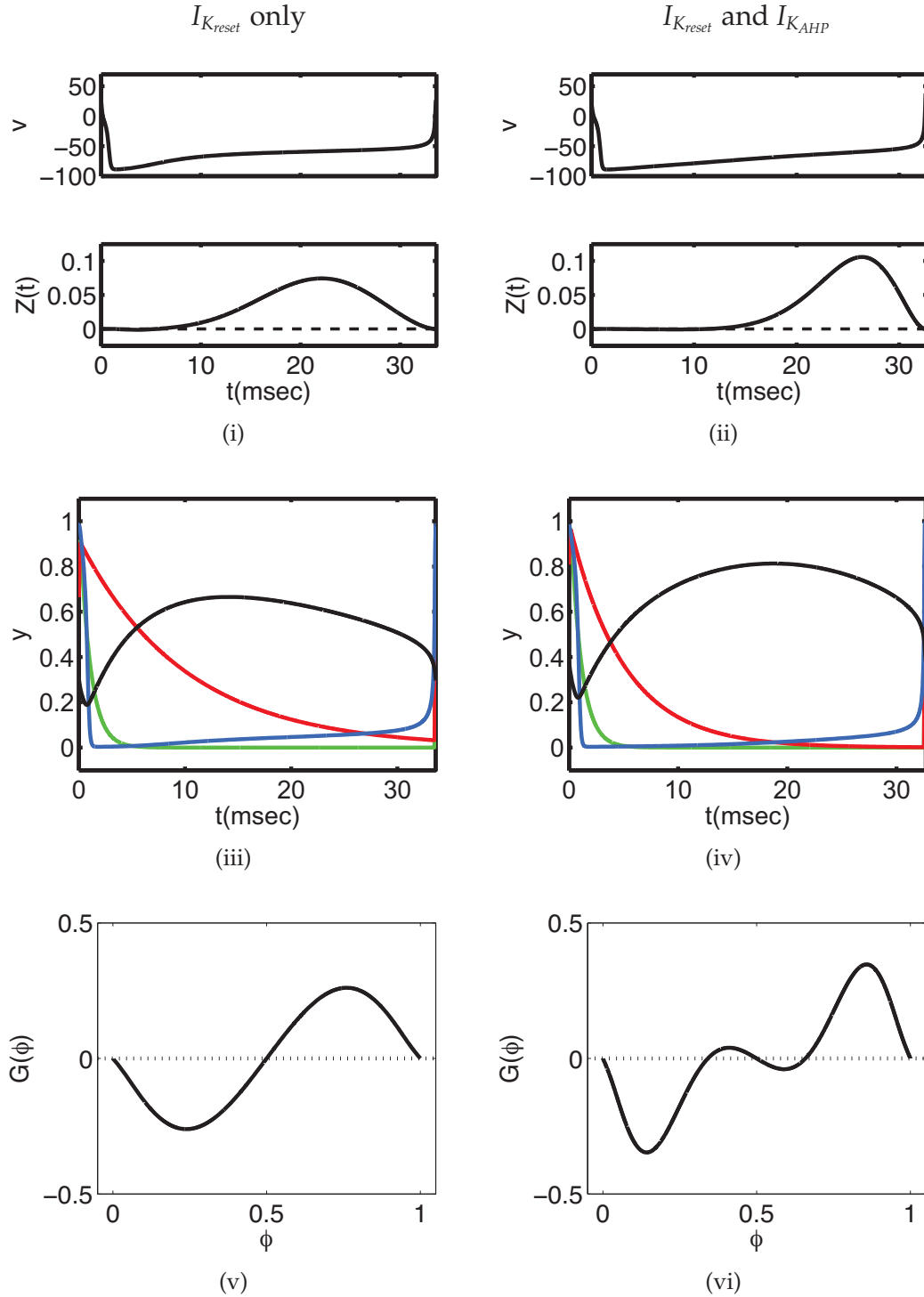


**Figure 4.3.1: Voltage Trace, PRC, Gating Variables, and  $G$ -functions for  $I_{K_{reset}}$  only (left column) and for both  $I_{K_{reset}}$  and  $I_{K_{AHP}}$  (right column).** In (i, iii, v),  $g_{K_{AHP}} = 0$ ,  $I_{applied} = 86\text{pA}$ ,  $f = 29.7\text{Hz}$ . In (ii, iv, vi),  $g_{K_{AHP}} = 100\text{nS}$ ,  $\tau_{d_{AHP}} = 5\text{ms}$ ,  $I_{applied} = 120\text{pA}$ ,  $f = 30.6\text{Hz}$ . In (iii) and (iv), black, blue, green, and red lines correspond to the value for the  $h$ ,  $m$ ,  $n_{reset}$ , and  $n_{AHP}$  gating variables.

with and without the AHP current. However, the  $m$ -gating variable achieves a higher value in the model with the AHP current, which leads to higher maximum sodium conductance, and thus a greater depolarization during the action potential. Regardless, the response of the model with and without the AHP current appear qualitatively similar. However, the  $G$ -functions illustrate that these seemingly small differences can foster a change in the phase-locking behavior of the electrically coupled neurons. In the model without the AHP current, the  $G$ -function indicates that only the synchronous state is stable; the antisynchronous state is unstable. Interestingly, in the model with the AHP current, the  $G$ -function indicates that both the synchronous and antisynchronous phase-locked states are stable for these values of  $g_{K_{AHP}}$  and  $\tau_{d_{AHP}}$ . It appears that the addition of the AHP current can stabilize the previously unstable antisynchronous state.

#### 4.3.1 Effects of varying $I_{applied}$ , $g_{K_{AHP}}$ , and $\tau_{d_{AHP}}$ on the $G$ -functions

From the previous chapters, we expect that as  $I_{applied}$  is increased, the firing frequency,  $f$ , increases, and the antisynchronous phase-locked state loses stability. Figure 4.3.2 shows that this pattern holds in our modified Hodgkin-Huxley model. When  $g_{K_{AHP}} = 100nS$  and  $\tau_{d_{AHP}} = 5$ , increasing  $I_{applied}$  causes the antisynchronous phase state to switch from being stable to unstable. When  $I_{applied} = 100pA$ , the antisynchronous phase-locked state is clearly stable (Figure 4.3.2(i)). As  $I_{applied}$  is increased to  $I_{applied} = 200pA$  and  $I_{applied} = 300pA$ , the anti-

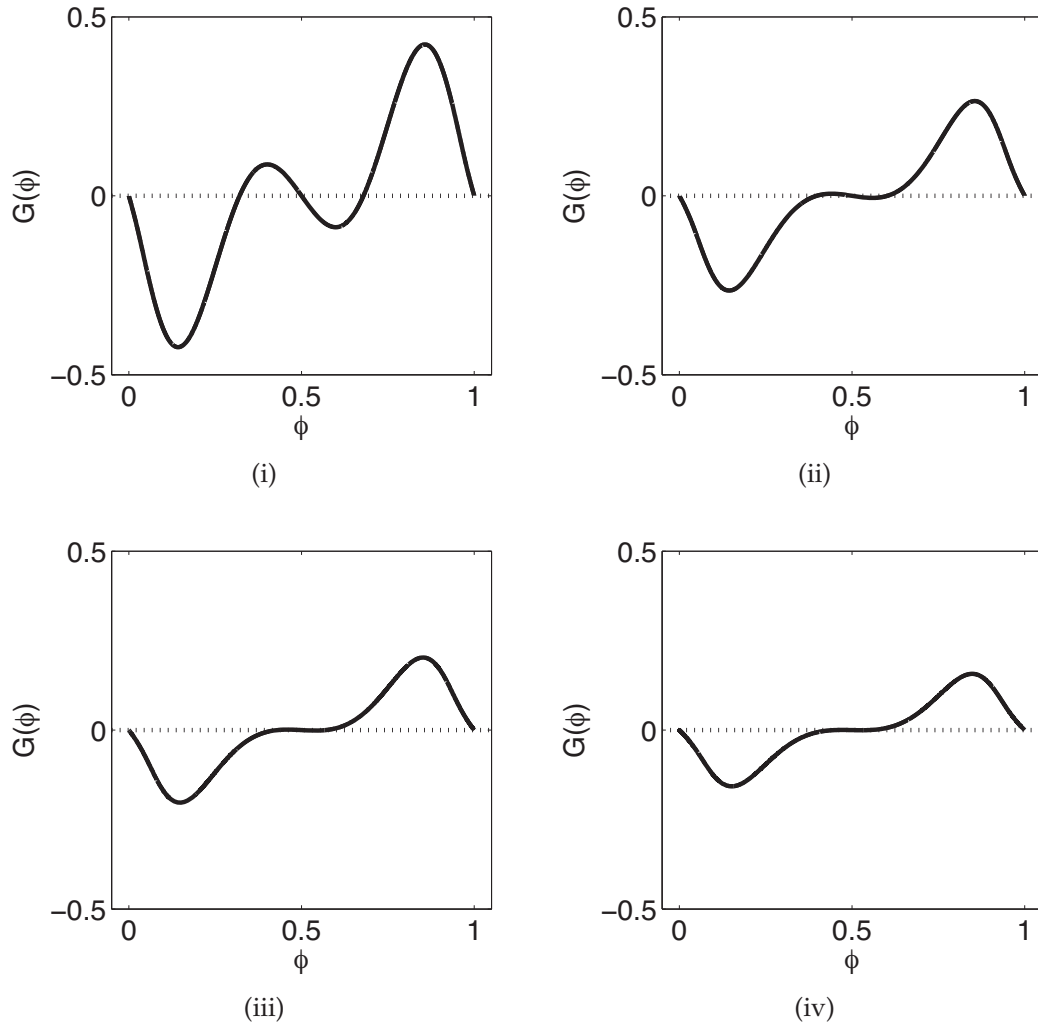


Figure 4.3.2: **G-functions for increasing values of  $I_{applied}$ .** For all plots,  $g_{K_{AHP}} = 100\text{nS}$  and  $\tau_{d_{AHP}} = 5\text{ms}$ . (i)  $I_{applied} = 100\text{pA}$ ,  $f = 26.5\text{Hz}$ . (ii)  $I_{applied} = 200\text{pA}$ ,  $f = 41.4\text{Hz}$ . (iii)  $I_{applied} = 300\text{pA}$ ,  $f = 51.0\text{Hz}$ . (iv)  $I_{applied} = 400\text{pA}$ ,  $f = 59.1\text{Hz}$ . As  $I_{applied}$  increases, the antisynchronous phase-locked state transitions from stable to unstable and the firing frequency  $f$  increases.

synchronous state remains stable, but much less robustly so. In (iv), as  $I_{applied}$  is increased to  $I_{applied} = 400\text{pA}$  the antisynchronous phase-locked transitions to being unstable. Thus as expected, as  $I_{applied}$  is increased, the firing frequency,  $f$ , increases, and antisynchronous oscillatory behavior appears to be suppressed.

Figure 4.3.3 shows that as  $g_{K_{AHP}}$  increases, the antisynchronous phase-locked

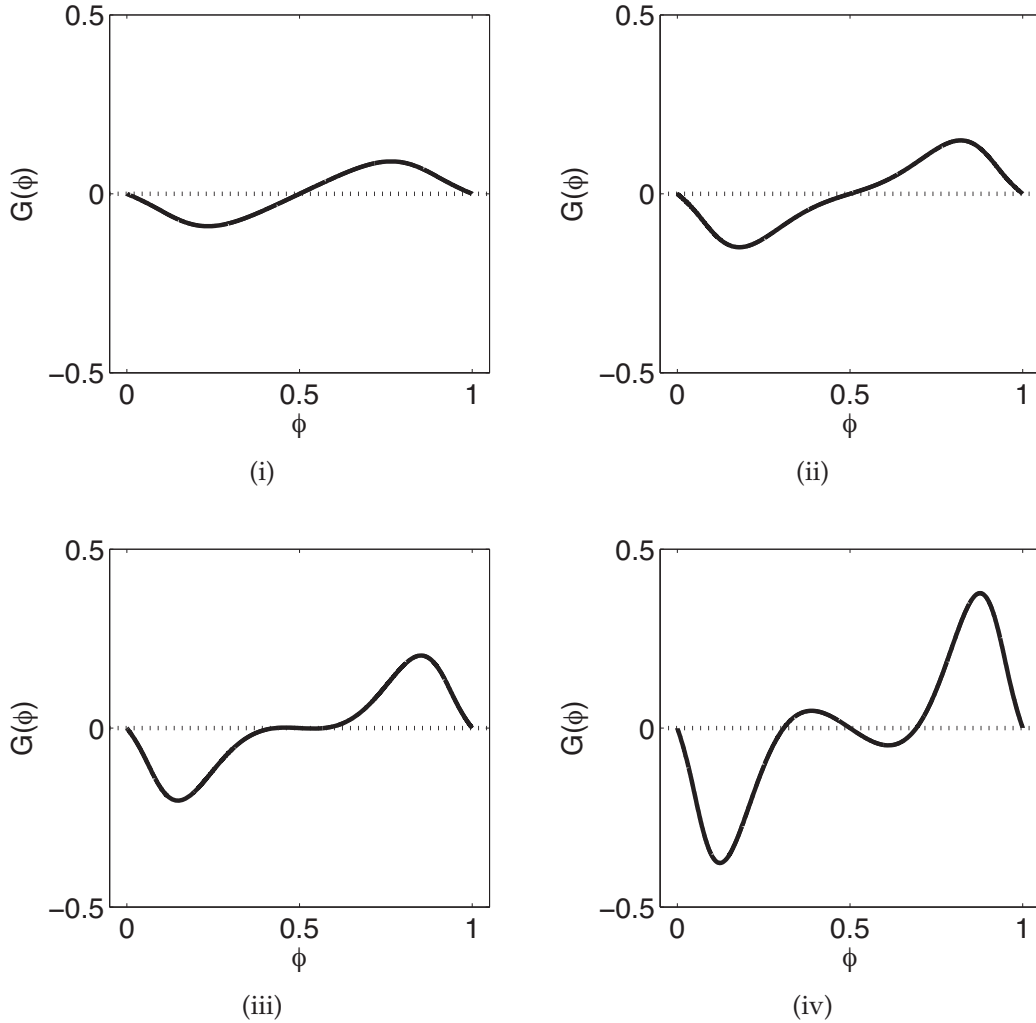


Figure 4.3.3: **G-functions for increasing values of  $g_{K_{AHP}}$ .** For all plots,  $\tau_{d_{AHP}} = 5ms$  and  $I_{applied} = 300pA$ . (i)  $g_{K_{AHP}} = 0nS, f = 94.7Hz$ . (ii)  $g_{K_{AHP}} = 50nS, f = 60.9Hz$ . (iii)  $g_{K_{AHP}} = 100nS, f = 51.0Hz$ . (iv)  $g_{K_{AHP}} = 200nS, f = 43.8Hz$ . As  $g_{K_{AHP}}$  increases, the antisynchronous phase-locked state transitions from being unstable to being stable. Additionally, the firing frequency  $f$  decreases as  $g_{K_{AHP}}$  increases.

state transitions from being unstable to being stable when  $\tau_{d_{AHP}} = 5ms$  and  $I_{applied} = 300pA$ . When  $g_{K_{AHP}} = 0nS$  and  $g_{K_{AHP}} = 50nS$ , the antisynchronous state is unstable (Figures 4.3.3(i) and 4.3.3(ii), respectively). When  $g_{K_{AHP}}$  is increased to  $g_{K_{AHP}} = 100nS$  and  $g_{K_{AHP}} = 200nS$ , the antisynchronous state becomes stable.

Thus, it appears that when  $\tau_{d_{AHP}} = 5ms$ , that the AHP potassium current,  $I_{K_{AHP}}$  promotes antisynchronous behavior. However, note that as  $g_{K_{AHP}}$  increases, the firing frequency decreased.

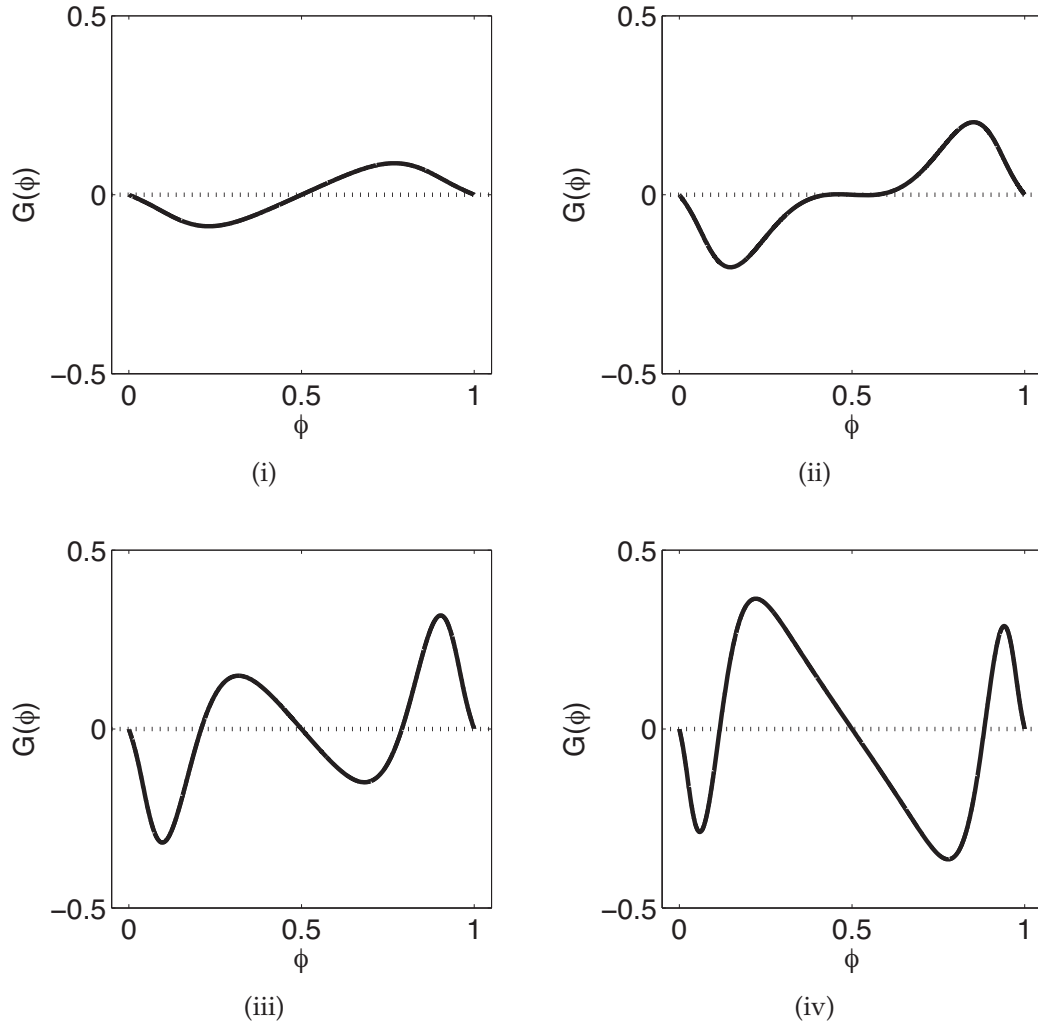


Figure 4.3.4: **G-functions for increasing values of  $\tau_{d_{AHP}}$ .** For all plots,  $g_{K_{AHP}} = 100nS$  and  $I_{applied} = 300pA$ . (i)  $\tau_{d_{AHP}} = 1ms, f = 94.6Hz$ . (ii)  $\tau_{d_{AHP}} = 5ms, f = 51.0Hz$ . (iii)  $\tau_{d_{AHP}} = 10ms, f = 29.9Hz$ . (iv)  $\tau_{d_{AHP}} = 20ms, f = 16.6Hz$ . As  $\tau_{d_{AHP}}$  increases, the antisynchronous phase-locked state transitions from being unstable to being stable. Additionally, the firing frequency  $f$  decreases as  $\tau_{d_{AHP}}$  increases.

Figure 4.3.4 shows that as  $\tau_{d_{AHP}}$  increases, the antisynchronous state tran-

sitions from being unstable to being stable when  $g_{K_{AHP}} = 100nS$  and  $I_{applied} = 300pA$ . For  $\tau_{d_{AHP}} = 1ms$ , the antisynchronous state is unstable (4.3.4(i)). As  $\tau_{d_{AHP}}$  is increased from  $\tau_{d_{AHP}} = 1ms$  to  $\tau_{d_{AHP}} = 5ms$ , the antisynchronous state becomes unstable. As  $\tau_{d_{AHP}}$  is further increased to  $\tau_{d_{AHP}} = 10ms$  and  $\tau_{d_{AHP}} = 20ms$ , the antisynchronous state becomes more robustly stable. Additionally, as  $\tau_{d_{AHP}}$  increased, the firing frequency  $f$  decreased.

Both Figures 4.3.4 and 4.3.3 showed that varying  $\tau_{d_{AHP}}$  and  $g_{K_{AHP}}$  can affect the stability of the antisynchronous phase-locked state. However, it is unclear whether the changes to the stability of the antisynchronous phase-locked state are due directly to the changes of  $\tau_{d_{AHP}}$  and  $g_{K_{AHP}}$ , or to the indirect effects of  $\tau_{d_{AHP}}$  and  $g_{K_{AHP}}$  on the firing frequency. As Figure 4.3.2 illustrated, changes in frequency can effect the stability of the antisynchronous state. Therefore, it behooves us to determine whether changes in  $\tau_{d_{AHP}}$  or  $g_{K_{AHP}}$  directly effect the stability of the antisynchronous state or only indirectly effect the stability of the antisynchronous state due their effects on the firing frequency.

By selecting an appropriate value of  $I_{applied}$ , we can tune the electrically coupled neurons to fire with the same frequency regardless of their values of  $\tau_{d_{AHP}}$  and  $g_{K_{AHP}}$ . Figure 4.3.5 shows that varying  $g_{K_{AHP}}$  effects the stability the antisynchronous phase-locked state even when the firing frequency is held at approximately constant. In each subfigure,  $\tau_{d_{AHP}} = 5ms$  and  $I_{applied}$  was chosen so that the firing frequency,  $f \approx 30Hz$ . For  $g_{K_{AHP}} = 0nS$ , the antisynchronous phase-locked state is unstable (Figure 4.3.5(i)). As  $g_{K_{AHP}}$  is increased to  $g_{K_{AHP}} = 50nS$ ,

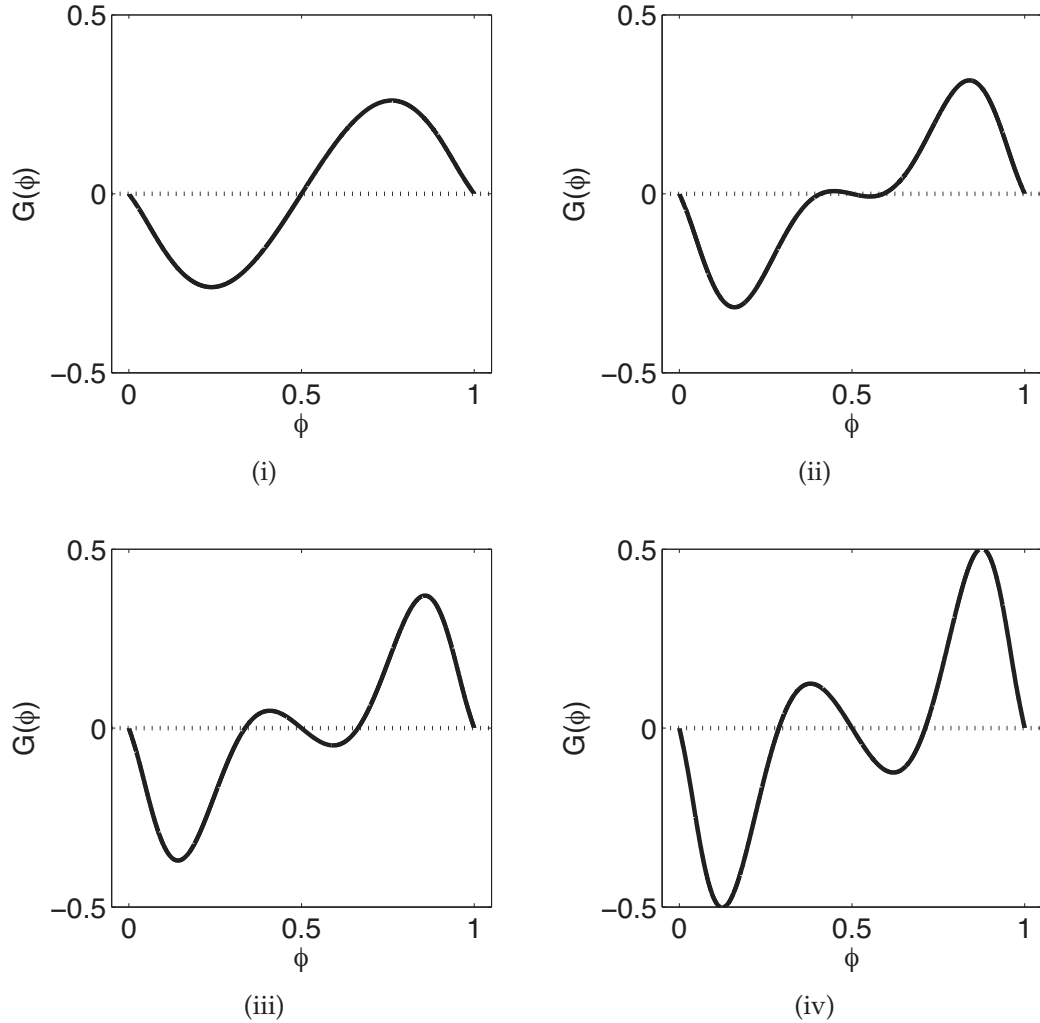


Figure 4.3.5: **G-functions for increasing values of  $g_{K_{AHP}}$  for the same  $f$ .** For all plots,  $\tau_{d_{AHP}} = 5ms$ . (i)  $g_{K_{AHP}} = 0nS, I_{applied} = 86pA, f = 29.7Hz$ . (ii)  $g_{K_{AHP}} = 50nS, I_{applied} = 105pA, f = 30.0Hz$ . (iii)  $g_{K_{AHP}} = 100nS, I_{applied} = 115pA, f = 29.7Hz$ . (iv)  $g_{K_{AHP}} = 200nS, I_{applied} = 135pA, f = 30.0Hz$ .

the antisynchronous phase-locked state becomes stable. Further increases in  $g_{K_{AHP}}$  to  $g_{K_{AHP}} = 100nS$  and  $g_{K_{AHP}} = 200nS$ , increase the robustness and basin of attraction of the stable antisynchronous state. It appears that the value of  $g_{K_{AHP}}$  can directly effect the stability of the antisynchronous phase-locked state. We note that similar response patterns for the stability of the antisynchronous

phase-locked state were observed in both Figure 4.3.3 and Figure 4.3.5, although differences exist regarding the robustness and the basin of attraction for the antisynchronous phase-locked state.

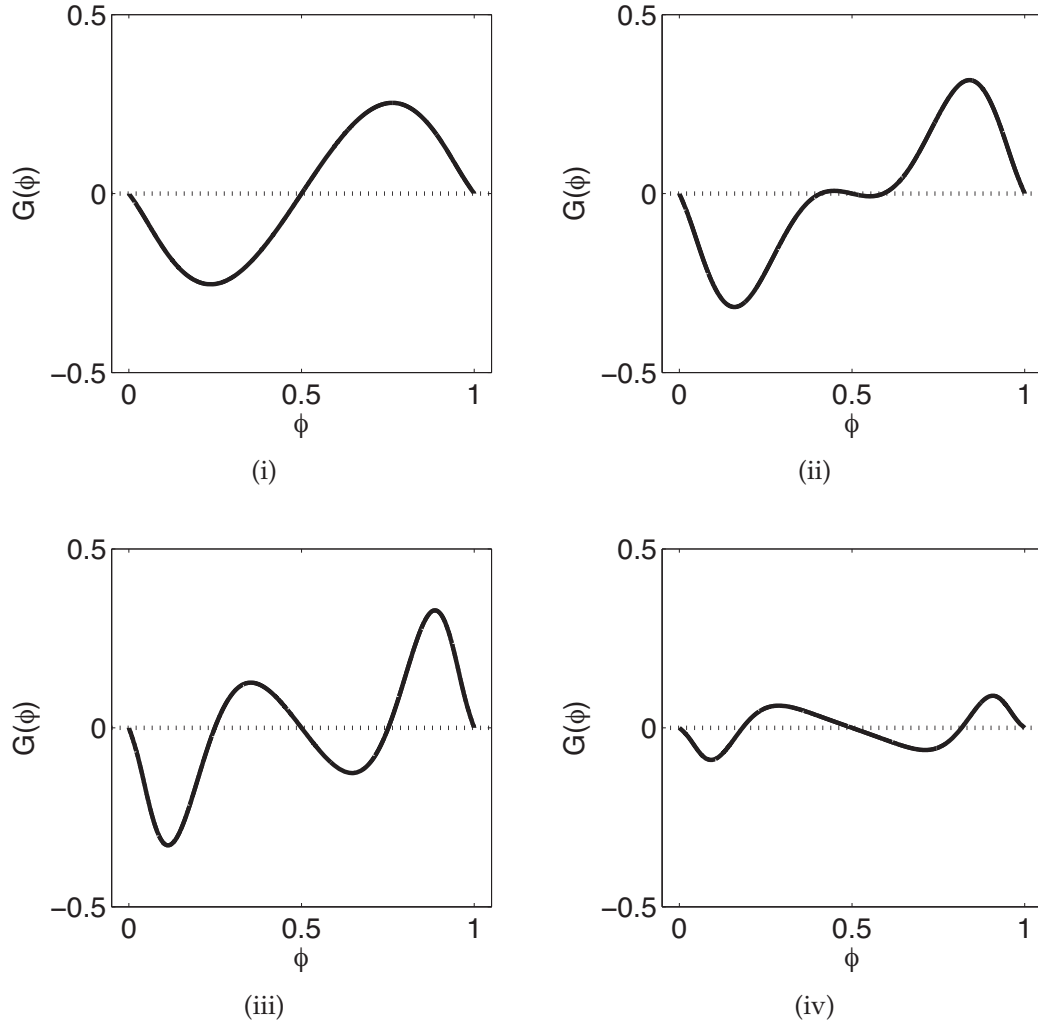


Figure 4.3.6: **G-functions for increasing values of  $\tau_{d_{AHP}}$  for same  $f$ .** For all plots,  $g_{K_{AHP}} = 50nS$ . (i)  $\tau_{d_{AHP}} = 1ms, I_{applied} = 86pA, f = 29.9Hz$ . (ii)  $\tau_{d_{AHP}} = 5ms, I_{applied} = 105pA, f = 30.0Hz$ . (iii)  $\tau_{d_{AHP}} = 10ms, I_{applied} = 205pA, f = 29.8Hz$ . (iv)  $\tau_{d_{AHP}} = 20ms, I_{applied} = 500pA, f = 30.2Hz$ .

Figures 4.3.6, 4.3.7, and 4.3.8 shows that changing  $\tau_{d_{AHP}}$  effects the stability of the antisynchronous state even when the firing frequency is kept approximately

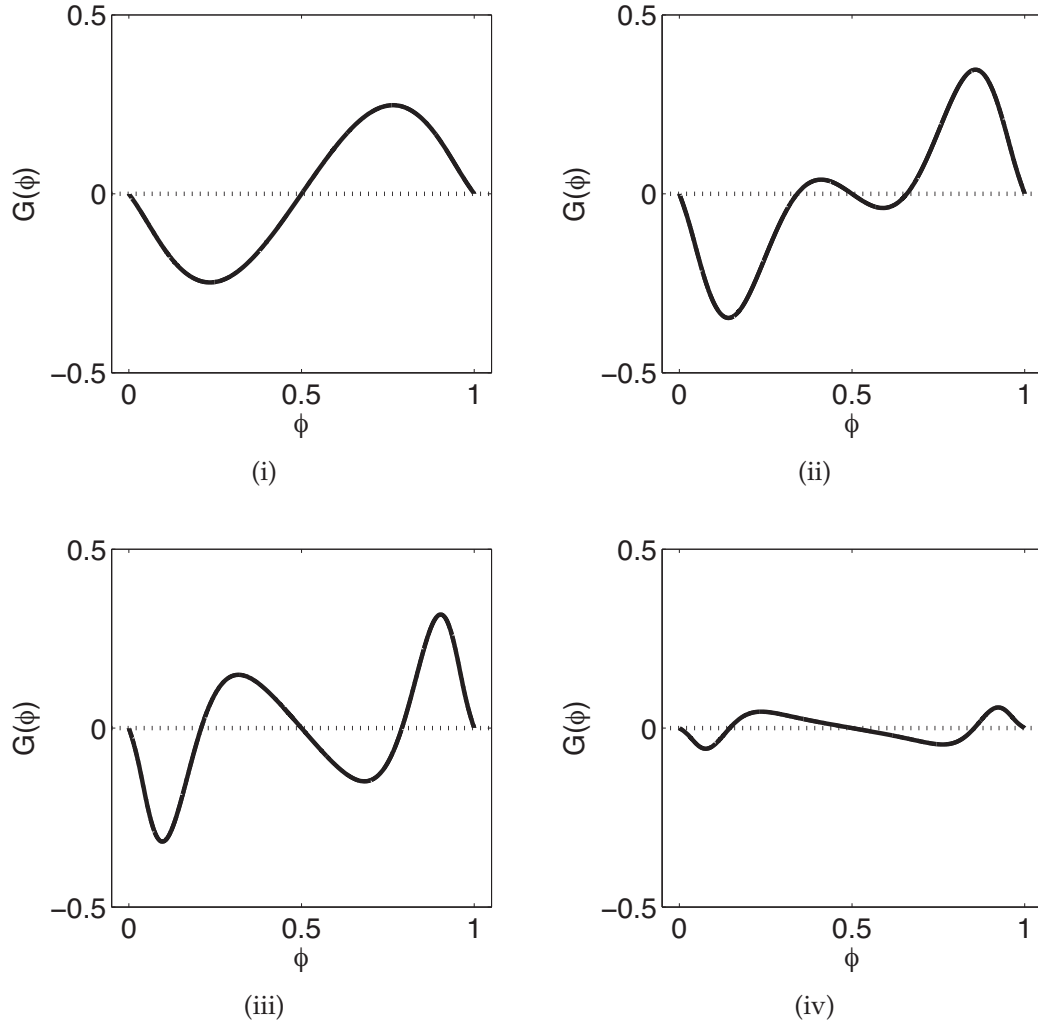


Figure 4.3.7: **G-functions for increasing values of  $\tau_{d_{AHP}}$  for same  $f$ .** For all plots,  $g_{K_{AHP}} = 100nS$ . (i)  $\tau_{d_{AHP}} = 1ms, I_{applied} = 86pA, f = 30.1Hz$ . (ii)  $\tau_{d_{AHP}} = 5ms, I_{applied} = 120pA, f = 30.6Hz$ . (iii)  $\tau_{d_{AHP}} = 10ms, I_{applied} = 300pA, f = 29.9Hz$ . (iv)  $\tau_{d_{AHP}} = 20ms, I_{applied} = 900pA, f = 30.7Hz$ .

equal. For Figures 4.3.6, 4.3.7, and 4.3.8,  $g_{K_{AHP}} = 50nS$ ,  $g_{K_{AHP}} = 100nS$ , and  $g_{K_{AHP}} = 200nS$ , respectively. In all figures and subfigures,  $I_{applied}$  was chosen so that  $f \approx 30Hz$ . When  $\tau_{d_{AHP}} = 1ms$ , the antisynchronous state is unstable (Figures 4.3.6(i), 4.3.7(i), and 4.3.8(i)). However, as  $\tau_{d_{AHP}}$  is increased to  $\tau_{d_{AHP}} = 5ms$ ,  $\tau_{d_{AHP}} = 10ms$ , and  $\tau_{d_{AHP}} = 20ms$ , the antisynchronous phase-locked state evolves

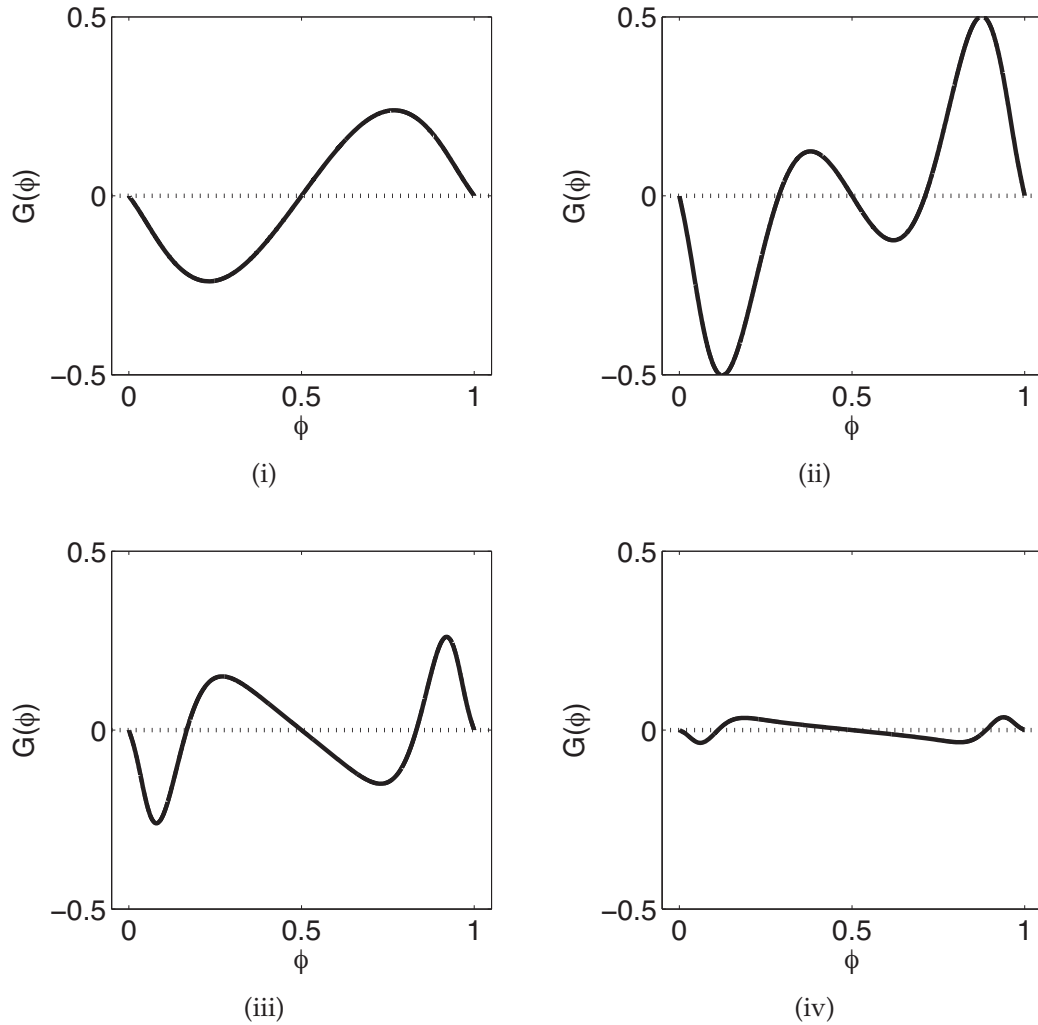


Figure 4.3.8: **G-functions for increasing values of  $\tau_{dAHP}$  for same  $f$ .** For all plots,  $g_{K_{AHP}} = 200\text{nS}$ . (i)  $\tau_{dAHP} = 1\text{ms}$ ,  $I_{\text{applied}} = 86\text{pA}$ ,  $f = 30.3\text{Hz}$ . (ii)  $\tau_{dAHP} = 5\text{ms}$ ,  $I_{\text{applied}} = 135\text{pA}$ ,  $f = 30.0\text{Hz}$ . (iii)  $\tau_{dAHP} = 10\text{ms}$ ,  $I_{\text{applied}} = 460\text{pA}$ ,  $f = 29.8\text{Hz}$ . (iv)  $\tau_{dAHP} = 20\text{ms}$ ,  $I_{\text{applied}} = 1600\text{pA}$ ,  $f = 30.0\text{Hz}$ .

to be stable in each figure. It appears that the value of  $\tau_{dAHP}$  can directly effect the stability of the antisynchronous phase-locked state. We note that similar response patterns for the stability of the antisynchronous phase-locked state were observed in both Figure 4.3.4 and Figure 4.3.7, although differences exist regarding the robustness and the basin of attraction for the antisynchronous

phase-locked state.

In addition to any indirect effects on the firing frequency due to increases of the deactivation time constant,  $\tau_{d_{AHP}}$ , or the magnitude of the AHP current,  $g_{K_{AHP}}$ , increasing  $\tau_{d_{AHP}}$  or  $g_{K_{AHP}}$  promotes the stability of the antisynchronous phase-locked state for the parameters we have investigated.

#### 4.4 Discussion and Conclusions

In this chapter, we investigated how the existence and stability of the phase-locked states for a pair of electrically coupled conductance-based model neurons are affected by changes to the dynamics of a constituent AHP potassium current. We used the theory of weakly coupled oscillators to gain insight into whether changes to the magnitude and the deactivation time constant of the AHP potassium current promoted or suppressed antisynchronous oscillatory behavior. Our work indicated that increasing the magnitude of the AHP current,  $g_{K_{AHP}}$ , and increasing the deactivation time constant,  $\tau$ , both promote antisynchronous oscillatory behavior.

It remains unclear how changes in  $\tau_{d_{AHP}}$  and  $g_{K_{AHP}}$  affect the mechanisms underlying the  $G$ -function. Further research into how  $I_{K_{AHP}}$  impacts the iPRC and the voltage trace should clarify where and how antisynchrony oscillatory behavior is promoted.

##### 4.4.1 Comparison to Previous Results of Pfeuty et al. and Mancilla et al.

The results for the electrically coupled Hodgkin-Huxley type conductance-

based model neurons reaffirm the main results of Chapters 2 and 3 – changes to the intrinsic dynamics of potassium conductances can affect the existence and stability of the antisynchronous phase-locked state. Our results immediately support those of Mancilla et al. (2007). That is, increasing the size of after-hyperpolarization by increasing the magnitude of the potassium current,  $g_{K_{AHP}}$ , promotes antisynchrony. Unlike our models of Chapter 2 and 3, our electrically coupled Hodgkin-Huxley type conductance-based model does not support the conclusions of Pfeuty et al. (2003). We did not observe synchronous oscillatory behavior being promoted due to the increase of the magnitude of the AHP potassium current,  $g_{K_{AHP}}$ . However, it is possible that such behavior exists. By investigating more values and larger values of  $\tau_{d_{AHP}}$ , a parameter space where increases to the magnitude of the potassium current,  $g_{K_{AHP}}$ , promote synchrony potentially may be found.

#### 4.4.2 Limitations of the Model

We intentionally limited our search for stable antisynchrony in this model to a set of lower frequencies, as this is the range of frequencies where antisynchrony is predicted to occur by previous models in this thesis and from similar models by others (see Chapters 2 and 3; Chow and Kopell, (2000); Lewis and Rinzel, (2003); Lewis, 2003; Mancilla et al., (2007)). It is possible that this model might show that stable antisynchrony exists at higher frequencies for suitable parameters; however, we did not investigate this possibility.

In order to study models that allow for analytic insight, this thesis is limited to the examination of the effects of a potassium current on the phase-locking behavior of a pair of identical, electrically coupled model neurons. We can create more biophysically realistic models in which to study the effects of potassium currents on oscillatory behavior in several ways. For instance, we can consider additional forms of cellular interactions, such as mutual inhibition due to chemical signaling. We can incorporate the natural heterogeneity exhibited by populations of neurons by considering non-identical model cells. We can examine more biophysically realistic subnetworks of neurons instead of only a pair of cells. We can introduce noise into our model, via the coupling current or the potassium current, and see if and how its inclusion effects the stability of phase-locked states. As stable, antisynchronous oscillatory activity has yet to be observed experimentally [Mancilla et al., 2007], it behooves us to see whether increasingly biophysically realistic theoretical models also predict the existence of stable antisynchrony.

Despite the limitations of our models, the results presented in this thesis support the need for accurate biophysical measurements, as even seemingly small differences in reported activity appear to affect the existence and stability of oscillatory activity.

---

## Appendix A

### A.1 The Infinitesimal Phase Resetting Curve $Z(t)$

The intrinsic dynamics of the LIF neuron with an explicit potassium current are given by the differential equation

$$\frac{dv}{dt} = -v + I - g_K \eta_K(t)$$

and the condition that when  $v$  reaches a threshold of 1, it is reset to  $v = 0$ . (Note that  $\eta_K(t)$  and  $A_K(\tau)$  are defined in Chapter 2.) When  $I > 1$ , the cell undergoes periodic firing. If the membrane potential of the cell starts out at  $v(0) = 0$ , then the  $T$ -periodic solution is given by

$$v_{LC}(t) = I(1 - e^{-t}) - g_K A_K(\tau) (e^{-t/\tau} - e^{-t}) + \beta \delta(t - T), \quad 0 \leq t < T.$$

We compute the iPRC by determining how a cell responds to a small  $\delta$ -function perturbation of strength  $\epsilon$  when the cell is at an arbitrary phase in the oscillations corresponding to  $t = \tilde{t}$ . The stimulus causes an instantaneous jump in  $v$  by  $\epsilon$ , i.e.  $v(\tilde{t}) = I(1 - e^{-\tilde{t}}) - g_K A_K(\tau) (e^{-\tilde{t}/\tau} - e^{-\tilde{t}}) + \epsilon$ , and thus altering the phase of the oscillation. To evaluate the magnitude and direction of the phase shift  $\Delta\phi$ , we use  $v(\tilde{t}) = I(1 - e^{-\tilde{t}}) - g_K A_K(\tau) (e^{-\tilde{t}/\tau} - e^{-\tilde{t}}) + \epsilon$  as the initial condition to

the system and solve for the time  $t = T - T\Delta\phi$  that the cell reaches threshold

$$v(T - T\Delta\phi) = 1.$$

$$1 = v(T - T\Delta\phi)$$

$$\begin{aligned} &= v(\tilde{t})e^{-(T-T\Delta\phi-\tilde{t})} + I(1 - e^{-(T-T\Delta\phi-\tilde{t})}) - g_K A_K(\tau)(e^{-(T-T\Delta\phi)/\tau} - e^{-\frac{\tilde{t}}{\tau}-(T-T\Delta\phi-\tilde{t})}) \\ &= \left[ I(1 - e^{-\tilde{t}}) - g_K A_K(\tau)(e^{-\frac{T-T\Delta\phi}{\tau}+(T-T\Delta\phi-\tilde{t})} - e^{-\tilde{t}}) + \epsilon \right] e^{-(T-T\Delta\phi-\tilde{t})} + I(1 - e^{-(T-T\Delta\phi-\tilde{t})}) \\ &= I(1 - e^{-(T-T\Delta\phi)}) - g_K A_K(\tau)(e^{-\frac{T-T\Delta\phi}{\tau}} - e^{-(T-T\Delta\phi)}) + \epsilon e^{-(T-T\Delta\phi-\tilde{t})} \end{aligned}$$

Because this equation is transcendental, we can not explicitly solve for the phase advance,  $\Delta\phi$ . However, with implicit differentiation, we can expand  $\Delta\phi$  around the small parameter  $\epsilon$ . This yields

$$\Delta\phi(\tilde{t}) = \frac{e^{\tilde{t}}}{T(I + g_K A_K(\tau)(\frac{1}{\tau}e^{T(\tau-1)/\tau} - 1))} \epsilon + O(\epsilon^2).$$

We normalize the phase shift  $\Delta\phi$  by the strength of  $\epsilon$  to obtain, the infinitesimal phase resetting curve (i.e. the PRC for sufficiently small  $\epsilon$ ). Thus

$$Z(\tilde{t}) = \frac{e^{\tilde{t}}}{T(I + g_K A_K(\tau)(\frac{1}{\tau}e^{T(\tau-1)/\tau} - 1))}.$$

Note that taking  $g_K \rightarrow 0$  (i.e. no explicit potassium current) yields the iPRC for the standard LIF model. The iPRC for the LIF model with a voltage dependent explicit potassium current (Chapter 3) is found using the steps outlined above.

## A.2 Reduction to Phase Model

Using the procedure outlined in the introduction, 1.3, the  $G$ -function for an

electrically coupled pair of LIF cells can be found by computing the integral

$$G(\phi) = \frac{1}{T} \int_0^T Z(t) g_c [(v_{LC}(t - \phi T) - v_{LC}(t + \phi T))] dt$$

We remind the reader that although  $Z(t)$  and  $v_{LC}(t)$  are periodic, they are only defined on  $t \in [0, T]$  for the LIF model neurons. Thus to appropriately evaluate  $G(\phi)$ , we must separate the integral over the appropriate subintervals.

$$\begin{aligned} G(\phi) &= \frac{1}{T} \int_0^T Z(t) g_c [(v_{LC}(t - \phi T) - v_{LC}(t + \phi T))] dt \\ &= \frac{g_c}{T} \left[ \int_0^T Z(t) (v_{LC}(t - \phi T) dt - \int_0^T Z(t) v_{LC}(t + \phi T) dt \right] \\ &= \frac{g_c}{T} \left[ \left( \int_0^{\phi T} Z(t) v_{LC}(t + (1 - \phi)T) dt + \int_{\phi T}^T Z(t) v_{LC}(t - \phi T) dt \right) \right. \\ &\quad \left. - \left( \int_0^{(1-\phi)T} Z(t) v_{LC}(t + \phi T) dt + \int_{(1-\phi)T}^T Z(t) v_{LC}(t - (1 - \phi)T) dt \right) \right] \end{aligned}$$

---

## Appendix B

### B.1 Choice of $\zeta(t)$

To facilitate comparisons between the LIF model with a conductance-based potassium current and the LIF model with a spike-triggered potassium current, ideally we would have chosen identical kernels. Unfortunately, it is not possible to find an analytic solution to the LIF model with a conductance-based potassium current if an exponentially decaying kernel, i.e.  $\eta_{K_{ns}}(t)$ , is used in place of  $\zeta(t)$ . In choosing  $\zeta(t)$ , we were mindful of choosing an equation that was qualitatively similar to  $\eta_{K_{ns}}(t)$  to keep comparisons reasonable. Thus we choose  $\zeta(t) = 1/(t + \tau)$ .

While analytic solutions to the LIF model with  $\eta_{K_{ns}}(t)$  as the kernel for the potassium conductance cannot be found, numerical solutions are possible. To show that the two kernels gives qualitatively similar results, Figure B.1.1 presents the pacing of non-dimensionalized electrically coupled LIF neurons with a conductance-based potassium current where the conductance kernel,  $\zeta(t)$  is replaced with  $\eta_{K_{ns}}(t)$ .

Both Figure B.1.1 with  $\eta_{K_{ns}}(t)$  as the potassium conductance kernel and Figure 3.2.1 with  $\zeta(t)$  as the potassium conductance kernel show that for small

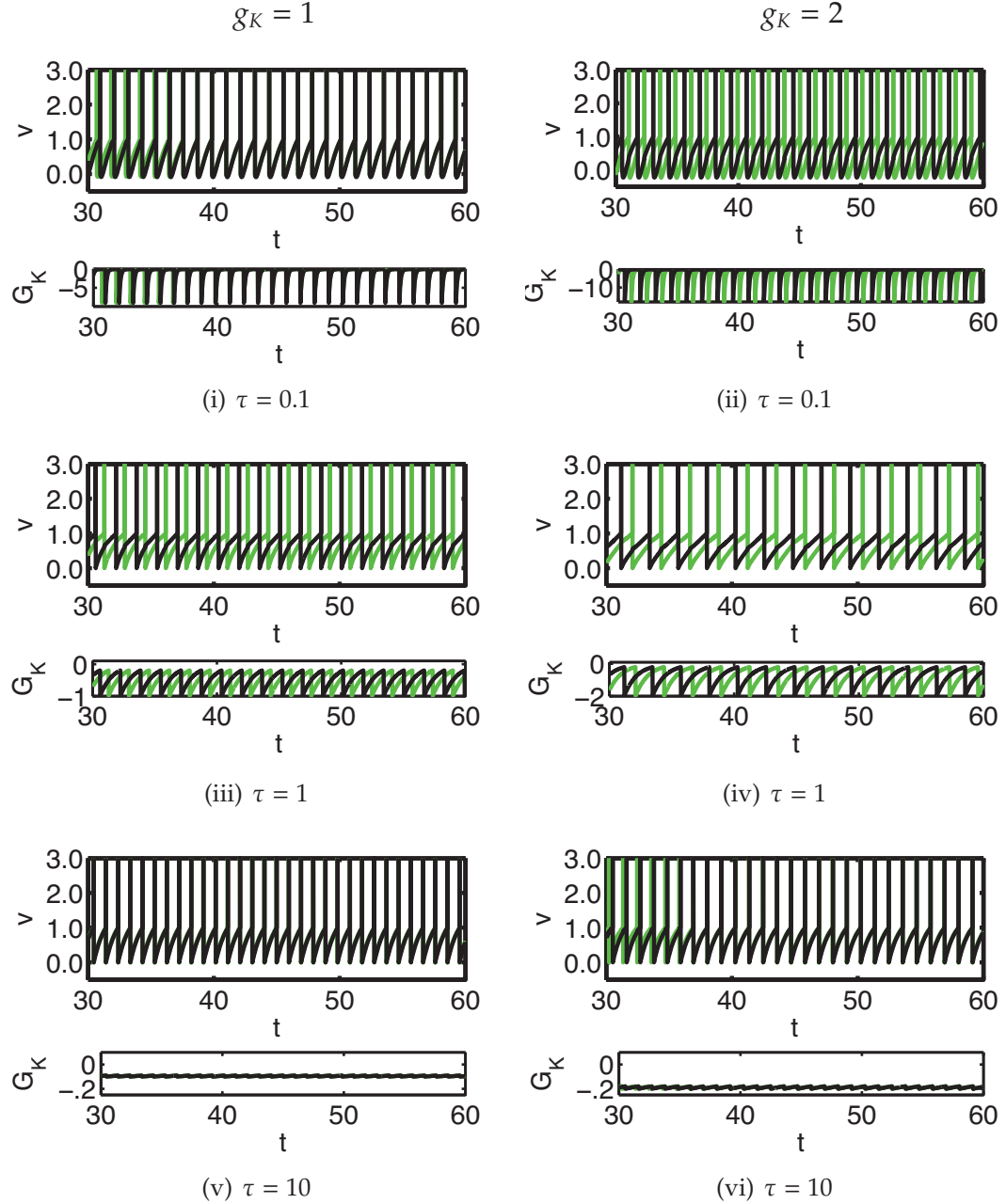


**Figure B.1.1: Electrically coupled LIF neurons with  $\eta_{K_{ns}}(t)$  as the kernel for the explicit potassium conductance with  $g_K = 1$  (left) and  $g_K = 2$  (right).** The cells oscillate independently from initial conditions  $v_1 = 0.83$  (black) and  $v_2 = 0.0$  (green) until the electrical coupling term was activated at  $t = 20$ . For  $\tau = 0.1$  and  $\tau = 1$ , the system evolves to antisynchrony for both  $g_K = 1$  and  $g_K = 2$ . For  $\tau = 10$ , the system evolves to synchrony for  $g_K = 1$  and  $g_K = 2$ . For all subfigures,  $I = 1.7$ ,  $E_K = -0.5$ ,  $g_c = 0.2$ , and  $\beta = 0.2$ .

$\tau$  that the electrically coupled cell-pair can evolve to antisynchrony. As  $\tau$  is increased, the system shifts and evolves to synchrony instead. However, the LIF model with a conductance-based potassium current with  $\eta_{K_{ns}}(t)$  as the potassium conductance kernel has a much higher firing frequency at low  $\tau$  than that of the model with  $\zeta(t)$ . As  $\tau$  increases, the differences in firing frequency between the use of the two kernels diminish.

Similarly, the LIF model with an explicit potassium current (Chapter 2) can be reinvestigated with  $\zeta(t)$  used in place of  $\eta_{K_{ns}}(t)$ . Unfortunately, when  $\zeta(t)$  is included in the differential equation in place of  $\eta_{K_{ns}}(t)$ , it is no longer possible to find an analytic solution to the modified differential equation. To show that the two kernels gives qualitatively similar results, Figure B.1.2 presents the numerical simulation of non-dimensionalized electrically coupled LIF neurons with a spike-triggered potassium current where the kernel,  $\eta_{K_{ns}}(t)$  is replaced with  $\zeta(t)$ .

Both Figure B.1.2 with  $\zeta(t)$  as the potassium current kernel and Figure 2.3.1 (right column) with  $\eta_{K_{ns}}(t)$  as the potassium current kernel shows that for small  $\tau$  that the use of either kernel allows the system to evolve to stable antisynchrony. As  $\tau$  is increased, the coupled system evolves to synchrony for both kernels. However, the use of  $\zeta(t)$  in place of  $\eta_{K_{ns}}(t)$  leads to a lower firing frequency for small  $\tau$ . However, this difference diminishes as  $\tau$  is increased.

Even though  $\zeta(t)$  and  $\eta_{K_{ns}}(t)$  differ in how quickly each decays and how much total current each contributes, they have similar qualitative effects on the

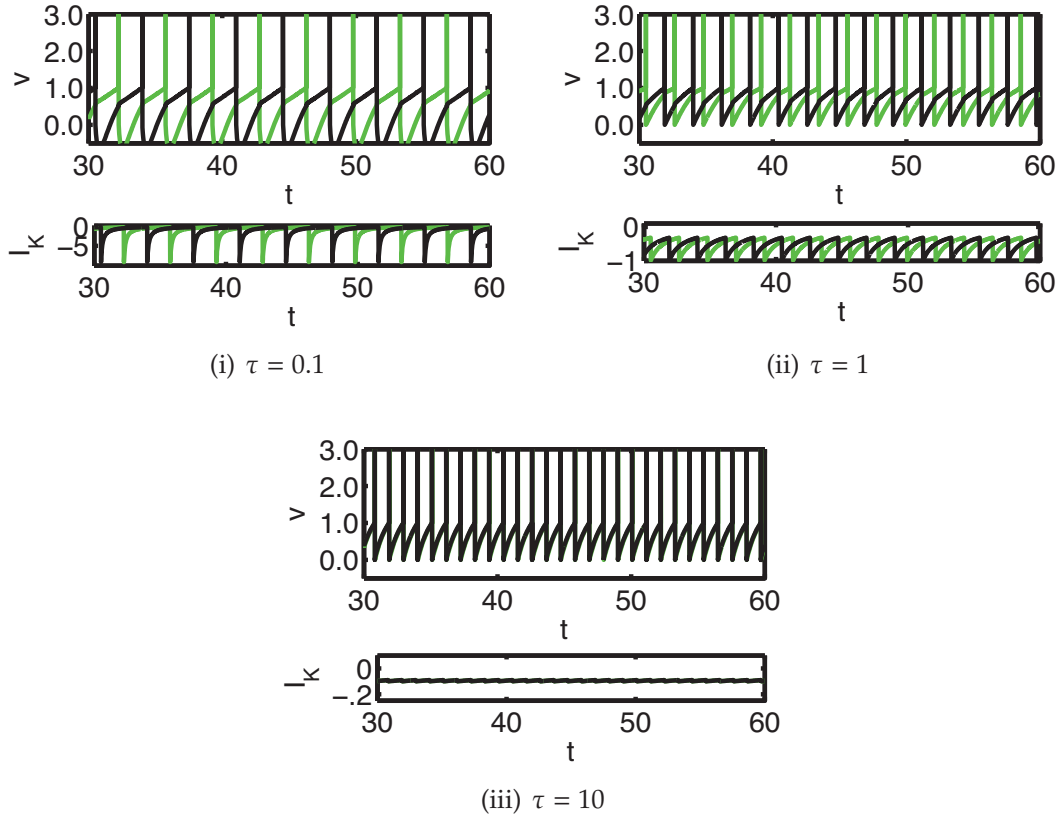


**Figure B.1.2: Electrically Coupled LIF neurons with  $\zeta(t)$  as the kernel for the spike-triggered potassium current.** The cells oscillate independently from initial conditions  $v_1 = 0.59$  (black) and  $v_2 = 0.0$  (green) until the coupling terms was activated at  $t = 10$ . (i – ii) For  $\tau = 0.1$  and  $\tau = 1$  the system evolves to antisynchrony. (iii) For  $\tau = 10$ , the system evolves to synchrony. For all graphs,  $I = 1.6$ ,  $g_K = 1$ ,  $g_c = 0.2$ , and  $\beta = 0.2$ .

LIF model. Furthermore, our choice of both kernels was arbitrary, as both were chosen to qualitatively capture the dynamics of a potassium channel rather than to adhere to biophysical dynamical measurements.

## B.2 Solutions for the LIF model with a Conductance-based Potassium Current for $g_K = 2$

In this section, we present the solutions for the LIF model with a conductance-

based potassium current for  $g_K = 2$ .

The corresponding solution to (3.2.1) for the differential equation (3.1.2) for

$g_K = 2$  is

$$\begin{aligned} v_{LC}(t) = & \frac{1}{(t + \tau)^2} \left[ (I(2 - 2\tau + \tau^2) + 2E_k(\tau - 1))(1 - e^{-(t-t_0)}) \right. \\ & + I(t(t + 2\tau - 2) - t_0(t_0 + 2\tau - 2)e^{-(t-t_0)}) \\ & \left. + 2E_k(t - t_0 e^{-(t-t_0)}) + v(t_0)(t_0 + \tau)^2 e^{-(t-t_0)} \right] + \beta \delta(t - (t_0 + T)) \quad t \in [t_0, t_0 + T]. \end{aligned} \quad (\text{B.2.1})$$

The corresponding solution to (3.2.2) to find the period,  $T$ , is

$$1 = \frac{1}{(T + \tau)^2} \left[ (I(2 - 2\tau + \tau^2) + 2E_k(\tau - 1))(1 - e^{-T}) + T(I(T + 2\tau - 2) + 2E_k) \right]. \quad (\text{B.2.2})$$

Equation (B.2.2) can be rearranged to give  $I$  as a function of the firing frequency  $f$  ( $= 1/T$ ). This corresponds to Equation (3.2.3).

$$I = \frac{(T + \tau)^2 - 2E_k[(\tau - 1)(1 - e^{-T}) + T]}{(2 - 2\tau + \tau^2)(1 - e^{-T}) + T(T + 2\tau - 2)} \quad (\text{B.2.3})$$

The iPRC,  $Z(t)$  for  $g_K = 2$ , which corresponds to (3.4.1) is

$$Z(t) = \frac{(t + \tau)^2 e^t}{2T[I(1 - \tau + \tau^2/2) + E_k(\tau - 1) + ((T + \tau)(I - 1) + E_k - I)e^T]}. \quad (\text{B.2.4})$$

The  $G$ -function for  $g_K = 2$ , which corresponds to (3.4.2) is

$$G(\phi) = \frac{g_c}{TD_2(\tau)} \left[ \left( \int_0^{\phi T} (t + \tau)^2 e^t v_{LC}(t + (1 - \phi)T) dt + \int_{\phi T}^T (t + \tau)^2 e^t v_{LC}(t - \phi T) dt \right. \right. \\ \left. \left. - \int_0^{T(1-\phi)} (t + \tau)^2 e^t v_{LC}(t + \phi T) dt - \int_{T(1-\phi)}^T (t + \tau)^2 e^t v_{LC}(t - (1 - \phi)T) dt \right) \right. \\ \left. + \beta [(\phi T + \tau)^2 e^{\phi T} - ((1 - \phi)T + \tau)^2 e^{(1-\phi)T}] \right]$$

$$\text{where } D_2(\tau) = 2T[I(1 - \tau + \tau^2/2) + E_k(\tau - 1) + ((T + \tau)(I - 1) + E_k - I)e^T] \quad (\text{B.2.5})$$

---

## Appendix C

### C.1 Model Parameters

Here we give the parameters for the modified Hodgkin-Huxley type model.

As a reminder, this model was described by

$$\begin{aligned} C_m \frac{dV}{dt} &= -g_L(V - E_L) - g_{Na}m^3h(V - E_{Na}) - (g_{K_{reset}}n_{reset} + g_{K_{AHP}}n_{AHP})(V - E_K) + I_{applied}, \\ \frac{dy}{dt} &= \alpha_y(V)(1 - y) - \beta_y(V)y, \text{ where } y = n, m, h. \end{aligned} \quad (\text{C.1.1})$$

We set each of the following to the given value,  $C_m = 40\text{pF}$ ,  $g_L = 10\text{nS}$ ,  $g_{Na} = 4500\text{nS}$ ,  $g_{K_{reset}} = 900\text{nS}$ ,  $E_L = -70\text{mV}$ ,  $E_{Na} = 74\text{mV}$ , and  $E_K = -90\text{mV}$  [Mancilla et al, 2007].

For  $m$ ,

$$\begin{aligned} \alpha_m(V) &= \frac{40.0(75.5 - V)}{e^{-(V-75.5)/13.5} - 1.0} \\ \beta_m(V) &= \frac{1.2262}{e^{V/42.248}}. \end{aligned} \quad (\text{C.1.2})$$

For  $h$ ,

$$\begin{aligned} \alpha_h(V) &= \frac{0.0035}{e^{V/42.186}} \\ \beta_h(V) &= \frac{-0.017(51.25 + V)}{e^{-(51.25+V)/5.2} - 1.0}. \end{aligned} \quad (\text{C.1.3})$$

For  $n_{reset}$ , we set  $V_{1/2} = 0mV$ ,  $\tau_{a_{reset}} = 0.1ms$ , and  $\tau_{d_{reset}} = 1ms$ .

$$\begin{aligned}\alpha_{n_{reset}}(V) &= \frac{e^{V+10}}{0.1e^{V+10} + 2} \\ \beta_{n_{reset}}(V) &= \frac{1}{0.1e^{V+10} + 2}.\end{aligned}\tag{C.1.4}$$

---

## Bibliography

- [1] Y Amitai, JR Gibson, M Beierlein, SL Patrick, AM Ho, BW Connors, and D Golomb, *The Spatial Dimensions of Electrically Coupled Networks of Interneurons in the Neocortex*, *Journal of Neuroscience*, Vol. 22, 4142 - 4152 (2002)
- [2] M Beierlein, JR Gibson, and BW Connors, *A Network of Electrically Coupling can Prevent Expression of Adult-like Properties in an Embryonic Neural Circuit*, *Nature Neuroscience*, Vol. 3, 904 - 910 (2000)
- [3] T Bem, Y Le Feuvre, J Simmers, and P Meyrand, *Electrical Coupling Can Prevent Expression of Adult-Like Properties in an Embryonic Neural Circuit*, *Journal of Neurophysiology*, Vol. 87, 538 - 547 (2002)
- [4] MVL Bennett and RS Zukin, *Electrical Coupling and Neuronal Synchronization in the Mammalian Brain*, *Neuron*, Vol. 41, 495 - 511 (2004)
- [5] G Buzsaki and A Draguhn, *Neuronal Oscillations in Cortical Networks*, *Science*, Vol. 204, 1926 - 1929 (2004)
- [6] G Buzsaki, *Theta Oscillations in the Hippocampus*, *Neuron*, Vol. 33, 325 - 340 (2002)
- [7] CC Chow and N Kopell, *Dynamics of Spiking Neurons with Electrical Coupling*, *Neural Computation*, Vol. 12, 1643 - 1678 (2000)
- [8] WA Coetzee, Y Amarilli, J Chiu, A Chow, D Lau, T McCormack, H Moreno, MS Nadal, A Ozaita, D Pountney, M Saganich, E Vega-Saenze de Miera, and B Rudy, *Molecular Diversity of K<sup>+</sup> Channels*, *Annals of the New York Academy of Science*, Vol. 868, 233 - 286 (1999)
- [9] P Dayan and LF Abbott, *Theoretical Neuroscience: Computational and Mathematical Modeling of Neural Systems*, ISBN 0-262-54185-8, The MIT Press, 2001
- [10] A Di Garbo, A Panarese, and S Chillemi, *Gap junctions promote synchronous activities in a network of inhibitory interneurons*, *Biosystems*, Vol. 79, 91 - 99 (2005)

- [11] A Erisir, D Lau, B Rudy, and CS Leonard, *Function of Specific  $K^+$  Channels in Sustained High-Frequency Firing of Fast-Spiking Neocortical Interneurons*, *Journal of Neurophysiology*, Vol. 82, 2476 - 2489 (1999)
- [12] GB Ermentrout and N Kopell, *Multiple Pulse Iteration and Averaging in Coupled Neural Oscillators*, *Journal of Mathematical Biology*, Vol. 29, 195 - 217 (1991)
- [13] GB Ermentrout and D Kleinfeld *Traveling Electrical Waves in Cortex: Insights from Phase Dynamics and Speculation on a Computational Role*, *Neuron*, Vol. 29, 33 - 44 (2001)
- [14] GB Ermentrout, M Pascal, and B Gutkin, *The Effects of Spike Frequency Adaptation and Negative Feedback on the Synchronization of Neural Oscillators*, *Neural Computation*, Vol. 13, 1285 - 1319 (2001)
- [15] P Fries, D Nikolic, and W Singer, *The Gamma Cycle*, *Trends in Neurosciences*, Vol. 30, 309 - 316 (2007)
- [16] M Galarreta and S Hestrin, *Electrical Synapses between GABA-releasing Interneurons*, *Nature Reviews Neuroscience*, Vol. 2, 425 - 433 (2001)
- [17] JR Gibson, M Beierlein, and BW Connors, *Two Networks of Electrically Coupled Inhibitory Neurons in Neocortex*, *Nature*, Vol. 402, 75 - 79 (1999)
- [18] JR Gibson, M Beierlein, and BW Connors, *Functional Properties of Electrical Synapses Between Inhibitory Interneurons of Neocortical Layer 4*, *Journal of Neurophysiology*, Vol. 93, 467 - 480 (2005)
- [19] D Golomb, D Hansel, and G Mato, *Theory of Synchrony of Neuronal Activity*, *Handbook of Biological Physics*, Vol 4: Neuro-informatics and Neural Modeling (S Gielen and M Moss, eds), pp 887 - 968 Amsterdam: Elsevier (2001)
- [20] ER Grannan, D Kleinfeld, and H Sompolinsky, *Stimulus-Dependent Synchronization of Neuronal Assemblies*, *Neural Computation*, Vol. 5, 550 - 569 (1993)
- [21] CM Gray, AK Engel, P Konig, and W Singer, *Synchronization of Oscillatory Neuronal Responses in Cat Striate Cortex: Temporal Properties*, *Vis. Neuroscience*, Vol. 8, 337 - 347 (1992)
- [22] D Hansel, G Mato, and C Meunier, *Mechanisms of Synchrony of Neural Activity in Large Networks*, In: F Moss, S Gielen, eds. *Handbook of Biological Physics*, Vol. R: Neuro-Informatics and Neural Modeling. Elsevier, Amsterdam. pp. 887 - 968 (2001)

- [23] A Hodgkin and A Huxley, *A Quantitative Description of Membrane Current and its Application to Conduction and Excitation in Nerve*, Journal of Physiology, Vol. 117, 500 - 544 (1952)
- [24] R Jolivet, TJ Lewis, and W Gerstner, *Generalized Integrate-and-Fire Models of Neuronal Activity Approximate Spike Trains of a Detailed Model to a High Degree of Accuracy*, Journal of Neurophysiology, Vol. 92, 959 - 976 (2004)
- [25] Y Kuramoto, *Chemical oscillations, waves, and turbulence*, Springer-Verlag, Berlin, (1984)
- [26] TJ Lewis and J Rinzel, *Dynamics of Spiking Neurons Connected by Both Inhibitory and Electrical Coupling*, Journal of Computational Neuroscience, Vol. 14, 283 - 309 (2003)
- [27] TJ Lewis and FK Skinner, *Understanding Activity in Electrically Coupled Networks using PRCs and the Theory of Weakly Coupled Oscillators*, Chapter in book: PRCs in Neuroscience: Theory, Experiment and Analysis (eds. N.Schultheiss, A.Prinz, R. Butera) Springer. (to appear) (2011)
- [28] JG Mancilla, TJ Lewis, DJ Pinto, J Rinzel, and BW Connors, *Synchronization of Electrically Coupled Pairs of Inhibitory Interneurons in Neocortex*, The Journal of Neuroscience, Vol. 27(8), 2053 - 2073 (2007)
- [29] EB Merriam, TI Netoff, and MI Banks, *Bistable Network Behavior of Layer I Interneurons in Auditory Cortex*, Journal of Neuroscience, Vol. 25, 6175 - 6186 (2005)
- [30] M Nomura, T Fukai, and T Aoyagi, *Synchrony of Fast-Spiking Interneurons Interconnected by GABAergic and Electrical Synapses*, Neural Computation, Vol. 15(9), 2179 - 2198 (2003)
- [31] B Pfeuty, G Mato, D Golomb, and D Hansel, *Electrical Synapses and Synchrony: The Role of Intrinsic Currents*, Journal of Neuroscience, Vol. 23(15), 6280 - 6294 (2003)
- [32] J Rinzel and GB Ermentrout, (1988). *Analysis of neural excitability and oscillations* Chapter in book: Methods in Neuronal Modeling: From Ions to Networks, 2nd ed. (eds. C.Koch, I.Segev). MIT Press, Cambridge MA. pp. 251- 191 (1988)
- [33] TJ Seynowski and O Paulsen, *Network Oscillations: Emerging Computational Principles*, Journal of Neuroscience, Vol. 26, 1673 - 1676 (2006)
- [34] A Sherman and J Rinzel, *Rhythmogenic Effects of Weak Electrotonic Coupling in Neuronal Models*, Proceedings of the National Academy of Science, Vol. 89, 2471 - 2474 (1992)

- [35] FK Skinner, L Zhang, JL Perez Velazquez, and PL Carlen, *Bursting in Inhibitory Interneuronal Networks: A Role for Gap-Junctional Coupling*, Journal of Neurophysiology, Vol. 81, 1274 - 1283 (1999)
- [36] SH Strogatz, *Nonlinear Dynamics and Chaos*, ISBN 0-7382-0453-6, Westview Press, 1994
- [37] RD Traub, N Kopell, A Bibbig, E Buhl, FEN Lebeau, and M Whittington, *Gap Junction Between Interneuron Dendrites can Enhance Synchrony of  $\gamma$  Oscillations in Distributed Networks*, Journal of Neuroscience, Vol. 21, 9478 - 9486 (2001)
- [38] LM Ward, *Synchronous Neural Oscillations and Cognitive Processes*, Trends in Cognitive Sciences, Vol. 7, 553 - 559 (2003)